Some exotic gapless states in insulating and conducting many-body systems

Francisco Zuniga Frias

A thesis submitted for the degree of PhD
at the
University of St Andrews

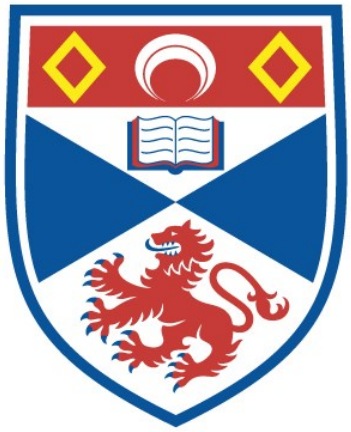

2025

Candidate's declaration

I, Francisco Zuniga Frias, do hereby certify that this thesis, submitted for the degree of PhD, which is approximately 36,000 words in length, has been written by me, and that it is the record of work carried out by me, or principally by myself in collaboration with others as acknowledged, and that it has not been submitted in any previous application for any degree. I confirm that any appendices included in my thesis contain only material permitted by the 'Assessment of Postgraduate Research Students' policy.

I was admitted as a research student at the University of St Andrews in January 2020.

I received funding from an organisation or institution and have acknowledged the funder(s) in the full text of my thesis.

Date 25/7/24 Signature of candidate

Supervisor's declaration

I hereby certify that the candidate has fulfilled the conditions of the Resolution and Regulations appropriate for the degree of PhD in the University of St Andrews and that the candidate is qualified to submit this thesis in application for that degree. I confirm that any appendices included in the thesis contain only material permitted by the 'Assessment of Postgraduate Research Students' policy.

Date 25/7/2024 Signature of supervisor

(Jonathan Keeling)

(Chris Hooley)

Permission for publication

In submitting this thesis to the University of St Andrews we understand that we are giving permission for it to be made available for use in accordance with the regulations of the University Library for the time being in force, subject to any copyright vested in the work not being affected thereby. We also understand, unless exempt by an award of an embargo as requested below, that the title and the abstract will be published, and that a copy of the work may be made and supplied to any bona fide library or research worker, that this thesis will be electronically accessible for personal or research use and that the library has the right to migrate this thesis into new electronic forms as required to ensure continued 2 5 us access to the thesis.

I, Francisco Zuniga Frias, confirm that my thesis does not contain any third-party material that requires copyright clearance.

The following is an agreed request by candidate and supervisor regarding the publication of this thesis:

Printed copy

No embargo on print copy.

Electronic copy

No embargo on electronic copy.

Date 25/7/24 Signature of candidate

Date 25/7/2024 Signature of supervisor

(Jonathan Keeling)

(Chris Hooley)

Underpinning Research Data or Digital Outputs

Candidate's declaration

I, Francisco Zuniga Frias, hereby certify that no requirements to deposit original research data or digital outputs apply to this thesis and that, where appropriate, secondary data used have been referenced in the full text of my thesis.

Date 25/7/24 Signature of candidate

Abstract

This thesis investigates two distinct classes of gapless, strongly correlated quantum systems. In the first part of this thesis, we examine quantum spin-1 systems, which allow for non-geometric frustration between bilinear and biquadratic interactions. For these systems, frustration leads to a rich phase diagram hosting exotic spin nematic phases with highly entangled ground states near SU (3)-symmetric points. We use tensor network renormalisation group methods to study the phase diagram of the spin-1 bilinear biquadratic Heisenberg model with focus on the phase transitions near SU (3)-symmetric points. Tensor network renormalisation methods are helpful in the study of both non-critical and critical phases and give insight to new mechanisms of spin-nematic phases and exotic ground states. In the second part of this thesis, we study non-Fermi liquids, characterised by the absence of quasiparticles and unusual symmetries. Based on the recent assumption that non-Fermi liquids have an emergent loop-U(1) group at the IR, we show the essential tools to quantise a loop-U(1) group. Using coadjoint orbits and their quantisation as the technology of choice, we propose a modest approach that might be helpful in the more profound problem of understanding the phenomenology of non-Fermi liquids.

Contents

Aknoledgements

I am deeply grateful to my supervisor, Professor Chris Hooley, whose guidance and support were instrumental in the completion of this thesis. His wide interests and deep knowledge of physics ignited my own and provided the foundation for this work. Collaborating with Chris has been both inspiring and intellectually stimulating, with an infectious enthusiasm for physics coupled with his rigorous critical thinking. I am particularly grateful to his ability to balance a clear direction while at the same time granting me the autonomy to explore my own ideas. His mentorship has been invaluable, shaping me as both a researcher and an individual. I would also like to thank Jonathan Keeling for all his very valuable academic advice. I would like to thank the professional community of St. Andrews which was a very insightful and enriching one. Finally I would like to thank my parents my brother and Alba for their love and support.

I would like to acknowledge FIDERH for financial support through the contract 1911110830.

Introduction

This thesis focuses on two primary areas: higher-spin insulators and quantum critical metals. These represent opposing ends of a broader spectrum within the realm of strongly correlated gapless systems. Strong correlations underpin a wide array of fascinating physical phenomena. Our specific interest lies in spin-1 systems at critical points and non-Fermi liquids.

Historically, these two areas share a common origin in the Hubbard model. This model, a fundamental tool in the study of strongly correlated systems, describes both insulating and metallic behaviour. At half-filling with strong on-site repulsion ($U \gg t$), the Hubbard model becomes an insulator with localised electrons possessing only spin degrees of freedom, leading to the Heisenberg model—the first part of this thesis explores a generalisation of the original Heisenberg model for spin-1 by adding a biquadratic term. In contrast, the weak coupling limit ($U \ll t$) yields a metallic state described by itinerant electrons. While Fermi liquid theory provides a qualitative framework for this metallic regime, the emergence of non-Fermi liquid behaviour near quantum critical points, characterised by anomalous properties such as linear-in-temperature resistivity and the absence of quasiparticles, challenges this conventional picture.

Higher-spin systems, particularly spin-1 systems, offer a unique opportunity to explore enhanced symmetries and novel phases of matter near critical points. In contrast to spin-1/2 systems, spin-1 systems can exhibit SU(3) symmetry, potentially leading to exotic spin liquid behaviour not possible in spin-1/2 systems. Non-Fermi liquids raise questions on possible uncommon renormalisation group flows and effective field theories where our best theories break down.

Both higher-spin insulators and quantum critical metals arise from strong correlations, providing fertile ground for the emergence of intriguing and unconventional phenomena.

Plan of the thesis

Spin-1 Systems

In Chapter 1 we introduce the basic notions of spin-1 systems, such as quadrupolar orders, the emergent SU(3) symmetry and its most useful representations. We describe quadrupolar states and compare them to spin coherent states. In Chapter 2.1, we introduce the basic background of phases of matter and tensor networks. Specific emphasis is made on the tensor renormalisation group methods which will be used in further chapters. Chapter 3 starts by setting the background of spin-1

chains, where the existence of a controversial critical nematic phase exists near an SU(3) critical point. We use tensor network renormalisation group methods to study this systems directly at criticality. Chapter 4 studies the analogous spin-1 systems but in 2D square lattices. We study the controversial Haldane phase residing near a critical SU(3) point. Again we propose a method for isotropising the tensor network and then renormalising it.

Non-Fermi liquids

This part introduces both Fermi liquids and non-Fermi liquids. The aim of this part of the thesis is to propose a way to quantise via the orbit method a conjectured loop-U(1) symmetry in the infrared in non-Fermi liquids. Chapter 5.1 introduces a relatively up-to-date revision of Fermi-liquid theory and it's main advances in the last decades, mostly focusing on renormalisation group methods. In Chapter **??** we introduce the abstract mathematical machinery of the orbit method, together with notions of general notions on how to obtain relevant information using symmetry arguments and making connections between representation theory and geometry. Chapter 8 is the formal proposition on how to quantise loop-U(1) groups using the orbit method or more general quantisation schemes and how to extract information relevant to the non-Fermi liquid phenomenology.

Part I

Spin-1 systems

The concept of matter organising into different phases is both familiar and profound. It might organise into ordinary liquids or conductors, as well as exotic states like quantum spin liquids or strange metals. The latter, however, are many-body phases of matter that lack successful theoretical explanations and often do not conform to classical notions of order parameters. Classical phase transitions involve a symmetric disordered phase transforming into an ordered phase that breaks symmetry, defined by local order parameters. However, some phases, such as topologically ordered phases, are not locally distinguishable and still undergo phase transitions. Quantum magnetism also offers numerous examples where strongly correlated systems exhibit non-classical phase transitions.

In this first part, our focus is on many-body spin-1 systems with emphasis on strongly interacting systems that cannot be reduced to effective one-particle systems. While one-particle systems approximate some real systems well, many strongly correlated materials lack an accurate free theory. In spin systems, strong interactions reveal the underlying quantum mechanics on large scales. Spin systems, central to much condensed matter theory, require advanced theoretical methods like renormalization groups, tensor networks, generalised symmetries, anomalies, among many more.

Spin-1 systems are quantum magnetic systems that, unlike classical magnets where magnetic order arises from dipolar interactions, exhibit a different type of magnetism. While dipolar interactions in classical magnets are more akin to a liquid crystallisation driven by thermal fluctuations, magnetic interactions in spin-1 systems are governed by quantum fluctuations. These fluctuations can be amplified by factors such as frustration and dimensionality. They can disrupt the magnetic order, leading to entirely new quantum states known as spin liquids. In lower dimensions, quantum fluctuations become more pronounced, potentially reducing or eliminating the ordering of a phase that would be stable in classical physics. For example, frustrated interactions—beyond just geometric ones—can contribute to this behaviour.

Spin-1 systems have been extensively studied [1, 77, 94, 58, 24] due to their potential to exhibit quantum phases with unique characteristics such as the Haldane phase [48], the anomalous magnetic and nematic ordering in iron superconductors [131], and various quantum spin liquid phenomena related to higher spins [70, 42, 82]. Experimental observations of spin liquids in spin-1 materials have been reported as well in [91, 20], including those with triangular and honeycomb antiferromagnets.

A significant challenge remains in that both larger spins exhibit reduced quantum fluctuations, and geometric frustration alone is insufficient to disrupt conventional magnetic order. This indicates that multiple forms of frustration may be necessary to stabilise novel quantum phases, making this somewhat intriguing area for further research. In spin-1 systems, the inclusion of biquadratic interactions alongside bilinear ones introduces another form of frustration, particularly when these interactions have comparable strengths, resulting in an enhanced symmetry. This leads to degeneracy of magnetic and non-magnetic orders, potentially giving rise to new phases. A central question would be if SU(3) symmetry enables spin liquid phenomena. Thus far, evidence for spin liquid phases in these systems is scarce, and research incorporating SU(3) symmetry has predominantly yielded

conventional ordered states. Nonetheless, the precise nature of phases near the SU(3) points within the bilinear-biquadratic model remains an open question in both one and two dimensions.

The first part of this thesis is organised as follows. The first chapter introduces the formalism for studying quadrupoles, along with the notation and general aspects of spin systems. The focus will then shift to the quadrupolar character of spin-1 wave functions, comparing quadrupolar states of spin-1 with spin coherent states of spin-1/2. Next, we explore the bilinear biquadratic Hamiltonian, a model that includes quadrupolar interactions as well as the typical interactions in spin systems. The subsequent chapters examine spin-1 chains using tensor renormalisation group methods around the controversial SU(3) points where a critical nematic phase remains controversial. The next chapter studies spin-1 systems on square lattices, again with the use of tensor network methods again near the critical SU(3) points where a Haldane phase is controversial.

Chapter 1

Spin-1 Systems

1.1 General aspects of spin-1 systems

This section shows general aspects of spin-1 systems, in particular, that a spin-1 wave function has quadrupoles, which are obtained through quadratic operators in the typical spin operators. Consequently, we may describe a state that has no magnetic moment that preserves time reversal invariance. After showing how to parametrise these states, we will see how an $SU(3)$ symmetry arises naturally and describe some useful representations. One of the most useful tools to study spin-1 lattices is the bilinear biquadratic model. After discussing its fundamental properties, we will explain different ansätze to make it more manageable. Finally we will comment on general ideas and conjectures that may appear in spin-1 many-body systems.

An efficient description of quadrupoles uses the following standard basis [73]

$$\begin{aligned} |x\rangle &= \frac{i}{\sqrt{2}}(|1\rangle - |\bar{1}\rangle), \\ |y\rangle &= \frac{1}{\sqrt{2}}(|1\rangle + |\bar{1}\rangle), \\ |z\rangle &= -i|0\rangle. \end{aligned} \tag{1.1}$$

By fixing a phase we can now characterise a wavefunction using four parameters, $\{\theta, \phi\} \in [0, \pi/2]$ and $\{\alpha, \beta\} \in [0, 2\pi)$, as follows

$$|\psi\rangle = e^{i\alpha} \sin\theta \cos\phi |x\rangle + e^{i\beta} \sin\theta \sin\phi |y\rangle + \cos\theta |z\rangle. \tag{1.2}$$

In this basis, the time-reversal operator $\mathcal{T}$ leaves (1.2) invariant since it interchanges $|\bar{1}\rangle$ for $|1\rangle$, it also flips the sign of $|0\rangle$, and it complex conjugates the amplitudes:

$$\begin{aligned} \mathcal{T}|x\rangle &= \frac{-i}{\sqrt{2}}(|\bar{1}\rangle - |1\rangle) = \frac{i}{\sqrt{2}}(|1\rangle - |\bar{1}\rangle) = |x\rangle \\ \mathcal{T}|y\rangle &= \frac{1}{\sqrt{2}}(|1\rangle + |\bar{1}\rangle) = |y\rangle \\ \mathcal{T}|z\rangle &= -(-i)(-|0\rangle) = |z\rangle. \end{aligned} \tag{1.3}$$

We can write the action of the spin operators on this basis as follows

$$S^a|b\rangle = i\sum_{c=x,y,z}\varepsilon_{abc}|c\rangle. \tag{1.4}$$

and thus

$$S^a|a\rangle = 0, \quad a = x, y, z. \tag{1.5}$$

In general, any self-adjoint operator $\hat{X}$ may be expressed as $\hat{X} = \sum_{\alpha,\beta=1}^{3} M_{\alpha\beta}|\alpha\rangle\langle\beta|$ where $\{|\alpha\rangle\}$ is a basis and $M^*_{\alpha\beta} = M_{\beta a}$. We can parametrise this three-dimensional self-adjoint matrix with nine real parameters, three of these are the S^α components, and five non-trivial components will have the spin operators to quadratic orders. Now following the typical construction, the components of a rank-l operator $O^{(l)}$ satisfy the following commutation relations

$$\begin{aligned}\left[S^z, O^{(l)}_q\right] &= qO^{(l)}_q,\\ \left[S^\pm, O^{(l)}_q\right] &= \sqrt{(l(l+1)-q(q\pm1))}O^{(l)}_{q\pm1}\end{aligned} \tag{1.6}$$

giving a total of $2l+1$ components for all q in $[-l, l]$. The $l = 1$ case gives

$$\begin{aligned}\left[S^z, O^{(1)}_{\pm1}\right] &= \pm O^{(1)}_{\pm1},\\ \left[S^z, O^{(1)}_0\right] &= 0,\end{aligned} \tag{1.7}$$

thus obtaining the ladder operators and S^z, respectively, while for $l = 2$ we get

$$\begin{aligned} O^{(2)}_{-2} &= S^-S^-, & O^{(2)}_{-1} &= \left\{S^-, S^z\right\},\\ O^{(2)}_0 &= \sqrt{6}(S^z)^2 - \sqrt{\frac{2}{3}}S(S+1), & O^{(2)}_1 &= -\left\{S^+, S^z\right\},\\ O^{(2)}_2 &= S^+S^+. \end{aligned} \tag{1.8}$$

Therefore obtaining a trace, which is the trivial scalar form, a rank-1 tensor with the three spin antisymmetric components (1.7), and a rank-2 tensor (1.8) which is a symmetric and traceless tensor which we can write as $Q^{\alpha\beta} = S^\alpha S^\beta + S^\beta S^\alpha - \frac{2}{3}S(S+1)\delta_{\alpha\beta}$ and composed of the above five independent components. The latter can be writen in a convenient way by taking the appropriate linear combinations of (1.8) as follows [73]

$$\mathbf{Q} = \begin{pmatrix} Q^{xy}\\ Q^{yz}\\ Q^{xz}\\ Q^{x^2-y^2}\\ Q^{3z^2-s^2}\end{pmatrix} = \begin{pmatrix} \{S^x, S^y\}\\ \{S^y, S^z\}\\ \{S^x, S^z\}\\ (S^x)^2 - (S^y)^2\\ -\frac{1}{\sqrt{3}}\left((S^x)^2 + (S^y)^2 - 2(S^z)^2\right)\end{pmatrix} \tag{1.9}$$

with $\{\ ,\ \}$ an anticommutator and where now each component is a quadrupolar order parameter. Therefore, in addition to spin ordering, a system of spin-1

particles inherently exhibits the potential for quadrupolar order. Furthermore, the interplay between the two order parameters $\mathbf{S}$ and $\mathbf{Q}$, for any spin-1 wavefunction, is $\langle\mathbf{S}\rangle^2 + \langle\mathbf{Q}\rangle^2 = \frac{16}{3}$ and the anticommutators give a hint to why the algebra is interesting.

Now, $|S, S^z\rangle$ is an eigenstate of $\mathbf{Q}^2$

$$\mathbf{Q}^2 |S, S^z\rangle = \left(\frac{4}{3}S^2(S+1)^2 - 1\right) |S, S^z\rangle , \tag{1.10}$$

and consequently

$$\left(\mathbf{Q}^2 + \mathbf{S}^2\right) |S, S^z\rangle = \frac{4}{3}S^2(S+1)^2 |S, S^z\rangle , \tag{1.11}$$

we may therefore view $\langle\mathbf{S}\rangle^2 + \langle\mathbf{Q}\rangle^2$ as a constraint for the possible local order parameters.

The Lie group SU(3) is the group of 3×3 unitary matrices with determinant one. The elements of this group may be obtained in the typical way: given a traceless, hermitian matrix A, we exponentiate iA. By applying the algorithm presented in Appendix A for $N = 3$, we obtain the well-known generators

$$\begin{aligned}
\lambda_1 &= \begin{pmatrix} 0 & 1 & 0 \\ 1 & 0 & 0 \\ 0 & 0 & 0 \end{pmatrix} \quad \lambda_2 = \begin{pmatrix} 0 & -i & 0 \\ i & 0 & 0 \\ 0 & 0 & 0 \end{pmatrix} \quad \lambda_3 = \begin{pmatrix} 1 & 0 & 0 \\ 0 & -1 & 0 \\ 0 & 0 & 0 \end{pmatrix} \\
\lambda_4 &= \begin{pmatrix} 0 & 0 & 1 \\ 0 & 0 & 0 \\ 1 & 0 & 0 \end{pmatrix} \quad \lambda_5 = \begin{pmatrix} 0 & 0 & -i \\ 0 & 0 & 0 \\ i & 0 & 0 \end{pmatrix} \\
\lambda_6 &= \begin{pmatrix} 0 & 0 & 0 \\ 0 & 0 & 1 \\ 0 & 1 & 0 \end{pmatrix} \quad \lambda_7 = \begin{pmatrix} 0 & 0 & 0 \\ 0 & 0 & -i \\ 0 & i & 0 \end{pmatrix} \quad \lambda_8 = \tfrac{1}{\sqrt{3}} \begin{pmatrix} 1 & 0 & 0 \\ 0 & 1 & 0 \\ 0 & 0 & -2 \end{pmatrix} .
\end{aligned} \tag{1.12}$$

The first three matrices are a clear embedding of an $SU(2)$ subalgebra, meaning they are Pauli matrices with added zero rows and columns. The third and eighth matrices are diagonal and when combined appropriately, i.e., $\frac{\sqrt{3}}{2}\lambda_8 - \frac{1}{2}\lambda_3$ and $\frac{\sqrt{3}}{2}\lambda_8 + \frac{1}{2}\lambda_3$ we obtain σ_3 for two sectors different than the one in λ_3. We thus obtain three different embeddings of $\mathfrak{su}(2)$ subalgebras. These three interrelated subalgebras make the $\mathfrak{su}(3)$ non-trivial.

Bosonic representation

This is a useful representation where we can see how the $SU(3)$ symmetry is related to quadrupolar degrees of freedom. The bosonic representation of $SU(3)$ is constructed by defining the generators via bosonic annihilation and creation operators, obeying

$$[a_i, a_j^\dagger] = \delta_{ij}, \quad [a_i, a_j] = 0; \quad i = 1, 2, 3. \tag{1.13}$$

We define the operator

$$Q_\alpha = \frac{1}{2}\hat{a}^\dagger \lambda_\alpha \hat{a}, \quad \alpha = 1, \dots 8, \tag{1.14}$$

where λ are the Gell-Mann matrices (1.12) and $\hat{a}^\dagger = \left(a_1^\dagger, a_2^\dagger, a_3^\dagger\right)$ thus

$$[\lambda_\alpha, \lambda_\beta] = 2i f_{\alpha\beta\gamma}\lambda_\gamma, \quad \alpha, \beta, \gamma = 1, 2, \dots 8 \tag{1.15}$$

with structure constants $f_{\alpha\beta\gamma}$. We can work with the Q_α operators and show that they obey the following

$$\begin{aligned}[Q_\alpha, Q_\beta] =& \frac{1}{4} a_i{}^\dagger a_j a_k{}^\dagger a_l \left(\lambda_{\alpha,ij}\lambda_{\beta,kl} - \lambda_{\beta,ij}\lambda_{\alpha,kl}\right) \\ =& i f_{\alpha\beta\gamma} Q_\gamma.\end{aligned} \tag{1.16}$$

thus, they obey an $\mathfrak{su}(3)$ algebra (1.15).

The constraint $\left[Q_\alpha, \hat{N}\right] = 0$ with $\hat{N} = \hat{a}^\dagger \hat{a}$, is fixing the number of bosons. Thus all representations of the group are obtained and they are in bijection with the integers. Now, the states $|n_1, n_2, n_3\rangle$ form a basis of occupation numbers satisfying

$$n_1 + n_2 + n_3 = N \tag{1.17}$$

where N is the number of bosons, and $|n_1, n_2, n_3\rangle$ is an eigenstate of $Q_\alpha Q_\alpha$ with eigenvalue $\frac{N}{3}(N+3)$.

In this representation a single spin-1, with $N = 1$, is thus

$$\mathbf{S} = \begin{pmatrix} S^x \\ S^y \\ S^z \end{pmatrix} = \begin{pmatrix} 2Q_5 \\ -2Q_7 \\ -2Q_2 \end{pmatrix}. \tag{1.18}$$

and

$$\mathbf{Q} = \begin{pmatrix} Q^{xy} \\ Q^{yz} \\ Q^{xz} \\ Q^{x^2-y^2} \\ Q^{3z^2-r^2} \end{pmatrix} = \begin{pmatrix} -2Q_1 \\ -2Q_4 \\ -2Q_6 \\ 2Q_3 \\ 2Q_8 \end{pmatrix}. \tag{1.19}$$

It is not too hard to see that

$$\left(\mathbf{Q}^2 + \mathbf{S}^2\right) = 4 Q_\alpha Q_\alpha \tag{1.20}$$

and also that $Q_\alpha Q_\alpha = \frac{N}{3}(N+3)\,|n_1, n_2, n_3\rangle$, and $\mathbf{S}^2\,|n_1, n_2, n_3\rangle = 2\,|n_1, n_2, n_3\rangle$. Also, it is straightforward to see that (1.18) and (1.19) satisfy (1.10) and (1.11).

Given an appropriate basis in which they are represented, both the operators are

$$\mathbf{S} = \begin{pmatrix} i[a_z^\dagger, a_y] \\ i[a_x^\dagger, a_z] \\ i[a_y^\dagger, a_x] \end{pmatrix} \tag{1.21}$$

and

$$\mathbf{Q} = \begin{pmatrix} -\left\{a_x^\dagger, a_y\right\} \\ -\left\{a_y^\dagger, a_z\right\} \\ -\left\{a_x^\dagger, a_z\right\} \\ a_y^\dagger a_y - a_x^\dagger a_x \\ \frac{1}{\sqrt{3}}\left(a_x^\dagger a_x + a_y^\dagger a_y - 2a_z^\dagger a_z\right) \end{pmatrix} \tag{1.22}$$

for the spin part and the quadrupolar part, respectively. The generalised Gell-Mann matrices for $N = 2$ produce the Pauli matrices and the method described above automatically produces an analogue of Schwinger bosons. Thus, for $N = 2$

$$S^\alpha = \frac{1}{2}\hat{a}^\dagger \lambda^\alpha \hat{a}, \quad \alpha = 1, 2, 3, \tag{1.23}$$

but now λ^α satisfy an $\mathfrak{su}2$ algebra, i.e. they are the Pauli matrices satisfying

$$\left[\lambda^\alpha, \lambda^\beta\right] = 2i\varepsilon_{\alpha\beta\gamma}\lambda^\gamma, \quad \alpha, \beta, \gamma = 1, 2, 3. \tag{1.24}$$

Finally, for the general SU(N) case, the above procedure is also applicable. In particular one can obtain all the generators of the $\mathfrak{su}$(N) Lie algebra, this is done in the same way by using the the generalised Gell-Mann matrices.

Quadrupolar states

A spin coherent state $|\mathbf{\Omega}\rangle$ is a maximally polarised state i.e., $\left(\langle\mathbf{\Omega}|\mathbf{S}|\mathbf{\Omega}\rangle\right)^2 = 1$ for a spin-1. It is parametrised by the unit vector $\mathbf{\Omega} = (\sin\theta\cos\theta, \sin\theta\sin\phi, \cos\theta)$ with polar angles $\{\theta, \phi\}$. Two important facts are that $|\mathbf{\Omega}\rangle$ is describing a spin parallel to $\mathbf{\Omega}$ [4]:

$$\langle\mathbf{\Omega}|\mathbf{S}|\mathbf{\Omega}\rangle = S\mathbf{\Omega} \tag{1.25}$$

with $\theta \in [0, \pi]$ and $\phi \in [0, 2\pi)$. Additionally, $|\mathbf{\Omega}\rangle$ satisfies the following

$$(\mathbf{\Omega}\cdot\mathbf{S})|\mathbf{\Omega}\rangle = S|\mathbf{\Omega}\rangle. \tag{1.26}$$

i.e., the state $|\mathbf{\Omega}\rangle$ is an eigenstate of the spin component that points in the direction of $\mathbf{\Omega}$.

Using the general formula [4]

$$|\mathbf{\Omega}\rangle = \sqrt{(2S)!}\sum_m \frac{u^{S+m}v^{S-m}}{\sqrt{(S+m)!(S-m)!}}|S, m\rangle \tag{1.27}$$

with $u = \cos\frac{\theta}{2}e^{-i\phi/2}$ and $v = \sin\frac{\theta}{2}e^{i\phi/2}$. One gets, for spin-1, the following:

$$|\mathbf{\Omega}\rangle = \frac{1+\cos\theta}{2}e^{-i\phi}|1\rangle + \frac{\sin\theta}{\sqrt{2}}|0\rangle + \frac{1-\cos\theta}{2}e^{i\phi}|\bar{1}\rangle.$$

Provided with a Haar integration measure $\frac{2S+1}{4\pi}d\hat{\mathbf{\Omega}} = \frac{2S+1}{4\pi}d\theta\sin\theta d\phi$, we can build the resolution of identity

$$\hat{I} = \frac{3}{4\pi}\int_{\theta=0}^{\pi}\int_{\phi=0}^{2\pi}\mathrm{d}\theta\mathrm{d}\phi\sin\theta|\mathbf{\Omega}\rangle\langle\mathbf{\Omega}|.$$

Applying $\hat{I}$ to an arbitrary spin-1 state $|\psi\rangle$ gives

$$|\psi\rangle = \hat{I}|\psi\rangle = \frac{3}{4\pi}\int_{\theta=0}^{\pi}\int_{\phi=0}^{2\pi}\mathrm{d}\theta\mathrm{d}\phi\sin\theta\langle\mathbf{\Omega}|\psi\rangle|\mathbf{\Omega}\rangle, \tag{1.28}$$

which expresses $|\psi\rangle$ in a spin coherent representation, which is an overcomplete basis.

The director, $|\mathbf{d}\rangle$, denotes a quadrupolar state if $(\langle\mathbf{d}|\mathbf{S}|\mathbf{d}\rangle)^2 = 0$. Spin fluctuations are perpendicular to $|\mathbf{d}\rangle$ and quadrupoles are parametrised, again, by a unit vector $\mathbf{d} = (\sin\theta\cos\phi, \sin\theta\sin\phi, \cos\theta)$; using (1.3) as follows [73]

$$|\mathbf{d}\rangle = \sum_{\alpha=x,y,z} d_\alpha|\alpha\rangle, \tag{1.29}$$

This shows that these states, characterised by $\mathbf{d}$ and $-\mathbf{d}$, are physically equivalent and now it should be obvious that $|\mathbf{d}\rangle$ is an eigenstate of of the spin component $(\mathbf{d}\cdot\mathbf{S})|\mathbf{d}\rangle = 0$.

As a remark, recall that it is not possible to have time-invariance for spin-1/2, due to Kramer's theorem. This generalises to any non integer spin $S = n/2$. However, as an example notice how a spin-3/2 state with zero spin length can be written as

$$|O\rangle = \frac{1}{\sqrt{2}}\left(\left|\frac{3}{2}\right\rangle + \left|-\frac{3}{2}\right\rangle\right). \tag{1.30}$$

This state $|O\rangle$ is neither a dipole nor a quadrupole, indicating an octupolar character.

Now we turn to the question of parametrisation. A general spin-1 state exhibits both spin and quadrupolar characteristics, and its physically relevant properties are determined by four independent real parameters (1.2). While various methods can be used to characterise spin-1 wavefunctions, a suitable parametrisation involves a pair of three-dimensional vectors. We express a general spin-1 state $|\psi\rangle$ as

$$|\psi\rangle = \sum_{\alpha=x,y,z}(u_\alpha + iv_\alpha)|\alpha\rangle \tag{1.31}$$

where the vectors satisfy a normalisation condition

$$\mathbf{u}^2 + \mathbf{v}^2 = 1 \tag{1.32}$$

and if one fixes a phase then

$$\mathbf{u} \cdot \mathbf{v} = 0. \tag{1.33}$$

Now the expectation value of an arbitrary state is given by the cross product

$$\langle\psi|\mathbf{S}|\psi\rangle = 2\mathbf{u} \times \mathbf{v}, \tag{1.34}$$

with length

$$\left(\langle\psi|\mathbf{S}|\psi\rangle\right)^2 = 4\mathbf{u}^2\mathbf{v}^2. \tag{1.35}$$

For spin coherent states both $\mathbf{u}^2$ and $\mathbf{v}^2$ equal 1/2. On the other hand, for quadrupoles, only one of them will be zero, while the other, non-zero vector, will be the director. For $0 < \left(\langle\psi|\mathbf{S}|\psi\rangle\right)^2 < 1$, the larger vector can be called the director. This will be clarified in the next paragraph.

Assume a normalised spin-1 state can be written as in (1.31) with conditions (1.32) and (1.33) satisfied. We explore which $\{\mathbf{u}, \mathbf{v}\}$ pairs are equivalent under a phase transformation. A restricted phase transformation of the state $|\psi\rangle$ gives:

$$|\psi'\rangle = e^{i\gamma}|\psi\rangle$$

with new vectors $\mathbf{u}'$ and $\mathbf{v}'$ satisfying (1.32) and (1.33)

$$\begin{pmatrix} \mathbf{u}' \\ \mathbf{v}' \end{pmatrix} = \begin{pmatrix} \cos\gamma & -\sin\gamma \\ \sin\gamma & \cos\gamma \end{pmatrix} \begin{pmatrix} \mathbf{u} \\ \mathbf{v} \end{pmatrix} \tag{1.36}$$

then, their scalar product becomes

$$\mathbf{u}' \cdot \mathbf{v}' = \cos^2\gamma\ \mathbf{u} \cdot \mathbf{v} - \sin^2\gamma\ \mathbf{u} \cdot \mathbf{v} + \frac{\sin 2\gamma}{2}\left(\mathbf{u}^2 - \mathbf{v}^2\right), \tag{1.37}$$

which leads to $\sin\gamma\cos\gamma\left(\mathbf{u}^2 - \mathbf{v}^2\right) = 0$. Now, If $\mathbf{u}^2 = \mathbf{v}^2$, correspond to simultaneous rotations of both vectors around an axis with length$\sqrt{1/2}$. If $\mathbf{u}^2 \neq \mathbf{v}^2$, γ takes only some specific values: $\gamma = 0$ (identity), $\gamma = \pi$ (opposite vectors), and $\gamma = \pi/2,\ -\pi/2$ (opposite of one vector and changing order). We can choose $\{\mathbf{u}, \mathbf{v}\}$ so that $\mathbf{v}^2 < \mathbf{u}^2$ and in this case we can use $\mathbf{u}$ as the director (recall that spin coherent states lack a director).

To prove this, consider a normalised spin-1 wavefunction with $\{\mathbf{u}, \mathbf{v}\}$ satisfying (1.32) but not (1.33). A phase transformation will produce a state $|\psi'\rangle$ with vectors satisfying both conditions. These vectors $\mathbf{u}'$ and $\mathbf{v}'$ satisfy (1.32) and their scalar product vanishes if:

$$\left(\cos^2\gamma - \sin^2\gamma\right)\mathbf{u} \cdot \mathbf{v} + \frac{\sin 2\gamma}{2}\left(\mathbf{u}^2 - \mathbf{v}^2\right) = 0. \tag{1.38}$$

When $\mathbf{u}^2 \neq \mathbf{v}^2$, then the angle is defined by:

$$\frac{\sin 2\gamma}{\cos 2\gamma} = \frac{2\mathbf{u}\cdot\mathbf{v}}{\mathbf{v}^2 - \mathbf{u}^2}, \tag{1.39}$$

with $\gamma \in (-\pi/4, \pi/4)$. Outside this interval, the choices correspond to equivalent sets of $\{\mathbf{u}', \mathbf{v}'\}$. If $\mathbf{u}^2 = \mathbf{v}^2$, one may choose $\gamma = \pi/4$.

This parametrisation distinguishes between wavefunctions with the same $\langle \mathbf{S} \rangle$ and less than full spin. The director $\mathbf{u}$ lies perpendicular to $\mathbf{S}$, and its length is determined by:

$$\mathbf{u}^2 = \frac{1}{2}\left(1 + \sqrt{1 - \left(\langle\psi|\mathbf{S}|\psi\rangle\right)^2}\right). \tag{1.40}$$

The director rotates freely in this plane, leading to different quadrupole moments, with configurations related by a π rotation being equivalent.

Biquadratic Interaction

We start with the fundamental formula:

$$O^{(m)} \otimes O^{(n)} = \bigoplus_{j=|m-n|}^{m+n} O^{(j)}, \tag{1.41}$$

where $O^{(j)}$ are irreducible representations of SU(2) parametrised by j. For spin-1 particles, if $m = 1$ and $n = 1$, the above expands into $O^{(0)} \oplus O^{(1)} \oplus O^{(2)}$, indicating possible singlet, triplet, and quintuplet states.

Applying (1.41) iteratively categorises operators in the Hilbert space:

$$(O^{(1)}) \otimes (O^{(1)}) = 3O^{(0)} \oplus 6O^{(1)} \oplus 6O^{(2)} \oplus 3O^{(3)} \oplus O^{(4)}, \tag{1.42}$$

yielding the following operators: three scalars, six dipoles, six quadrupoles, three octupoles, and one hexadecupole.

Contrasting this with spin-half particles, where $\mathbf{S}_1 \cdot \mathbf{S}_2$, $\mathbf{S}_1 \pm \mathbf{S}_2$, $\mathbf{S}_1 \times \mathbf{S}_2$, and a quadrupolar operator suffice. Formula (1.42) shows that there are three scalar operators of which two are non-trivial. To find a general SU(2) invariant Hamiltonian for spin-1, we need to rely on these scalar operators, which can be built either from spin operators or quadrupolar ones, i.e., the Hamiltonian should depend on the scalar product of $\mathbf{S}_1 \cdot \mathbf{S}_2$ and of $\mathbf{Q}_1 \cdot \mathbf{Q}_2$. The familiar bilinear-biquadratic takes the form

$$H = J\cos\theta\, \mathbf{S}_1 \cdot \mathbf{S}_2 + J\sin\theta (\mathbf{S}_1 \cdot \mathbf{S}_2)^2, \tag{1.43}$$

where the angle $\theta \in [0, 2\pi)$ sets the relative contributions between the bilinear and the biquadratic terms (and will be relevant in the next chapters when both terms are similar). This is because higher-order scalar products $\mathbf{S}_1 \cdot \mathbf{S}_2$ preserve the Hamiltonian form (1.43). A brief examination of (1.42), leads us to the fact that all independent scalar operators for spin-S pairs arise from on-site order parameter scalar products. This allows re-expressing $(\mathbf{S}_1 \cdot \mathbf{S}_2)^2$ in terms of $\mathbf{S}_1 \cdot \mathbf{S}_2$

and $\mathbf{Q}_1 \cdot \mathbf{Q}_2$ giving

$$\mathbf{Q}_1 \cdot \mathbf{Q}_2 = 2(\mathbf{S}_1 \cdot \mathbf{S}_2)^2 + \mathbf{S}_1 \cdot \mathbf{S}_2 - \frac{2}{3}S^2(S+1)^2. \tag{1.44}$$

which is the most elementary isotropic quadrupolar interaction. Substituting (1.44) into (1.43) we get

$$H = J\left(\cos\theta - \frac{\sin\theta}{2}\right)\mathbf{S}_1 \cdot \mathbf{S}_2 + J\frac{\sin\theta}{2}\mathbf{Q}_1 \cdot \mathbf{Q}_2 + \frac{J_2}{3}S^2(S+1)^2 \tag{1.45}$$

and setting spin length to one refines the bilinear-biquadratic Hamiltonian to

$$H = J\left(\cos\theta - \frac{\sin\theta}{2}\right)\mathbf{S}_1 \cdot \mathbf{S}_2 + J\frac{\sin\theta}{2}\mathbf{Q}_1 \cdot \mathbf{Q}_2 + J\frac{4\sin\theta}{3}. \tag{1.46}$$

Or in its general form

$$H = \sum_{\langle i,j \rangle} J\left(\cos\theta - \frac{\sin\theta}{2}\right)\mathbf{S}_i \cdot \mathbf{S}_j + J\frac{\sin\theta}{2}\mathbf{Q}_i \cdot \mathbf{Q}_j + \frac{J_2}{3}S^2(S+1)^2. \tag{1.47}$$

1.2 Introduction to Spin-1 chains and the Haldane phenomena

Quantum spin chains are one-dimensional arrays of interacting quantum spins, where each spin can be viewed as a quantum mechanical magnetic moment. These systems are described by Hamiltonians that dictate how spins interact with each other and with external fields. Understanding their behaviour is crucial for various applications in condensed matter physics, including magnetic materials and quantum information processing. Spin-1 chains, are interesting among other things because they harbour Haldane phenomena, in particular Haldane gaps and Haldane phases. Introduced in [48, 49] the existence of a gap in integer spin chains challenged conventional wisdom about the nature of quantum spin systems, particularly those with integer spin. Before Haldane's proposal, it was widely believed that one-dimensional spin chains with integer spins would behave similarly to those with half-integer spins, where gaps were absent or different in nature. This gap, arises due to the unique topological properties and quantum fluctuations inherent in integer spin systems. Theoretical investigations into the Haldane gap typically employ models such as the Heisenberg model and its variants. This idea has been confirmed numerically and mathematically through the AKLT model [1]. This was somehow unexpected and led to further discoveries like Haldane phases, which are a type of symmetry protected topological phase (SPT).

Central to understanding the Haldane gap is its relation to symmetries and topological phases in quantum spin systems. Integer spin chains possess internal symmetries that differ from those in half-integer spin chains, leading to distinct topological phases and ground state degeneracies. These symmetries are crucial for characterising the nature of the Haldane gap and its robustness against per-

turbations. Experimental verification of the Haldane gap has also been achieved in various magnetic materials and quantum systems. Techniques such as neutron scattering, NMR spectroscopy, and magnetisation measurements have provided evidence for the predicted gaps and ground state properties in real materials. These experiments corroborate theoretical predictions and highlight the relevance of the Haldane gap in practical applications. Numerical methods are a further way of verifying this affirmations, and several methods exist such as exact diagonalization and the density matrix renormalization group (DMRG), or more generally tensor networks. These simulations allow us to study finite-size effects, boundary conditions, and quantum phase transitions associated with the Haldane phase. Exact results from these simulations provide benchmarks for theoretical models and insights into the nature of the Haldane gap. Several works have studied higher-dimensional spin systems, spin liquids, and exotic quantum phases aim to deepen our understanding of quantum spin dynamics and topological orders. Moreover, interdisciplinary efforts in quantum information theory and materials science promise new applications and discoveries related to the Haldane gap.

We can discuss the general idea by Haldane by using the one-dimensional antiferromagnetic Heisenberg model for general spin of length N with periodic boundary conditions. The Hamiltonian is given by

$$H = \sum_{j=1}^{N} \boldsymbol{S}_j \cdot \boldsymbol{S}_{j+1}. \tag{1.48}$$

The Lieb-Mattis theorem [81] forces a unique ground state with total spin zero. The particular case of the spin-1/2 Heisenberg chain is well known for its exact solvability through the Bethe ansatz. Briefly, we know that this system has a unique ground state independent of system size, has gapless excitations, and has a power-law decay of correlations.

While the uniqueness of the ground state for finite systems is rigorously established by the Lieb-Mattis' theorem, its extension to infinite systems is closely related to the absence of long-range order. The gapless nature implies a continuum of excited states above the ground state in the thermodynamic limit, although a finite gap exists for finite systems and closes as the system size increases. The power-law decay of correlations, while strongly supported by numerical and analytical studies, remains a conjecture.

The ground state two-point correlation function is conjectured to exhibit the following asymptotic behaviour for large distances:

$$(-1)^{x-y} \frac{\sqrt{\log|x-y|}}{|x-y|}. \tag{1.49}$$

The dominant term, $(-1)^{x-y}/|x-y|$, reflects the antiferromagnetic correlations, while the logarithmic correction is a subtle effect. This power-law decay with logarithmic correction is reminiscent of critical phenomena, suggesting that the ground state of the $S = 1/2$ Heisenberg chain represents a quantum critical point.

From a quantum field theory perspective, the properties of a unique ground state, gapless excitations, and power-law correlations indicate a massless theory

without spontaneous symmetry breaking. This suggests that low-energy excitations can be described by a massless particle.

The exponential decay of correlations in the case of integer spin leads to the following asymptotic behaviour:

$$\frac{(-1)^{x-y}}{|x-y|^{1/2}} e^{-\frac{|x-y|}{\xi}}. \tag{1.50}$$

This rapid, exponentially decaying correlation function, is in strong contrast to the power-law behaviour of the half-integer spin chain. The existence of a finite energy gap and exponentially localised correlations clearly differentiates the integer spin Heisenberg chain from its half-integer counterpart, and established the Haldane gap as a fundamentally new phase of matter.

Haldane's prediction of this dramatic difference between integer and half-integer spin chains was a groundbreaking discovery that has stimulated extensive theoretical and experimental investigations in the field of quantum magnetism.

For length scales significantly larger than the correlation length, the correlation function exhibits the following asymptotic behaviour (1.50) The power-law factor of $|x-y|^{-1/2}$ is a common feature of one-dimensional disordered systems, while the exponential decay with characteristic length scale ξ is a signature of gapped systems. The overall behaviour resembles the Ornstein-Zernike form observed in classical two-dimensional systems above the critical temperature. This unexpected similarity between a ground state and a high-temperature state highlights the concept of "quantum disorder" induced by strong quantum fluctuations in the integer spin chain.

The gapped behaviour of the integer spin chain can be attributed to a massive field theory, where the energy gap corresponds to the mass of the particle. This interpretation is supported by the exponential decay of correlations, akin to the short-range interactions mediated by massive particles.

Haldane's seminal work established the qualitative difference between integer and half-integer spin chains through two complementary approaches. The first approach involved analysing quantisation conditions in a nonlinear sigma model, while the second focused on semiclassical quantisation of solitons. Both methods pointed to a critical, gapless phase for half-integer spins and a gapped, disordered phase for integer spins.

Chapter 2

Tensor networks

The quantum many-body problem is an overarching concept referring to the complexity of interactions among quantum particles. Systems from nearly every field in physics consist of numerous particles interacting under quantum mechanics sometimes resulting in exotic phenomena. Arguably, in many cases, this complexity is based on entanglement[1], meaning that the state of a many-particle system cannot be understood by examining individual particles. Information is distributed non-locally among particles, causing the number of possible states to grow exponentially with the number of particles, making it impossible to describe even an ungenerous number of particles.

On the bright side, many quantum systems like some spin chains or spin lattices have limited and structured entanglement near ground states, allowing for relatively efficient descriptions using specific quantum information methods. Roughly stated, quantum information involves understanding, describing, quantifying, and utilising entanglement. Techniques like tensor networks and quantum circuits enable representations of quantum systems that distribute this entanglement incrementally, extending traditional mean-field approaches that avoid entanglement. These representations express many-body quantum states compactly and allow direct analysis of their entanglement structure, crucial for understanding emergent phenomena.

Quantum phases of matter are the typical examples of entangled many-body systems. Here, entanglement is essential. Unlike conventional phases characterised by local order parameters and the conventional notions of symmetry, quantum phases are much more complicated for different reasons. For example topological orders have ground states with a long range entanglement structure. Thus classifying different phases becomes a problem of understanding the entanglement structure. Quantum computation is another example where entanglement is a resource. Again, entanglement becomes crucial, and it is here where the whole area of quantum advantage thrives.

The theory of quantum information and of quantum phases of matter have matured and evolved together in the past decades. Quantum phases of matter are practical and natural ways of storing and processing quantum information. A notable example is topological quantum computation, based on topologically

[1]Entanglement is not the only measure of complexity see [114] and other measures like magic or negativity can be measured with tensor networks [126]

ordered systems based on anyon physics or the connection between symmetry-protected topological phases and quantum circuits.

The concept of symmetry itself is undergoing a generalisation. We now have the notions of generalised symmetries, non-invertible symmetries, categorical symmetries, subsystem symmetries, among others. The relation between symmetries and the different quantum information methods are becoming clearer and clearer. Among others, this has come with a mathematical enrichment, for example, the use of category theory is a natural language for tensor networks and most of topological orders, critical phases, topological field theories, among others.

2.1 Tensor Networks

Tensor Networks (TNs) may be roughly defined as mathematical representations of quantum states of many-body systems. They are theoretical and computational technology that provide a natural language of the complexity of physical systems [98]. Today, the use of tensor networks is widespread in physics including their use in topological order [28, 43], topological field theory [63], holography [35], quantum gravity [22], gauge theory [115, 15, 23], quantum cellular automata [102] and conformal field theory [89] among many more. However, their most prevalent use is still in estimating ground states and excitation spectra of many-body systems. Rather than having some coefficients in a certain basis, a state is described by a network of tensors which depict the entanglement structure of a system. In that way we can speak of tensor network states as quantum states given in a specific entanglement representation. Furthermore, similar to Feynman diagrams, tensor networks have a useful and intuitive graphical representation as shown in Fig. 2.1.

In general, quantum Hamiltonians are difficult to simulate due to an exponentially large number of degrees of freedom. For example, it is of order 2^N for N spin-1/2 systems—while only $2N$ for classical spin systems. Therefore, the complete solution of (1.47) is a formidable problem and almost always intractable even for supercomputers. Formally, the complexity of both the Hubbard and the Heisenberg models is summarised by saying that they are QMA-complete problems (these represent the quantum extension to NP-complete problems in complexity theory) which are problems with very difficult solutions, but given a solution, it should be easy to verify that the solution is correct using a quantum computer [65, 12, 21]. However, in many calculations we don't need to explore the gigantic Hilbert space of states, we only need to explore a subset of physically relevant states exhibiting low entanglement or, in other words, satisfying an area law. This is where tensor networks shine: low-entanglement states can be well approximated by using tensor network methods, and the reason for them being ubiquitous is the fact that ground states satisfy area laws.

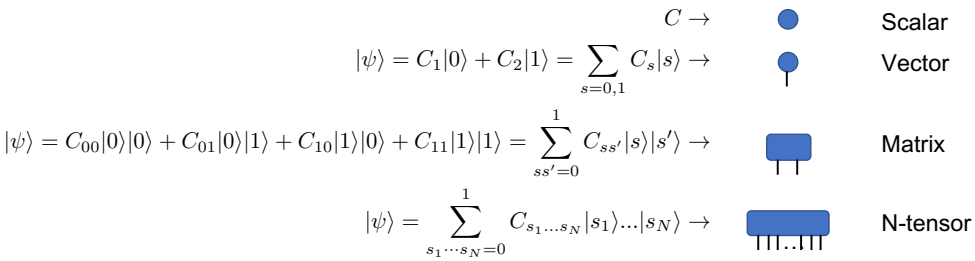

Figure 2.1: **Graphical representation of common mathematical objects.** Each amplitude C has a diagrammatic representation: A scalar C with no indices has a representation with no legs; a vector C_s has one index and a diagrammatic representation with one leg. In general an amplitude $C_{s_1,\ldots,s_N}$ is an N-index tensor represented by an N-leg diagram.

2.2 Matrix Product States (MPS)

Matrix product states [101, 109] are one-dimensional tensor networks and accurate representations of many-body ground states [122]. These states can be described as a quantum system with N sites which can be seen as identical subsystems in a finite Hilbert space of dimension d. Quantum states of the system are therefore defined by vectors in the Hilbert space $\mathcal{H}_N \equiv \mathbb{C}^d \otimes \cdots \otimes \mathbb{C}^d$. A basis of product states is defined by $|s\rangle = |s_1\rangle_d \otimes |s_2\rangle_d \cdots \otimes |s_N\rangle_d$, where $s_i = 1, \ldots, d$ is an orthonormal basis for $\mathbb{C}^d$. A state in this basis may be seen as

$$|\psi\rangle = \sum_{s_1 \cdots s_N} \underbrace{\psi_{s_1 \ldots s_N}}_{N-tensor} |s_1 \ldots s_N\rangle. \tag{2.1}$$

The MPS ansatz for this state reduces a problem with size growing exponentially as $\sim \exp N$ to a problem of polynomial size (see Fig. 2.2)

$$\underbrace{\psi_{s_1 \ldots s_N}}_{\exp(N)} \approx \underbrace{\tilde{\psi}_{s_1 \ldots s_N}}_{\text{poly}(N)} = \sum_{a_1, \ldots, a_{N-1}} A^{s_1}_{a_1} A^{s_2}_{a_1, a_2} \ldots A^{s_{N-1}}_{a_{N-2}, a_{N-1}} A^{s_N}_{a_{N-1}}. \tag{2.2}$$

In this last equation $\approx$ means that the exponentially large tensor is well approximated by a polynomially large one. Simplifying notation, we can rewrite the components $\langle s|\psi\rangle = \psi_s$. $|\psi\rangle$ is now regarded as a rank-N tensor with components ψ_s. Thus, an MPS is a tensor of the form

$$\psi_s = A^{s_1}_1 A^{s_2}_2 \cdots A^{s_N}_N = \tag{2.3}$$

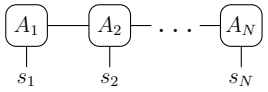

where each A has dimension $\chi \times \chi \times d$ where χ is the bond dimension and d the Hilbert space dimension. In graphical representation the squared norm of a state is

$$\langle \psi|\psi\rangle = \sum_s \bar{\psi}_s \psi_s = \tag{2.4}$$

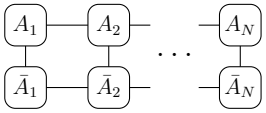

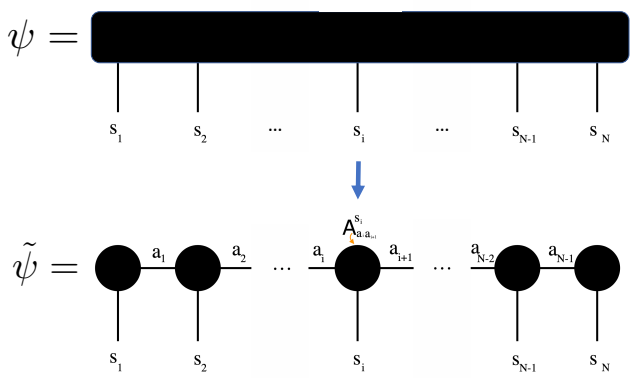

Figure 2.2: **Graphical representation of the MPS tensor network ansatz**.

From (2.3) we see that if each one of the A_i has bond dimension χ, we would still have χ^N coefficients, however these new coefficients are not independent anymore, rather they are related to each other by the contraction of the tensor network. In other words, we decomposed our big tensor ψ into tensors of smaller rank. While doing so, the tensor network is also giving a good approximation to the entanglement structure of the problem (which is a precise object related to entanglement entropy of the system), and the final tensor network state depends only on a polynomial number of parameters.

This is explained by the *Schmidt decomposition*—this is the formal step where the state is reduced to its final form—which relies on a singular value decomposition (SVD). Very generally we can divide our system into two subsystems A and B and describe a general pure state $|\psi\rangle = \sum_{ij} C_{ij}|i_A\rangle|j_B\rangle$, by its reduced density matrices

$$\hat{\rho}_A = \mathrm{Tr}_B|\psi\rangle\langle\psi| \qquad \hat{\rho}_B = \mathrm{Tr}_A|\psi\rangle\langle\psi| \tag{2.5}$$

By taking an SVD of C_{ij}, we obtain a Schmidt decomposition

$$|\psi\rangle = \sum_{ij} \sum_{a=1}^{\min(N_A,N_B)} U_{ia}S_{aa}V^*_{ja}|i_A\rangle|j_B\rangle = \sum_{a=1}^{\min(N_A,N_B)} s_a|a_A\rangle|a_B\rangle. \tag{2.6}$$

This is the von Neumann entanglement entropy

$$S_{A|B}(|\psi\rangle) = -\mathrm{Tr}\hat{\rho}_A \log_2 \hat{\rho}_A = -\sum_{a=1}^{r} s_a^2 \log_2 s_a^2, \tag{2.7}$$

which is an upper bound to the area law, and where s_a^2 are the singular values of the SVD. The set $\{s_a^2\}$ determines an entanglement structure $P_a(s_1^2, s_2^2, \ldots, s_r^2)$ which characterises the entanglement of the system.

For example, in 2D, if we consider a lattice arrangement of our tensors (this tensor network is called Projected Entangled Pair States), one subsystem may be the inside of a square of $N \times N$ bonds, and the second subsystem the complement of it. For each side we would have our square crossing N bonds of dimension

χ, therefore we would have χ^{4N}, by (2.7) $S = -\mathrm{Tr}\hat{\rho}_{A=in}\log_2\hat{\rho}_{A=in} \leq 4N\log(\chi)$. Therefore the entanglement structure is related to both the geometry of the tensor network (tells us how many Ns) and to the bond dimension. Here it is clear that if $\chi = 1$ we have no entanglement entropy.

2.3 Finite-depth circuits

Finite-depth circuits are a natural extension of matrix product states into quantum circuits [101, 9]. From the discussion above, there are some important things to notice. The MPS representation shows gauge freedom, meaning that under certain transformations $A^s_{(i)} \to T_{i-1}A^s_{(i)}T_i^{-1}$ for $i = 2, \ldots N-1$ the tensor ψ_s of eq. (2.3) remains invariant. Here we are concerned with canonical transformations of the form

$$\sum_s A^{s\dagger}_{(i)}A^s_{(i)} = \mathbf{1} = \quad . \tag{2.8}$$

and general contractions of the form

$$= \Lambda_{i-1} = \sum_s \mathcal{A}^{s,1}_i \Lambda_i \mathcal{A}^{1,s\dagger}_i = \quad . \tag{2.9}$$

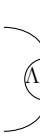

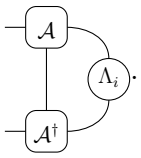

Where $A^\sigma_{ab} = \mathcal{A}^{\sigma\delta}_{ab}v^\delta$, and v^δ are spinor components of the vector state $|\mathbf{v}\rangle$. We will interpret $\mathcal{A}^{(a,s)}_{(b,\delta)}$ as a quantum circuit because it makes sequential unitary maps that preserve the canonical transformations (2.8). Formally, an m-local unitary circuit of depth D is a unitary operator [9]

$$U = \prod_{i=1}^{D}\prod_{j=0}^{m-1}\left(U^i_j \otimes U^i_{m+j} \otimes U^i_{2m+j} \otimes \ldots\right),$$

where U^i_n is a unitary operator that acts on at most m consecutive sites starting at site n. This unitary transformation is what takes product states into entangled states, i.e., it is constructing a tensor network with finite depth and variable (possibly infinite) width. Fig. 2.3 shows a finite depth circuit for the case of spinless fermions. In that image it is shown how an SVD leads to a decomposition of the tensor network similar to that seen for MPS. In this case, however unitary circuits correspond to matrix product states in canonical form. This representation still follows an area law and can modulate the entanglement structure very easily.

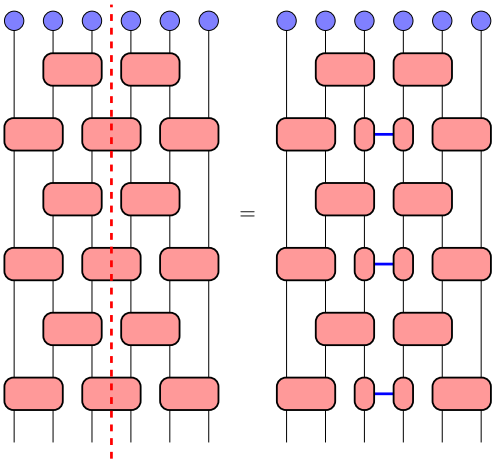

Figure 2.3: Example of a finite-depth circuit. The blue dots represent a product state $|\psi\rangle$. This image shows how the state becomes entangled by an $(m = 2)$-local finite-depth circuit transformation of depth $D = 3$. The red dashed line represents the location of the partition that is being used to calculate the entanglement entropy, it is directly related to the amount of operators it crosses (in this representation, the maximum entanglement is 3). The right side of the figure shows an SVD of the operators to the left. Image reproduced from [9]

2.4 Feynman Path Integrals over Tensor Networks

The path-integral approach to quantum mechanics is a generalisation of the principle of stationary action, where a quantum amplitude is obtained by performing a weighted sum over all possible trajectories. The partition function in this formalism is represented by an integral of the field configurations and provides both important insight into the physical system and powerful approximations by means of saddle points, instantons, solitons, perturbation methods, among others. The partition function reads as follows

$$\mathcal{Z} = \operatorname{Tr} e^{-\beta \mathcal{H}} = \int \mathcal{D}\psi(\tau) e^{-\mathcal{S}[\psi]}, \tag{2.10}$$

where the field integral is constructed in the usual way by breaking the time interval of the imaginary time evolution operator into infinitesimal steps, and taken over coherent states to attain a general many-body Hamiltonian. The over-complete basis of coherent states allows us to include resolutions of the identity in the form

$$\mathbf{1} = \int d\psi |\psi\rangle\langle\psi|, \tag{2.11}$$

where $|\psi\rangle$ is a product state and $d\psi$ is a gauge invariant measure. This approach, however, shows no entanglement at the saddle-point. The main purpose to include

entanglement to the functional integral is to take product states $|\psi_A\rangle$ with a general form as in (2.2) (in this case (2.2) represents matrix product states, but the general idea is generalisable to other types of tensor networks), which already include an entanglement structure. To define the path integral over tensor networks, we must redefine our resolution of identity to

$$\mathbf{1} = \int dA |\psi_A\rangle\langle\psi_A|, \tag{2.12}$$

where the new gauge-invariant measure dA and states $|\psi_A\rangle$ form a new overcomplete basis. To make it consistent with both tensor network and with the functional integral we reinterpret our product states as quantum circuits, $\mathcal{A}^{s\delta}_{a_i,a_{i+1}}$, defined by introducing a reference state $|\mathbf{v}\rangle = v^\delta|\delta\rangle$ in an appropriate basis and by defining a matrix product operator $A^s_{a_i,a_{i+1}} = \mathcal{A}^{s\delta}_{a_i,a_{i+1}} v^\delta$. As shown in [41], the quantum circuit $\mathcal{A}^{(a,s)}_{(b,\delta)}$ makes sequential unitary maps from the reference space + auxiliary space to a physical space + auxiliary space at the following site. This quantum circuit now lives in $SU(\chi d)$ where the gauge-invariant measure may be now formally constructed. The contraction of the tensor network follows now as a series of matrix multiplications

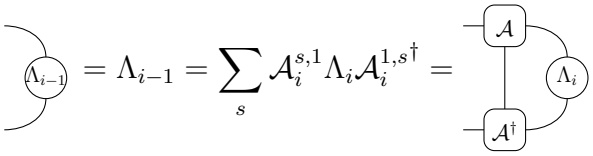

(2.13)

for which the field integral takes the final form of a path integral constructed over the contraction Λ and the SU(χd) elements $\mathcal{A}$

$$\mathcal{Z} \;=\; \int \mathcal{D}\mathcal{A}\mathcal{D}\Lambda\, \delta\left[\Lambda_{i-1} - \sum_s \mathcal{A}_i^{s,1}\Lambda_i\mathcal{A}_i^{1,s^\dagger}\right] e^{-\mathcal{S}[\mathcal{A}]}. \tag{2.14}$$

As mentioned above, this new formulation is convenient because it includes entanglement and offers some notable conceptual differences from other formulations:*(i)* This provides a semiclassical description of the field integral in the sense that new collective coordinates emerge (in this case the product states of the tensor network). It is semiclassical because the number of states escalates polynomially as the size of the system (a classical property) but it shows entanglement (a quantum property).*(ii)* In this formulation, there is a remarkable connection between saddle points and ground states. This is seen through the bond order where a low-bond order is adiabatically connected to the actual saddle points. This extends even to quantum critical points where entanglement diverges.*(iii)* A tensor network path integral captures naturally the proliferation of instantons. This is possible because tensor networks include by construction an entanglement structure which translates as classical trajectories transferring weight to other classical ones (i.e., tunneling achieved through instantons in the coherent-state theory).

2.5 MPS in the thermodynamic limit

In this section we introduce theoretical representations of tensor network states as differential manifolds where a geometrical analysis of its tangent space gives insights into a unified version of stationary and time-dependent approaches. These methods work in the thermodynamic limit by applying Dirac's time-dependent variational principle (TDVP) [27] and construct efficient variational ansätze for elementary excitations on top of tensor network ground states [118, 45, 128, 119]. Moreover, these methods are a natural language for the application of field-theoretical techniques over tensor networks [41] where, for example, Berry phases emerge effortlessly. In particular, the combination of path integrals and tangent spaces render these methodologies a generalisation suitable to describe strongly correlated systems and non-trivial topological excitations—e.g., anyons. Here we only focus on MPS.

The application of the TDVP to MPS provides an efficient method to obtain time-evolution, bulk excitations, and other quantities without the use of a Lie-Trotter-Suzuki (LTS) decomposition. In contrast with the time-evolving block decimation method (TEBD), the TDVP involves no LTS error while truncating the bond dimension (which breaks the symplectic structure of the manifold of states). Therefore the TDVP preserves symmetries and conservation laws as well as the symplectic structure of the manifold [45, 47, 55, 121]. The excitations turn out to be related to the tangent space of the manifold and all the calculations can be performed in the thermodynamic limit of systems with infinite size.

For space and clarity reasons, most of the results shown are not rigorous but heuristical. In turn this lets us write every result both in mathematical form as well as in diagrammatic form. Assuming the definitions of 2.2 we now take the limit $N \to \infty$ of infinite size where now the system is defined as a lattice with magnitude equal to the cardinality of the integers $|\mathbb{Z}|$.

A translation invariant or uniform uMPS state (in the thermodynamic limit) is defined as

$$|\Psi(A)\rangle = \sum_{\{s\}} \boldsymbol{v}_L^\dagger \prod_{m\in Z} A^{s_m} \boldsymbol{v}_R \, |\{s\}\rangle = \ldots$$

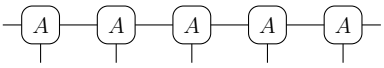

$$\ldots \quad (2.15)$$

where each A^s is a $\chi \times \chi$ matrix. A may be viewed as a tensor of dimensions $\chi \times d \times \chi$, with d the physical dimension at every site in the chain and χ the bond dimension. In an infinite system—and in particular for the so-called injective MPS— the vectors $\boldsymbol{v}_L^\dagger$ and $\boldsymbol{v}_R$ are irrelevant.

States (2.15) are gauge invariant and form a differential manifold $\mathcal{M} \subset \mathcal{H}$. By taking a specific subset of states from an open set called injective MPS (see [55] for rigorous definition of these manifolds), this space is diffeomorphic to $\mathcal{M}$ and thus it inherits the properties of a smooth complex manifold. This manifold is symplectic and the problem of finding expectation values or excitations reduces to the solution of non-linear differential equations, in similar fashion to that of classical mechanics.

The transfer matrix operating on the space of $\chi \times \chi$ matrices, defined as

$$E = \sum_{s=1}^{d} A^s \otimes \bar{A}^s = \quad , \tag{2.16}$$

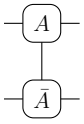

will be the workhorse for the TDVP. E has precisely one eigenvalue equivalent to the spectral radius of E, $\lambda^1 = \rho(E)$ which upon normalisation may be taken as unity, and the corresponding left and right eigenvectors ($l|$ and $|r$) of length χ^2 (or by "reshaping", $\chi \times \chi$ matrices l and r). The fact that the transfer matrix has only one eigenvalue is a consequence of working in the space of injective MPS. The spectral radius of $E - |r)(l|$ is smaller than 1 and will be relevant when obtaining overlaps between MPS and tangent states. The eigenvectors ($l|$ and $|r$) may be written as positive-semidefinite Hermitian matrices. Given the normalisation condition $Tr(lr) = 1$ these may be written in the following representation

$(l|E =$ $= l$, $E|r) =$ $= r$, (2.17)

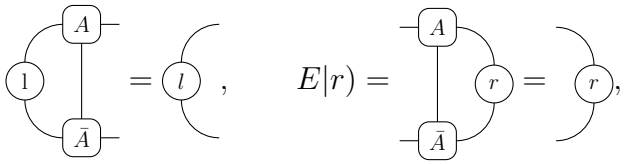

and $\mathrm{Tr}(lr) =$ $= 1.$ (2.18)

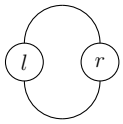

Diagrammatically, the norm of a uMPS state is written as

$$\begin{aligned}
\langle \Psi(\bar{A}) | \Psi(A) \rangle &= \sum_{\{s\}} \boldsymbol{v}_L \left[\prod_{m \in Z} \bar{A}^{s_m} \right] \boldsymbol{v}_R \dagger \, \langle \{s\} | \sum_{\{s\}} \boldsymbol{v}_L^\dagger \left[\prod_{m \in Z} A^{s_m} \right] \boldsymbol{v}_R \, | \{s\} \rangle \\
&= (\boldsymbol{v}_L \boldsymbol{v}_L \dagger) \left(\prod_{m \in \mathbb{Z}} E \right) (\boldsymbol{v}_R \boldsymbol{v}_R \dagger) \\
&= \cdots \quad \cdots \qquad (2.19) \\
&= \quad \overset{m \to \infty}{\quad} \quad = 1 \qquad (2.20)
\end{aligned}$$

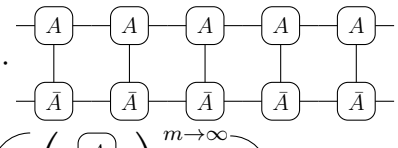

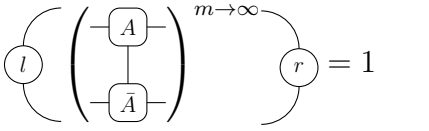

where in the last step we are assuming that the MPS is normalised and that the boundary vectors are irrelevant in the infinite limit. Therefore, in the infinite limit $E^N \to [N \to \infty]|r)(l|$ becomes a projector. Now we want to obtain the overlaps of two different states. Given two normalised MPS $|\Psi(A)\rangle$ and $|\Psi(B)\rangle$,

the overlap is given by

$$\langle\Psi(\bar{B})|\Psi(A)\rangle = \cdots$$ 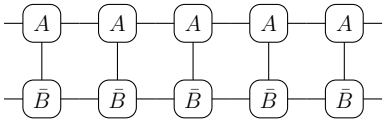 $$\cdots \tag{2.21}$$

where we now define the quantity

$$E_B^A = \sum_{s=1}^{d} A^s \otimes \bar{B}^s =$$ 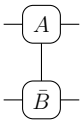 . $$\tag{2.22}$$

Eq. (2.21) shows that the maximum eigenvalue $\lambda_{\max}$ of E_B^A is the one determining the value of the overlap. If it is less than unity it vanishes, if it is unity it stays as unity. This result will repeat again when obtaining overlaps with tangent vectors. Following this logic the expectation values of operators $O = \frac{1}{N}\sum_{n\in\mathbb{Z}} O_n$ is

$$\langle\Psi(\bar{A})|\, O\,|\Psi(A)\rangle = (l|\frac{1}{N}\sum_{n\in\mathbb{Z}} O_n \sum_{\{s\}} \left[\prod_{n\in Z} \bar{A}^{s_n}\right] \otimes \left[\prod_{m\in Z} A^{s_m}\right] |r)$$

$$= \cdots$$ 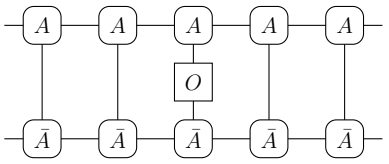 $$\cdots$$

$$\rightarrow$$ 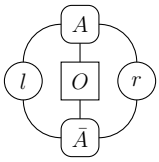 . $$\tag{2.23}$$

similarly, the local two-site hamiltonian H

$$\langle\Psi(\bar{A})|\, H\,|\Psi(A)\rangle =$$ 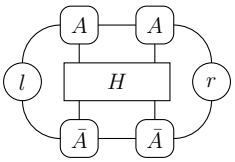 $$\tag{2.24}$$

By taking into account that the complement of the projector $C \equiv 1 - |r)(l|$, we first note that a general two-point connected correlation function of two local

operators O^α and O^β may be computed

$$\begin{aligned}\Omega^{\alpha\beta}(n) &= (l|E_{O^\alpha}E^{n-1}E_{O^\beta}|r) - (l|E_{O^\alpha}|r)(l|E_{O^\beta}|r)\\ &= (l|E_{O^\alpha}\left[E^{n-1} - |r)(l|\right]E_{O^\beta}|r)\\ &= (l|E_{O^\alpha}\left[CE^{n-1}C\right]E_{O^\beta}|r)\\ &= (l|E_{O^\alpha}\left[C(CEC)^{n-1}C\right]E_{O^\beta}|r)\end{aligned}$$

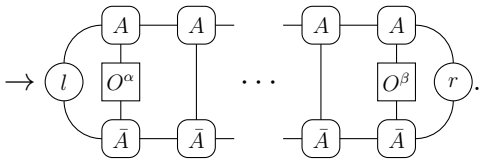

(2.25)

2.6 Tangent space

The tangent space of the manifold $\mathcal{M}_{\mathcal{MPS}}$ is formed by the generalised tangent vectors [47]

$$|\Phi_p(\mathbf{B};A)\rangle = \sum_{n\in\mathbb{Z}} e^{ipn} \sum_{\{s_n\}=1}^{d} \boldsymbol{v}_{\mathrm{L}}^\dagger \left[\left(\prod_{m<n} A^{s_m}\right) B^{s_n} \left(\prod_{m'>n} A^{s_{m'}}\right)\right] \boldsymbol{v}_{\mathrm{R}} \,|\boldsymbol{s}\rangle\,. \tag{2.26}$$

The above is well defined because tangent spaces are linear vector subspaces of Hilbert space, but are now parametrised by linear combinations of (derivatives of) B. The tangent space however includes both translationally invariant states and site-dependent ones. In the expression above we restrict to the tangent space sector where translation invariance is made explicit by including the momentum-dependent prefactors e^{ipn}. By setting $p = 0$ we obtain the translationally invariant sector of tangent states that are not orthogonal to the original state $|\psi(A)\rangle$

$$\begin{aligned}|\Phi(B;A)\rangle := B^i\partial_i|\Psi(A)\rangle &= \sum_{n\in\mathbb{Z}}\sum_{\{s_n\}=1}^{d} \boldsymbol{v}_{\mathrm{L}}^\dagger \left[\left(\prod_{m<n} A^{s_m}\right) B^{s_n} \left(\prod_{m'>n} A^{s_{m'}}\right)\right] \boldsymbol{v}_{\mathrm{R}} \,|\boldsymbol{s}\rangle\\ &= \sum_n \cdots$$

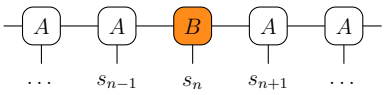

$$\cdots \tag{2.27}$$

Note that

$$\langle\Phi(\bar{B}';\bar{A})|\Phi(B;A)\rangle = \bar{B}^{i\prime}\,\langle\partial_i\Psi(\bar{A})|\partial_j\Psi(A)\rangle\,B^j \equiv \bar{B}^{i\prime}G_{ij}(\bar{A},A)B^j, \tag{2.28}$$

where G_{ij} is called the Gram matrix and may be interpreted as a norm matrix, and more specifically when $p = 0$ it is the norm of the uMPS manifold.

Now we can evaluate the overlap between MPS and tangent states

$$\begin{aligned}\langle\Psi(\bar{A})|\Phi(B;A)\rangle &= \sum_{n\in\mathbb{Z}} e^{ipn}(l|E_A^B|r) = 2\pi\delta(p)(l|E_A^B|r)\\ &\xrightarrow{p\to 0} 2\pi\delta(0)(l|E_A^B|r)\end{aligned} \tag{2.29}$$

where $2\pi\delta(0) = |\mathbb{Z}|$. And the overlap among tangent states

$$\begin{aligned}
\langle \Phi_p(\overline{B};\overline{A}) \mid \Phi_{p'}(B';A)\rangle = \sum_{n=-\infty}^{+\infty}\sum_{n'=-\infty}^{+\infty} e^{+ip'n'-ipn}\Big[&\delta_{n,n'}(l|E_B^{B'}|r) \\
&+\theta_{n',n}(l|E_B^A(E)^{n'-n-1}E_A^{B'}|r)\Big] \qquad (2.30)\\
&+\theta_{n,n'}(l|E_A^{B'}(E)^{n-n'-1}E_B^A|r)\Big] \\
= \sum_{n_0=-\infty}^{+\infty} e^{i(p'-p)n_0}\sum_{\Delta n=-\infty}^{+\infty} e^{ip\Delta n}\Big[&(l|E_B^{B'}|r) \\
&+\theta(\Delta n>0)(l|E_B^A C E^{\Delta n-1} C E_A^{B'}|r) \qquad (2.31)\\
&+\theta(\Delta n<0)(l|E_A^{B'} C E^{-\Delta n-1} C E_B^A|r)\Big] \\
+ (l|E_B^A|r)(l|E_A^{B'}|r)\sum_{n=-\infty}^{+\infty}\sum_{n'=-\infty}^{n-1} &e^{ip'n'-ipn} \\
+ (l|E_A^{B'}|r)(l|E_B^A|r)\sum_{n=-\infty}^{+\infty}\sum_{n'=n+1}^{+\infty} &e^{ip'n'-ipn} \\
= 2\pi\delta(p'-p)\Big[&(l|E_B^{B'}|r) + (l|E_B^A C(\mathbb{1}-e^{ip}CEC)^{-1}CE_A^{B'}|r \\
&+(l|E_A^{B'}C(\mathbb{1}-e^{-ip}CEC)^{-1}CE_B^A|r) \qquad (2.32)\\
&+(2\pi\delta(p)-1)(l|E_A^{B'}|r)(l|E_B^A|r)\Big] \qquad (2.33)
\end{aligned}$$

Where in the last equation, we used (2.25) and the geometric series expansion $\sum_n^\infty C(e^{-ip}E)^{n-1}C = \sum_n^\infty C^n(e^{-ip}E)^{n-1}C^n = \sum_n^\infty C(Ce^{-ip}EC)^{n-1}C = C(1-e^{-ip}CEC)^{-1}C$. This is true because the operator's spectral radius is less than one.[2]

2.7 Time-dependent variational principle (TDVP)

The main idea behind the TVDP is to *approximate* the solution to the Schrödinger equation for a uMPS

$$i\partial_t |\Psi(A)\rangle = H|\Psi(A)\rangle\,. \qquad (2.34)$$

This equation has no exact solution because $i\frac{\partial}{\partial t}|\Psi(A)\rangle = |\Phi(\dot{A},A)\rangle$ lives in the tangent space manifold, which is not the manifold where $H|\Psi(A)\rangle$ lives, and it is not possible to integrate exactly the equation. However, by orthogonally projecting $H|\Psi(A)\rangle$ onto the tangent space, we can obtain the best approximation to the time evolution of a uMPS. This implies that solving the equation for the

[2]Here we use the power theorem [56] which tells us that $A \in \mathbb{C}^{n\times n}$ has $\rho(A) < 1$ iff $A^k \xrightarrow{k\to\infty} 0$

projected Hamiltonian

$$i\frac{\partial}{\partial t}\left|\Psi(A(t))\right\rangle = P_{T_A} H \left|\Psi(A(t))\right\rangle \tag{2.35}$$

is the same as minimising the expression $(i\frac{\partial}{\partial t}\left|\Psi(A)\right\rangle - H\left|\Psi(A)\right\rangle)$. First we note that the tangent vector takes the form

$$\partial_t \left|\psi(A(t))\right\rangle = \partial_t A_i \partial_{A_i} \left|\psi(A)\right\rangle \tag{2.36}$$

and the projector may be defined in terms of the Gram matrix of tangent vectors (2.28)

$$P_{T_A} = \left(\partial_{A_i}\left|\Psi(A)\right\rangle\right)\left(G^{-1}\right)^{ij}\left(\partial_{\bar{A}_i}\left\langle\Psi(\bar{A})\right|\right) \tag{2.37}$$

Therefore our projected Schrödinger equation now reads

$$\partial_t A_i \partial_{A_i}\left|\psi(A)\right\rangle = -iP_{T_A} H\left|\Psi(A(t))\right\rangle = -i\left(\partial_{A_i}\left|\Psi(A)\right\rangle\right)\left(G^{-1}\right)^{ij}\left(\partial_{\bar{A}_i}\left\langle\Psi(\bar{A})\right|\right) H\left|\Psi(A)\right\rangle \tag{2.38}$$

or, using (2.36)

$$G_{ij}\partial_t A_i = -i\partial_{\bar{A}_i}\left\langle\Psi(\bar{A})\right| H\left|\Psi(A)\right\rangle. \tag{2.39}$$

Before evaluating

$$\left\langle\Phi(B;A)\right| H\left|\Psi(A)\right\rangle \tag{2.40}$$

we note that whenever the tensor B is to the right of the two-site Hamiltonian we may "contract" using the pseudo inverse operator, which was obtained as the geometric series expansion in (2.33)

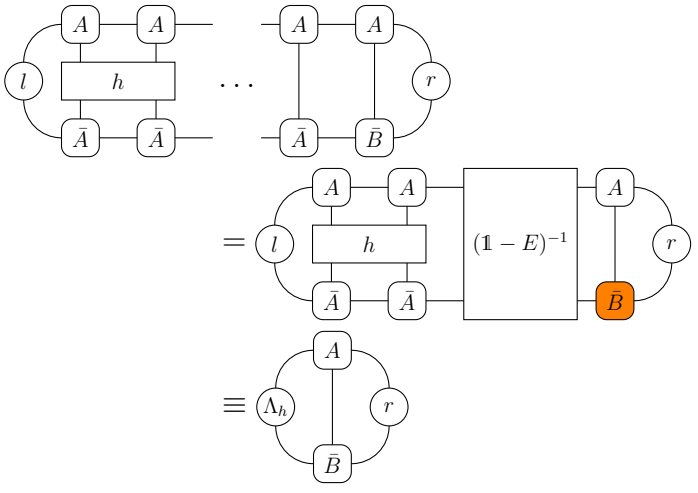

(2.41)

The analogous happens when evaluating B to the left of the two-site Hamiltonian. Hence, (2.40), takes the form

$\langle \Phi(B;A)| H |\Psi(A)\rangle =$

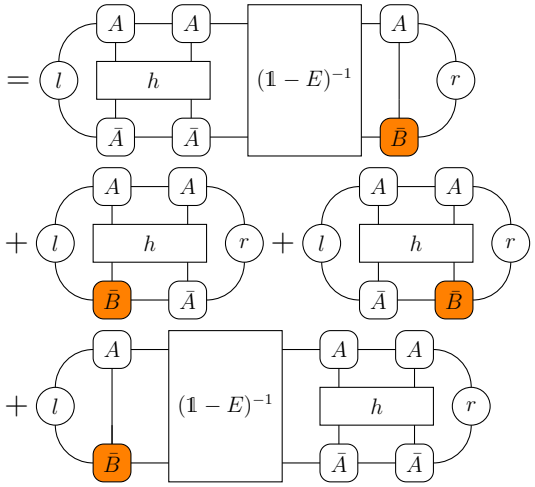

(2.42)

The projection onto the tangent space is obtained by taking $\partial_{\bar{B}_i}$ of (2.42), giving in turn a three-index tensor $\overline{E}$ by removing each tensor B from the equation above while leaving the legs open. To completely solve the problem we must obtain the three-index tensor $\dot{A}$ in terms of the new tensor F by solving a set of non-linear differential equations. Tensor F has the form [45]

$$
\begin{aligned}
F = &\sum_{s,t=1}^{d} (V_L^s)^\dagger l^{1/2} C^{st} r (A^t)^\dagger r^{-1/2} \\
&+ \sum_{s=1}^{d} (V_L^s)^\dagger l^{-1/2} \left(\sum_{t=1}^{d} (A^t)^\dagger l C^{ts} + K A^s \right) r^{1/2}
\end{aligned}
$$

$=$

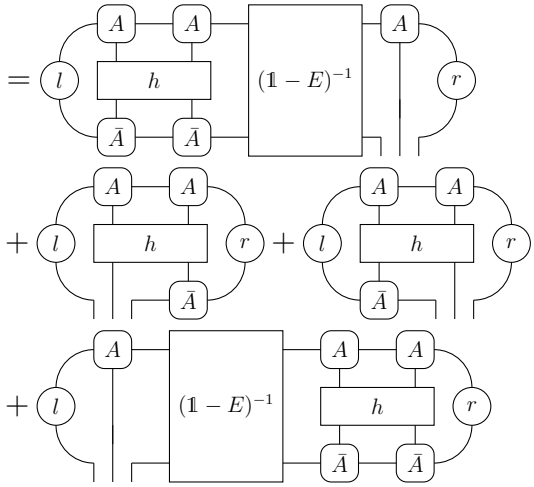

(2.43)

where V_L represents the null space of $\bar{A}$ i.e. $LV_L = 0$ for $L_{\alpha,(s,\beta)} = [A^{s\dagger} l^{1/2}]_{\alpha,\beta}$, and $C^{st} = \sum_{uv} \langle st| h |uv\rangle A^u A^v$. With this equation we can now minimise the expression

$$||B^i(x)\partial_i |\psi(A)\rangle - H |\psi(A)\rangle ||^2 \tag{2.44}$$

where the parametrisation $B^s(x) = l^{-1/2} V_l^s x r^{-1/2}$ is used, giving as a result

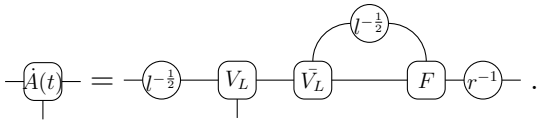

(2.45)

This equation may be solved by noting that the gauge-fixing $(l|E_A^{B(x)} = 0$ (because V_L contains only null vectors) and $\bar{B}^{i\prime} \langle \partial_i \Psi(\bar{A}) | \partial_j \Psi(A) \rangle B^j \equiv \bar{B}^{i\prime} = |\mathbb{Z}| \mathrm{tr}[\mathrm{x}^\dagger \mathrm{y}] = 1$.

2.7.1 Path integrals over uMPS

Now we want to relate the equations above to the Berry phase by realising a parametrisation of the MPS manifold in terms of spin-coherent states [128, 41]. The projection of the Hamiltonian onto tangent space provided us a solution of time-evolution in Eq. (2.45), which is an operator containing the information of both the MPS and the tangent space. To understand this, we may start by considering small paths about some state ψ as in (2.15). A tangent vector in this case is obtained by replacing a tensor on site i, say $A^\sigma_{ab(i)}(x) = A^\sigma_{ab(i)} + dA^\sigma_{ab(i)}(x)$ by $dA^\sigma_{ab(i)}(x)$, which should be chosen orthogonal to the MPS manifold. $dA^\sigma_{ab(i)}(x)$ is then parametrised by tensors $x^{\sigma\neq 1}_{ab(i)}$ of $\chi \times (d-1) \times \chi$ size.

Now we can use MPO notation (a tensor with four indices) and represent the variation of a tangent vector as follows [41]

$$dA^\sigma_{ad}(x) = \mathcal{A}^{\sigma,\delta\neq 1}_{ab} x^{\delta\neq 1}_{bc} \Lambda^{-1/2}_{cd}. \tag{2.46}$$

The convenience of this MPO notation is that it contains both the reference MPS and information about the tangent space orthogonal to the MPS manifold. With this in mind, the Berry phase in terms of those tensors is

$$\mathcal{S}_B = \sum_i \int dt \sum_{s\neq 1} Tr[x^{s\dagger}_i \dot{x}^s_i] \tag{2.47}$$

When the time-dependent parameters x (with simplified notation) are defined as a representation of spin-coherent states, the Berry phase generalises the notion of a spinor representation, for example, for $\chi = 1$ it reduces to the coherent state Berry phase. A simple example is the MPS representation of the SU(2)spinor x [128, 41], taking the simple form

$$|A(x)\rangle = \exp\left[x_\downarrow \Lambda^{-1/2} \sigma^+ x^\dagger_\downarrow \Lambda^{-1/2} \sigma^-\right] |\uparrow\rangle \tag{2.48}$$

where [41]

$$\hat{A}_i(x) = \begin{pmatrix} 0 & |\mathbf{l}_i\rangle\langle\uparrow| & |-\mathbf{l}_i\rangle\langle\uparrow| \\ n_{1,i-1}|\mathbf{l}_i\rangle\langle\uparrow| & 0 & 0 \\ n_{2,i-1}|-\mathbf{l}_i\rangle\langle\uparrow| & 0 & 0 \end{pmatrix} + \begin{pmatrix} 0 & 0 & 0 \\ \tilde{n}_{1,i-1}|\mathbf{l}_i\rangle\langle\downarrow| & 0 & |-\mathbf{l}_i\rangle\langle\downarrow| \\ \tilde{n}_{2,i-1}|-\mathbf{l}_i\rangle\langle\downarrow| & |\mathbf{l}_i\rangle\langle\downarrow| & 0 \end{pmatrix}, \tag{2.49}$$

with corresponding Berry phase

$$\mathcal{S}_B = \sum_i \sum_\sigma \int dt \mathrm{Tr}[{x^\sigma_{(i)}}^\dagger \dot{x}^\sigma_{(i)}]. \tag{2.50}$$

The results above show that tangent-space methods of tensor networks may serve as a formalism for developing field theories on lattice systems. This is highly extendable to other types of tensor networks [120].

Sketch of the problem: Path integral over MPS for the spin-1 BBH model in 1D

Here we give a brief sketch on how to formulate and which phases are relevant of the BBH model. Just as before, for this model we need to determine a suitable coherent-state basis that captures the entanglement of bonds

$$|\mathbf{A}\rangle = \left(\prod_i A_i\right)|v\rangle. \tag{2.51}$$

From (1.47)

$$H = \sum_{\langle i,j\rangle} \cos(\theta)\mathbf{S}_i \cdot \mathbf{S}_j + \sin(\theta)(\mathbf{S}_i \cdot \mathbf{S}_j)^2$$

This Hamiltonian reduces to the Heisenberg and the AKLT Hamiltonians for $\theta = 0$ and $\theta = \sin^{-1}(-1/3)$, respectively. This model presents no AFM order but it does present FM. The ground state or Haldane phase is in a gapped symmetry protected topological phase with its lowest excitation in a spin-1 triplet. At $\theta = \pi/4$ the transition is of the Berezinskii–Kosterlitz–Thouless (BKT) type. Just as before, for this model we need to determine a suitable coherent-state basis that captures the entanglement of bonds.

The general problem of finding a path integral reduces in part to finding an appropriate measure, where given $\prod_i d\Omega_i = [\mathcal{D}\mathbf{A}]$,

$$\int [\mathcal{D}\mathbf{A}]|\mathbf{A}\rangle\langle\mathbf{A}| = I_{3^N\times 3^N}. \tag{2.52}$$

The time-evolution amplitude over an infinitesimal time interval δt may be written as

$$\frac{\langle \mathbf{A}(t+\delta t)|e^{-i\delta t H}|\mathbf{A}(t)\rangle}{\langle \mathbf{A}(t)|\mathbf{A}(t)\rangle} \simeq \exp\left(i\delta t[-i\frac{\langle \partial_t \mathbf{A}(t)|\mathbf{A}(t)\rangle}{\langle \mathbf{A}(t)|\mathbf{A}(t)\rangle} - \frac{\langle \mathbf{A}(t)|H|\mathbf{A}(t)\rangle}{\langle \mathbf{A}(t)|\mathbf{A}(t)\rangle}]\right), \tag{2.53}$$

with $|\mathbf{A}(t)\rangle$ denoting the entangled coherent state (2.51) at time t.

We will need to find the quantities $|\partial_t \mathbf{A}\rangle$ and $H|\mathbf{A}\rangle$ and show the properties of over-completeness of the MPS states. These properties will be needed to find an explicit form of the expectation value of the spin-1 bilinear-biquadratic Heisenberg Hamiltonian (2.52), namely

$$E = \sum_n \frac{\langle \mathbf{A}|H_n|\mathbf{A}\rangle}{\langle \mathbf{A}|\mathbf{A}\rangle} \tag{2.54}$$

and the Berry phase term

$$-i\frac{\langle \partial_t \mathbf{A}|\mathbf{A}\rangle}{\langle \mathbf{A}|\mathbf{A}\rangle}. \tag{2.55}$$

The representation in which the MPS can be depicted is crucial to compute the above quantities. One such representation is that of Schwinger bosons where the singlet and triplet operators take simple forms.

2.8 Tensor Renormalisation Group (TRG)

This section covers general tensor renormalisation group methods. These are useful in the understanding of emergent phenomena, strong correlations, and entanglement, which are some of the major challenges and concepts in theoretical physics. Ideally, knowing the microscopics of a many-body system would allow to write its path integral containing all the information about the system's collective properties. However, calculating these functions is notoriously difficult. The spin-blocking procedure by lattice coarse-graining was the first nonperturbative attempt to address this problem [62]. Forty years later, Levin and Nave [80] improved this with a versatile real-space coarse-graining method called the tensor renormalisation group (TRG) for 2D classical partition functions and 1D quantum systems.

In general, real-time correlations can be computed using tensor network methods. In 1D, for instance, the real-time evolution of a matrix product state (MPS) is achieved by various methods. One approach involves applying the evolution operator e^{-iHt} to an MPS, where e^{-iHt} can be decomposed using a Suzuki-Trotter expansion. Key methods using this decomposition include time-evolving block decimation (TEBD) [123], which truncates the evolved state via singular value decomposition (SVD), and time-dependent density matrix renormalisation group (tDMRG) [127], which updates the state using the variational principle. Another class of time evolution methods are tangent-space methods [46, 132], which project

the evolved state onto the MPS manifold. The most relevant schemes are the time-dependent variational principle (TDVP) [46] and the variational uniform matrix product state (VUMPS) [132]. Additional algorithms for time evolution include Krylov-based methods [61], which approximate the state using linear combinations of Krylov vectors, and methods based on Chebyshev expansions [125].

Both MPS-based and TRG methods come with their own challenges. For MPS methods, the entanglement entropy of a (1+1)D quantum state grows linearly with time, necessitating an exponential increase in bond dimension to describe the evolved state. In contrast, TRG-based algorithms offer a direct approach to dealing with partition functions in (1+1)D, enabling physical measurements like equal-time correlation functions using the ensemble method. However, the original TRG scheme fails to eliminate some short-range correlations (entanglement) in the partition function (path integral), leaving the coarse-grained system with unwanted microscopic information. This conflicts with the renormalisation group (RG) concept and results in an RG flow with incorrect noncritical fixed points. Computationally, accumulating short-range entanglement over successive TRG coarse-graining transformations leads to TRG's breakdown at criticality.

The limitations of the tensor renormalization group (TRG) method were solved by the tensor network renormalization (TNR) [36]. TNR is a renormalization group (RG) transformation that delivers accurate RG flows and significantly more precise observables than TRG, albeit at a higher computational cost. The key difference between TRG and TNR lies in the refinement of the renormalization process, where TNR incorporates additional optimisation steps to capture more detailed information, leading to improved accuracy and control over the renormalisation group flow of the system at the cost of increased computational complexity.Subsequent techniques, including Loop-TNR [129], TNR+ [6], and GILT-TNR [52], have also proposed similar solutions to the limitations of TRG, effectively eliminating all the microscopic information during the coarse-graining procedure.

2.8.1 Graph-Independent Local Truncations (GILT)

To overcome the limitations of TRG in coarse-graining, it is essential to implement additional local truncations. These adjustments, which eliminate short-range information, must retain the network's geometry and uniformity to ensure the tensor space flow remains consistent. Several methods, including tensor network renormalisation (TNR) [34], loop-TNR [129], and TNR+ [7], have been developed to address TRG's shortcomings and establish accurate RG flows. A recent method known as GILT (graph-independent local truncations) [52] offers a new approach.

GILT is a simple algorithm that allows to locally—at each bond or edge of the network— truncate the bond dimension of a network while preserving the overall geometry. By truncating the selected legs, GILT effectively removes short-range information surrounding these legs. For instance, consider a network plaquette with a particular leg of bond dimension χ. The GILT algorithm replaces this leg, initially represented by an identity matrix, with a low-rank matrix. This matrix is then split and contracted with neighbouring tensors, thereby reducing the bond dimension of the original leg, as shown in Fig.2.4 and Fig.2.5.

To determine this low-rank matrix, the network is analysed without the leg to be truncated, followed by a singular value decomposition (SVD), as depicted in Fig.2.5. In this process, the vector t represents the partial trace of the three-index tensor U.

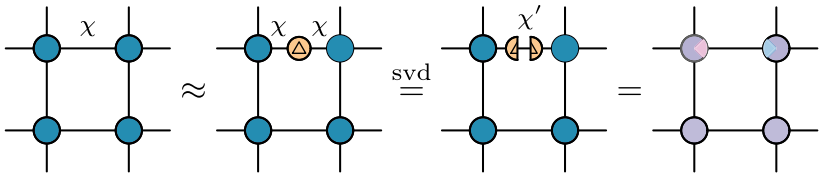

Figure 2.4: SVD of a single leg. The Δ tensor is decomposed into two tensors followed by a truncation in bond dimension. The new bond dimension χ' is less than the original bond dimension χ

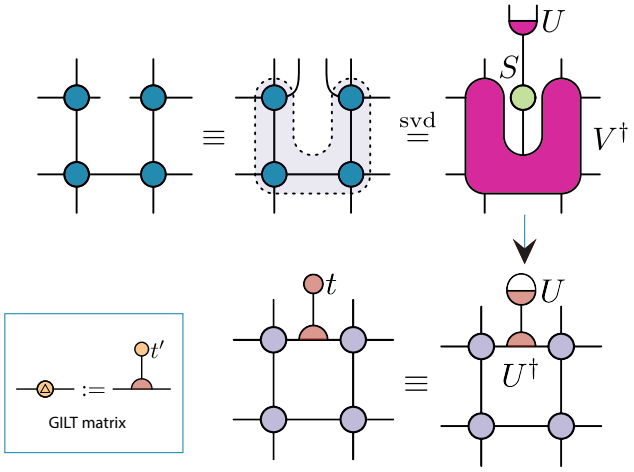

Figure 2.5: GILT matrix. For a given plaquette, we apply an singular value decomposition (SVD) to a single leg. The idea is that one can define a vector t to approximate the original tensor Δ using the spectrum of the SVD.

The GILT matrix depends on defining the following:

$$t'_i := t_i \frac{S_i^2}{S_i^2 + \epsilon_{\text{GILT}}^2} \tag{2.56}$$

where S_i denotes the singular values obtained from the SVD in Fig.2.5. This formula applies a gentle truncation to the singular values of S. This approach is considered optimal for a cost function that prefers low-rank matrices [52], i.e. it minimises the rank of the matrix while maximising the similarity between the original and the modified network. The parameter ϵ_{GILT} is chosen manually based on model variables and simulation settings, such as the maximum bond dimension. Although selecting ϵ_{GILT} manually is not ideal, it balances rank reduction with

accuracy. A larger ϵ_{GILT} leads to more significant rank reduction but may introduce larger local errors, whereas a smaller ϵ_{GILT} results in less rank reduction, similar to TRG, where irrelevant information persists across scales.

Choosing an appropriate ϵ_{GILT} involves heuristic considerations and monitoring the truncation extent to identify an optimal range relative to bond dimensions. For example, [52] suggests $\epsilon_{\text{GILT}} = 8 \times 10^{-7}$ for bond dimensions ranging from 10 to 100, though more precise values are preferable. This parameter should ensure that the algorithm's error is mainly due to the coarse-graining step, implying that ϵ should decrease as χ increases. Minor deviations around the optimal ϵ generally have little impact on the renormalisation flow, with the optimal ϵ usually found at a stationary point. Near this value, a smaller ϵ tends to favour the symmetry-broken phase, while a larger ϵ favours a disordered phase.

The GILT algorithm effectively solves the issue of the original tensor renormalisation group which couldn't establish a proper renormalisation group flow due to its inability to eliminate short-range information. In Ref. [52] it was demonstrated that applying the GILT algorithm along the bonds of a tensor network they could obtain a proper renormalisation group flow. Specifically, iterating the GILT algorithm on all surrounding legs of such a plaquette removes the correlation loop within.

Figures 2.5 and 2.6 illustrate the GILT procedure when applied to a tensor network.

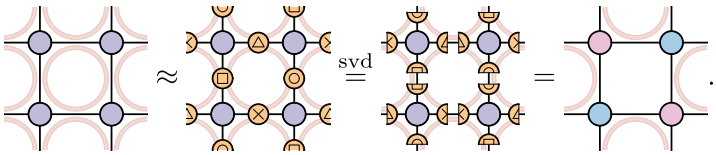

Figure 2.6: GILT procedure 1

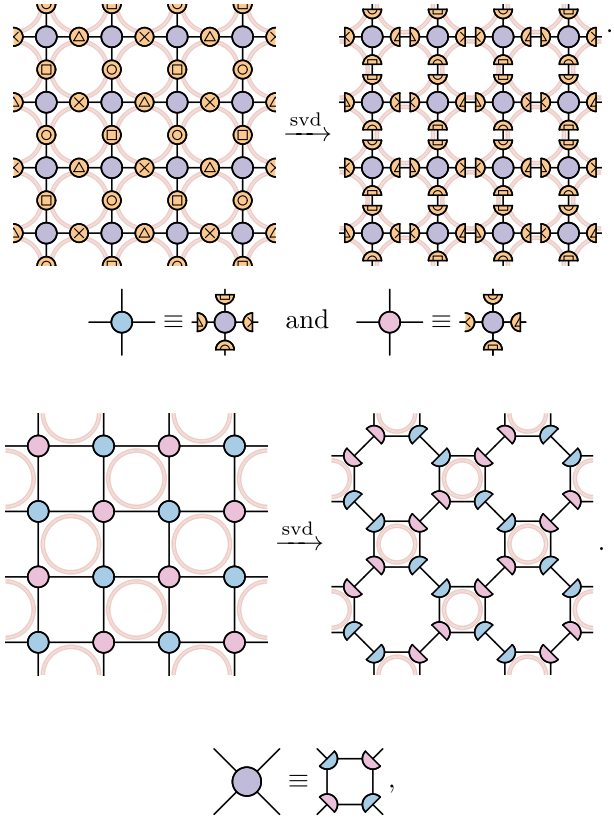

Figure 2.7: GILT procedure 2

Chapter 3

Tensor renormalisation of quantum spin-1 systems in 1D

3.1 Critical ferromagnetic $SU(3)$ point of the spin-1 chain

The spin-1 bilinear-biquadratic model in 1D is described by the Hamiltonian

$$H = \sum_i J \cos\theta \, \mathbf{S}_i \cdot \mathbf{S}_{i+1} + J \sin\theta (\mathbf{S}_i \cdot \mathbf{S}_{i+1})^2. \tag{3.1}$$

This model has been studied profusely from very different perspectives [1, 48, 8, 38, 24]. The phase diagram is depicted in Fig. 3.1. Probably the most remarkable phases to notice here are the Haldane phase, which is an example of a symmetry protected topological phase, with a Haldane gap as mentioned in 1.2; notoriously, the antiferromagnet at $\theta = 0$ is adiabatically connected to the the Affleck-Kennedy-Lieb-Tasaki (AKLT) [1] point at $\theta = \arctan(1/3)$, an example of a ground state with valence-bond solid (VBS) state and very relevant to the development of tensor networks. To this date the most controversial point in the phase diagram is maybe the point $\theta = 5\pi/4$, where the model has an enhanced $SU(3)$ symmetry, where there is no decisive evidence of what type of phase transition is happening.

The existence of a nematic phase near the SU(3) point has been a subject of extensive theoretical and experimental investigations. Early analytic studies [8] predicted a gapped nematic phase, while subsequent numerical works [38] suggested a direct, first-order, gapless transition (not nematic). Further studies by Buchta, Fáth, Legeza, and Sólyom [14] using DMRG found a dimerised phase prevailing down to the $SU(3)$ point. Läuchli, Schmid, and Trebst [77] employed numerical methods to propose a possible crossover to a critical nematic phase. However, analytic work by Grover and Senthil and more recent numerical studies by Rakov and Weyrauch [107] and Dai, Shi, Zhou, and McCulloch [24] consistently indicate the absence of a critical nematic phase near the $SU(3)$ point. However, as shown in Ref. [24], when using tensor networks one must tread softly, for there are several numerical artefacts that arise when studying this model near the SU(3) points. The two main artefacts proposed in that article are a conformal regime

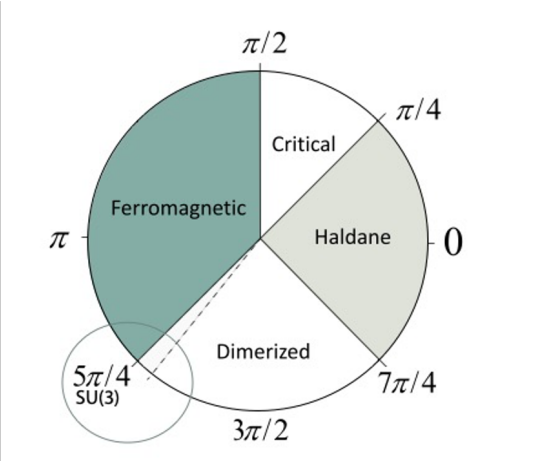

Figure 3.1: Ground state phase diagram for the one-dimensional spin-1 bilinear-biquadratic model. The parameter θ varies from 0 to 2π, with particular emphasis on the region around the $SU(3)$ ferromagnetic point at $\theta = 5\pi/4\theta$. The dotted line indicates a potentially critical nematic phase, which is a controversial point in the diagram.

and a fractal scale-invariant regime, both of them are due to enhanced entangled ground states and the SU(3) point. Two different techniques may be used in characterising them, namely, the counting of Nambu-Goldstone modes [124] and a fractal dimension [18]:

$$S(n) = \frac{d_f}{2} \ln n + b.$$

Where, d_f is the fractal dimension, and b is an additive constant.

As of now, the controversy mostly persistent between Ref. [8] and Ref. [38] is that the former—predicting a gapped nematic phase—may be dismissed, but has still some truth to it in the following sense. There are two critical nematic phases with central charge $c = 1$ that are nearly adjacent to the SU(3) ferromagnetic point. The proximity to these critical nematic phases explains the small gap that opens exponentially away from the SU(3) ferromagnetic point. This results in an essential singularity. Furthermore, the transition from the ferromagnetic phase to the dimerised phase is direct, aligning with Ref. [38]. The transition occurs at the SU(3) ferromagnetic point and features scale-invariant ground states with a fractal dimension of 2. SU(2) ferromagnetic states smoothly evolve into SU(3) ferromagnetic states within the ferromagnetic phase. In contrast, approaching the SU(3) ferromagnetic point from the dimerised phase reveals an essential singularity, indicating that the transition is not first-order, contrary to Ref. [38]. Finally, according to Ref. [24], rather than a simple crossover, the phenomena involve a pseudo first-order phase transition and pseudo critical points, proving to be more complex than initially expected.

In this chapter, we analyse the critical behaviour of the spin-1 chain using tensor renormalisation methods. These results are partial, but contrary to previous methods work directly at criticality, and extracting universal features should be

easier.

3.2 Tensor Renormalisation Group for 1D Spin-1 Systems

The core procedure for applying a tensor renormalisation group to spin systems is illustrated in Fig. 3.2.

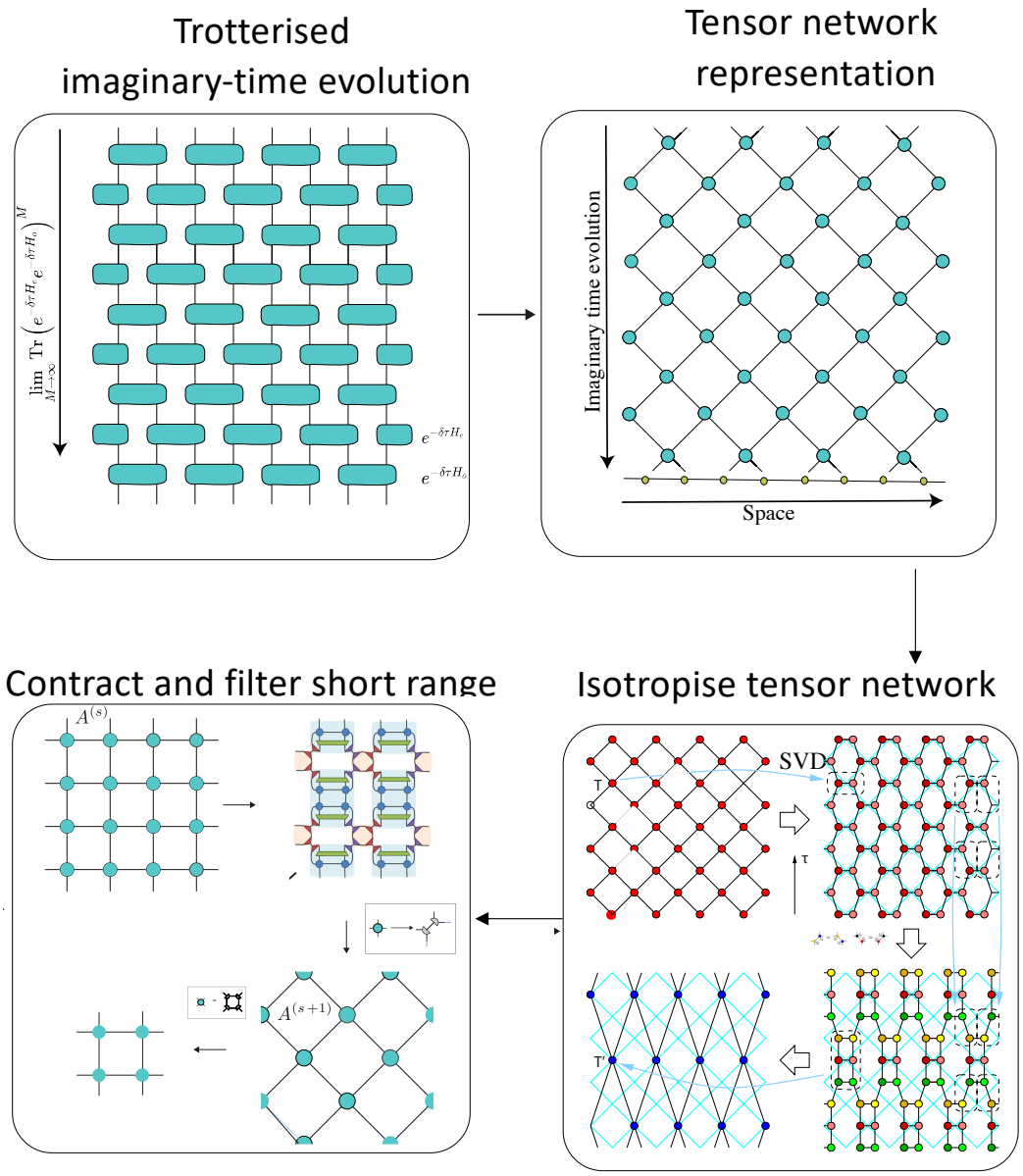

Figure 3.2: Steps of tensor network renormalisation for a spin chain. [44, 33]

For a quantum system with Hamiltonian H in 1D, the time evolution operator $e^{-\beta H}$ can be represented using a tensor network via Trotter decomposition.

Assuming H is a sum of local terms h,

$$H = \sum_r h_{r,r+1}, \tag{3.2}$$

we can now write the evolution operator as a product over small time steps τ:

$$e^{-\beta H} = \left(e^{-\tau H}\right)^{\beta/\tau}. \tag{3.3}$$

The evolution $e^{-\tau H}$ for a small time step τ is approximated by

$$e^{-\tau H} \approx e^{-\tau H_{\text{odd}}} e^{-\tau H_{\text{even}}}, \tag{3.4}$$

where H_{odd} and H_{even} denote contributions from odd and even bonds, respectively. This approximation introduces an error of order $O(\tau)$. Higher-order Suzuki-Trotter decompositions can improve this error to $O(\tau^n)$, where $n > 1$.

Since H_{odd} consists of commuting terms acting on different sites, $e^{-\tau H_{\text{odd}}}$ simplifies to a product of two-site gates, and similarly for $e^{-\tau H_{\text{even}}}$:

$$e^{-\tau H_{\text{odd}}} = \prod_{\text{odd } r} e^{-\tau h_{r,r+1}}, \tag{3.5}$$

$$e^{-\tau H_{\text{even}}} = \prod_{\text{even } r} e^{-\tau h_{r,r+1}}. \tag{3.6}$$

Thus, by considering each gate $e^{-\tau h}$ as a tensor T_{ijkl} and substituting into the equations above, we obtain a tensor network representation of the Euclidean path integral $e^{-\beta H}$ on a square lattice. Note that this representation introduces an error of order $O(\beta\tau)$, which can be mitigated by reducing the time step τ.

Isotropisation Step

Although this network serves as a starting point for tensor network renormalisation, preliminary manipulations can enhance its utility. This initial manipulation involves transforming the network to a new square lattice that is tilted by 45 degrees relative to the original, followed by a renormalisation in the time direction. Since $e^{-\tau h} \approx 1$ when $\tau \to 0$ the initial tensor network is highly anisotropic. The step of renormalising or coarse-graining in the time direction yields a more isotropic tensor network representation of $e^{-\beta H}$, making it more suitable for renormalisation. This process we call the isotropisation step and is depicted in Fig. 3.2.

Coarse Graining Step

Consider a tensor network $\mathcal{G}$ composed of identical tensors T_{ijkl} arranged in a square lattice with periodic boundary conditions. We want to compute the scalar expectation value $\langle\mathcal{G}\rangle$, which involves contracting the network or calculating the system's partition function. Given the exponential scaling of exact contraction with system size L, approximate methods become crucial for large-scale networks. We first provide an overview of general local approximation methods suitable for

such contractions, then examine the truncated singular value decomposition (SVD) used within the tensor renormalisation group (TRG) framework, and finally discuss specific local approximation classes in various tensor renormalisation algorithms.

Let $\mathcal{F}$ denote a subset of tensors, or equivalently a subnetwork, within $\mathcal{G}$. Coarse-graining methods for tensor networks rely on local approximations, where a subset $\mathcal{F}$ can be replaced by a different network of tensors $\tilde{\mathcal{F}}$ if their difference $\varepsilon \equiv \|\mathcal{F} - \tilde{\mathcal{F}}\|$ is sufficiently small. For simplicity, $\|\mathcal{F}\| = 1$ is often assumed. The scalar $\langle \mathcal{G} \rangle$ from contracting network $\mathcal{G}$ should only differ by a small amount $O(\varepsilon)$ when substituting $\mathcal{F}$ with $\tilde{\mathcal{F}}$. The norm

$$\|T\| = \sqrt{\mathrm{tTr}\,(T \otimes T^{\dagger})}, \tag{3.7}$$

represents the typical Hilbert-Schmidt norm, where we are taking the trace, i.e., we are contracting all indices between tensors of equal dimensions. Tensor network renormalisation schemes, including TRG and its more advanced variants, iteratively apply local approximations across the tensor network, alongside contractions, to produce coarser tensor networks.

In principle, any local approximation method that achieves a sufficiently small error ε can be incorporated into a coarse-graining scheme. The original Tensor Renormalisation Group (TRG) [80] and its subsequent refinements heavily rely on the truncated singular value decomposition (SVD) of individual tensors or its generalisation, the higher-order SVD (HOSVD).

Consider a tensor T_{ijkl} with four indices, each of dimension χ. By reshaping T into a $\chi^2 \times \chi^2$ matrix, we apply the standard SVD:

$$T_{ijkl} = \sum_{m=1}^{\chi^2} U_{ijm} S_{mm} V_{mkl} \tag{3.8}$$

Here, U and V are unitary matrices—with an appropriate reshaping—- and S is a diagonal matrix with positive singular values λ arranged in descending order. Truncating the SVD to the χ' largest singular values (where $\chi' < \chi^2$) provides an approximation:

$$T_{ijkl} \approx \sum_{m=1}^{\chi'} U_{ijm} S_{mm} V_{mkl} \tag{3.9}$$

The truncation error ε is given by the square root of the sum of the squares of the discarded singular values:

$$\varepsilon = \sqrt{\sum_{m=\chi'+1}^{\chi^2} \lambda_m^2}. \tag{3.10}$$

To simplify computations, we usually normalise the tensor T so that its norm equals unity, meaning the sum of the squares of its singular values is one. The SVD is particularly helpful in this context because it offers the optimal low-rank approximation of a tensor, a universal property in many tensor network renormalisation methods.

3.3 Isotropisation and tensor renormalisation for spin-1 systems: results

Isotropisation and tensor renormalisation for different angles

In Fig. 3.3 we see the results of the isotropisation and renormalisation steps done in different regions of the phase diagram for a bond dimension of $\chi = 50$. This image, is obtained by applying the procedure explained before, i.e., an isotropisation step followed by a renormalisation step using TNR. The results are produced by plotting the tensors at each coarse-graining (or RG) step, thus we can see how the structure of the tensors evolves when flowing to a fixed point. To create the plots shown, the tensors are reshaped into a matrix and graphed as heatmaps. The brighter colours represent larger values of elements of the matrix. For example, as seen Fig. 3.3 at the ferromagnetic phase with angle $\theta = \pi$ the renormalisation scheme would flow very fast leaving only two, faint yellow points. At the critical point and in the dimerised phases the tensors preserve much more structure. At the critical point we see scale-invariant tensors, while deep in the dimerised phases we see tensors preserving some structure, but not as much as at criticality.

Isotropisation and tensor renormalisation at the critical point

At the critical point we can see that the tensors clearly preserve the structure when the bond dimension goes up to $\chi = 70$. All the structure is mainly preserved which is what one would expect at the critical point. See Fig. 3.4

Isotropisation and tensor renormalisation near the critical point

In Fig. 3.5 it is shown the critical phase up to bond dimension $\chi = 72$. In particular one can see a point near the critical phase on the dimerised side. This procedure, at this limited bond dimension shows that all tensors preserve a structure, very similar to that at the critical point. This might suggest that the critical phase is extended near $\theta = 5\pi/4$. This method at this sstem sizes cannot make a clear distinction between the critical point and this near points.

Discussion

This chapter introduced a novel method for isotropisation followed by a proper tensor renormalisation of a quantum spin-1 chain in 1D. The method is effective in identifying fixed points in ordered phases, and allows for the visualisation of the critical behaviour of the system, i.e., we can visualise how the tensor structure is preserved even with a relatively small bond dimension. However, the current results are limited due to the heuristic nature of the presented results Further testing with larger clusters and higher bond dimensions is required for more conclusive results. In a way, significant computational limitations hinder further exploration. Some advancements also depend on developing appropriate algorithms and computational technology to extract features like the number of Nambu-Goldstone bosons, which would be helpful in distinguishing between fractal and conformal regimes near SU(3) points. This includes obtaining universality

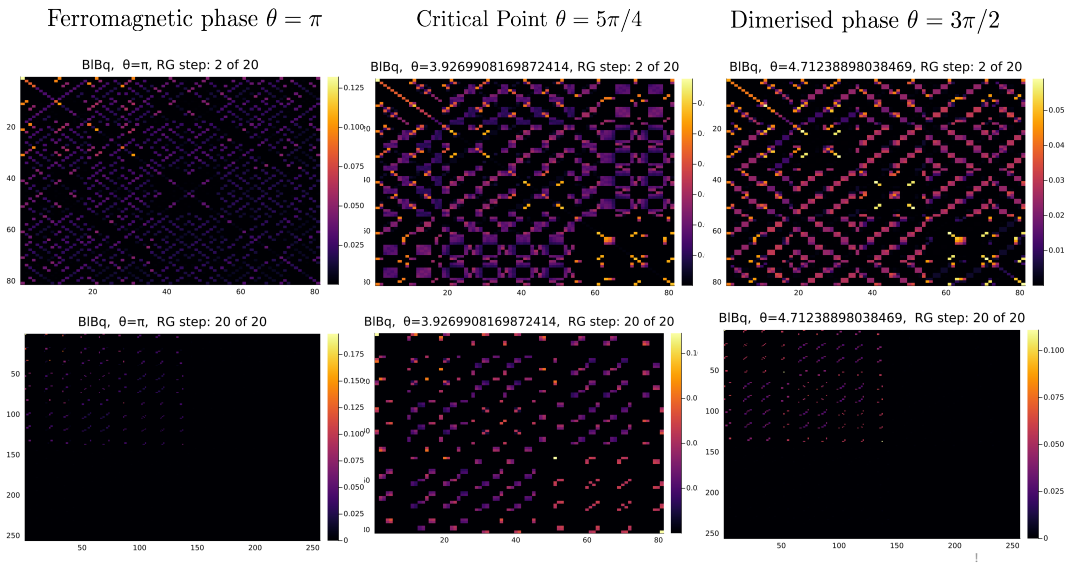

Figure 3.3: Isotropisation and tensor renormalisation of a spin-1 bilinear biquadratic model for fixed bond dimension $\chi = 50$. The top three images show the initial tensors before coarse-graining. The lower images show the coarse grained tensors for 20 iterations of the TNR method. The first column shows the case for the ferromagnetic phase at an angle $\theta = \pi$, with two fixed points, one at the top left corner and one in the middle diagonal; the middle column shows the critical point at $\theta = 5\pi/4$, which flows to no fixed point, preserving quite a lot of structure; and the third column shows the dimerised phase at $\theta = 5\pi/4$, where the tensors preserve quite a lot of structure but not as much as in the critical point. The image shows plotted tensors, the color code helps find fixed points, which usually appear in yellow (higher values). All the results were obtained using the CDT cluster in Edinburgh.

data from renormalised tensors, such as scaling dimensions, topological operators, and defects.

Another promising avenue for exploration is studying non-invertible symmetries or generalised topological operators with scaling properties which one would expect to persist in the renormalised tensors. Whether these symmetries exist in the bilinear biquadratic spin-1 model remains an open question. Furthermore, these methods could be leveraged to formally extract fixed points, owing to the straightforward theoretical method found in Refs. [67, 66].

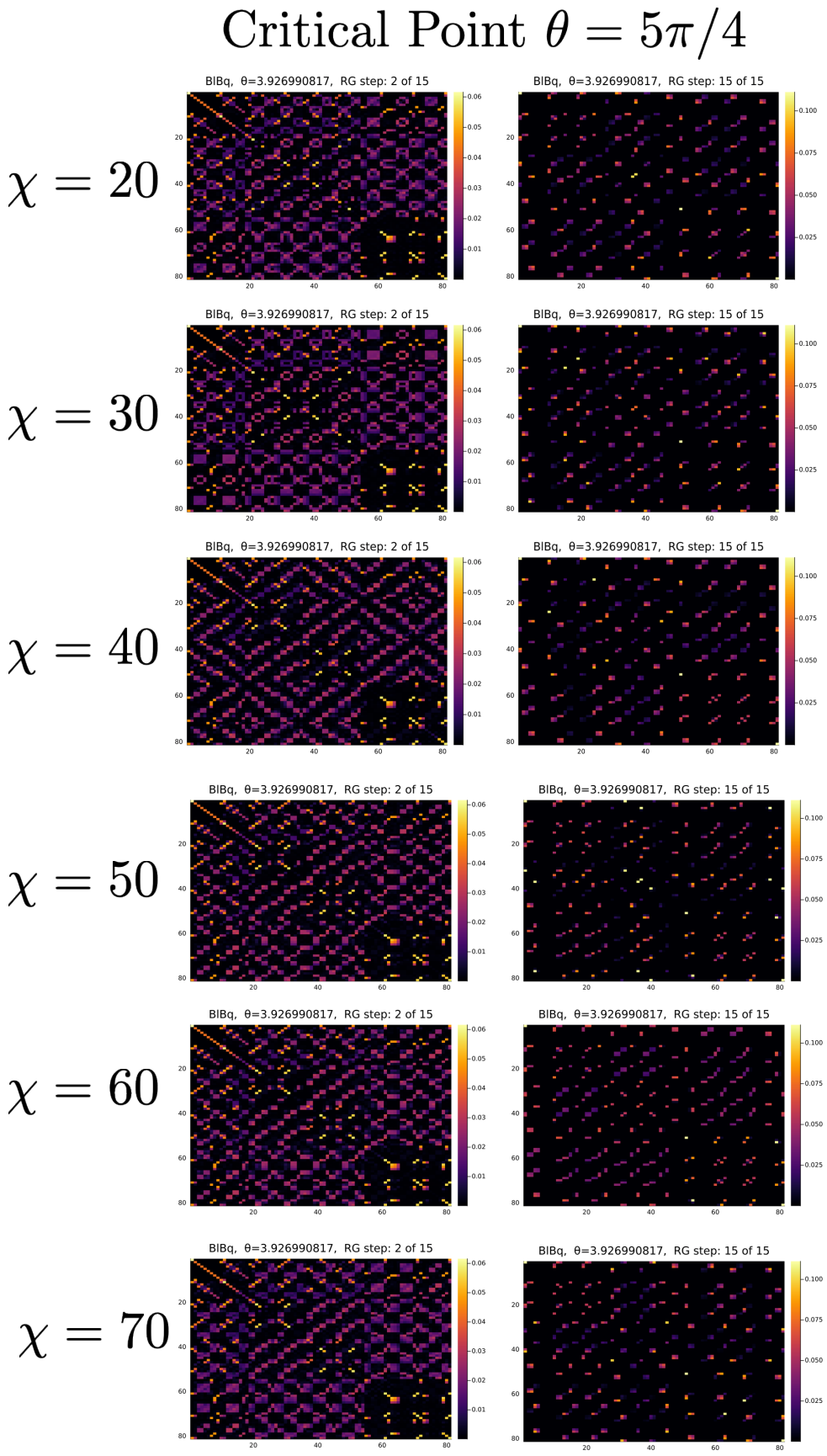

Figure 3.4: Isotropisation and tensor renormalisation at the critical point for fixed coarse-graining iterations and angle $\theta = 5\pi/4$. We can see in this image that even when greatly increasing the bond dimension the tensors preserve their structure no matter the bond dimension.

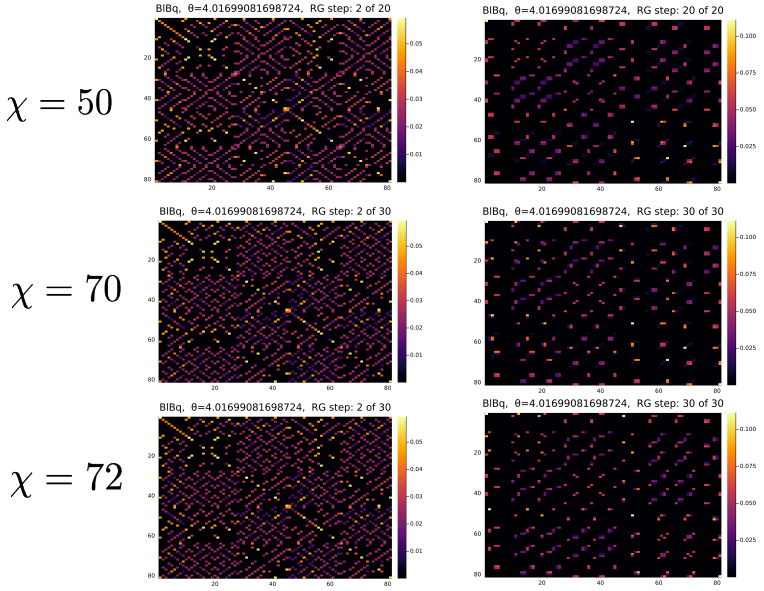

Figure 3.5: Isotropisation and tensor renormalisation near the critical point for fixed coarse-graining iterations and fixed angle $\theta \approx 4.017$. At this point the results show a renormalisation process but there is no great difference from that at criticality.

Chapter 4

Tensor renormalisation of Spin-1 systems in 2D

4.1 Bilinear Biquadratic Heisenberg Model

Just as in 1D, the study of spin-1 systems in 2D has also been a very active research area in the last decades [37, 127, 77, 131, 94], showing promise in describing difficult quantum phases like iron-based superconductors or nematic orders [3, 39, 113, 74, 58] and of particular recent interest, due to their relation with non-Abelian chiral spin-1 liquids as candidates for quantum computation [82]. Just as before, we start with the bilinear-biquadratic Hamiltonian

$$H = J\cos\theta\,\mathbf{S}_1\cdot\mathbf{S}_2 + J\sin\theta(\mathbf{S}_1\cdot\mathbf{S}_2)^2. \tag{4.1}$$

where $\mathbf{S}_i = (S_i^x, S_i^y, S_i^z)$ is the spin-1 operator at site i.

The phase diagram of the bilinear biquadratic Heisenberg in 2D model has been studied with classical and semiclassical methods [99, 116, 96], but due to a sign problem in the top right quadrant of the phase diagram (see Fig. 4.1) the use of tensor network methods [95] is sensible. Interesting phenomena take place at specific values of θ, where we see a rich phase diagram showing classically ordered phases (FM, AFM, etc.) and a top right quadrant with inaccessible phases for classical, semiclassical or even quantum Monte Carlo methods. For example, a Haldane-AFM phase transition was seen only recently using the iPEPS tensor network [95]. Also, for $\theta = \pi/4$ an emergent analogue of the $SU(3)$ Heisenberg model emerges, showing a sign-problem [83]. Experimental realisations of this model include ultra-cold atom experiments [19, 40], where it may be useful in the construction of quantum clocks and in quantum information processing. On the other hand, it may describe exotic phases of matter that can be readily verified experimentally such as spin-nematic phases in $NiGa_2S_4$ [117]. These phases still have open questions which may be understood by applying the methods proposed in this project.

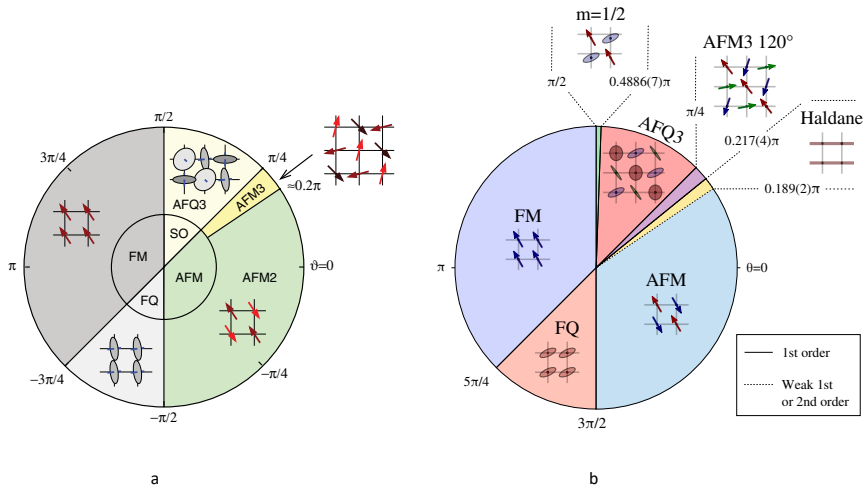

Figure 4.1: **Phase diagram of the $S = 1$ BBH model on the square lattice.** **a**) The inner circle shows a variational approach, while the outer one a numerical result by exact diagonalisation. Ferromagnetic and antiferromagnetic are ferro- and antiferromagnetic, FQ is ferroquadrupolar, while SO stands for semiordered. Shown in the outer circle are the three-sublattice ordered antiferromagnetic (AFM3) and antiferroquadrupolar (AFQ3) phases between $\theta \approx 0.2\pi$ and $\pi/4$ and between $\pi/4$ and $\pi/2$, respectively (Figure reproduced from [116]). **b**) Phase diagram using the iPEPS tensor network. Two new phases are shown, a gapped Haldane phase and a partially nematic and partially magnetic phase $m = 1/2$ in the region near $\theta = \pi/2$. (Figure reproduced from [94]).

4.2 Phase diagram for the spin-1 bilinear-biquadratic Heisenberg model in 2D

In 1988, Papanicolaou [99] examined the spin-1 bilinear-biquadratic Heisenberg (BBH) model by analysing its product states. The bipartite property of the square lattice guarantees some simplification. The results of Ref. [99], similar to those of 1D, revealed distinct ordered or semi-ordered phases. To minimise the energy of two interacting particles, one sublattice state must be quadrupolar while the other could be quadrupolar with a perpendicular director, magnetic with a moment aligned to the first sublattice's director, or a combination of both.

The phase diagram (see Fig.4.1) shows several $SU(3)$ points when the sine and cosine have the same value. A notable finding is that at each SU(3) point, the product ground states on either side are simultaneously valid. These states may be rotated into each other using elements of the $SU(3)$ group. The significant possible quantum fluctuations on the top right quadrant near these points suggests high degeneracy of the product ground state. The discovery of diverse ground states opens up intriguing possibilities for various types of ordering. For example, the ability for neighbouring directors to be perpendicular in three orientations enables a three-sublattice ground state—a surprising feature given the nearest-neighbour interactions on a bipartite lattice.

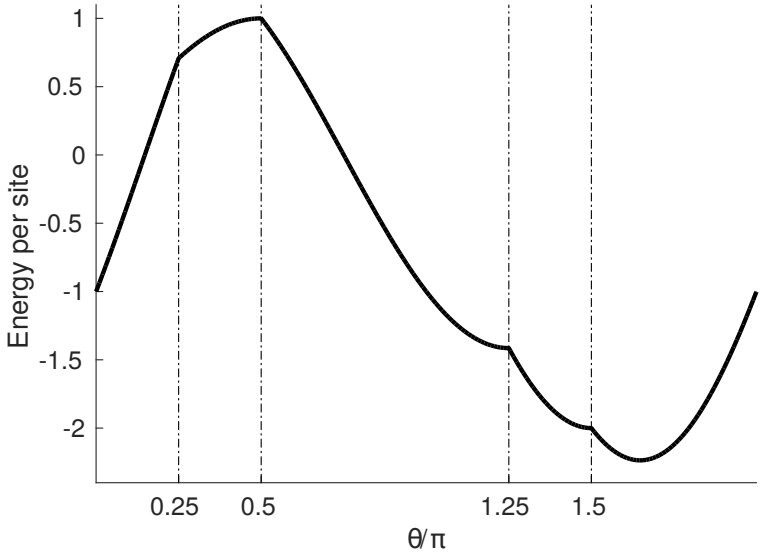

Figure 4.2: Energy per site for the product ground state, showing distinct jumps at the SU(3)-symmetric points, suggests that phase transitions are of first order.[116]

In 2002, Harada and Kawashima [51] studied the lower half of the phase diagram ($-\pi \leq \theta \leq 0$) using quantum Monte Carlo methods, noting the absence of sign problems. Their findings confirmed and matched Papanicolaou's phase diagram. The main observations were the existence of kinks in the quadrupolar order parameter near the SU(3) points $\theta = 5\pi/4$ and $3\pi/2$, consistent with the results and analysis of Ref. [99]. This, at least partially, confirmed that the phase transitions from the AFM phase to the FM phase, and from the FQ phase to the FM phase are first order.

Building on this, [116] used exact diagonalisation and linear-flavour-wave methods to study the SU(3)-symmetric point $\theta = \pi/4$ in 2010. They found that the ground state prefers a three-sublattice configuration over a two-sublattice one due to its lower zero-point energy. This three-sublattice order was further validated by DMRG and iPEPS simulations.

In Ref. [116] the investigation was extended to understand if the three-sublattice phase persists beyond $\theta = \pi/4$. They identified a three-sublattice antiferro-quadrupolar (AFQ3) state within the semi-ordered phase, where neighbouring sites have perpendicular directors. Interestingly, they also observed that the AFQ3 state extends into the AFM region, where, for $0.2\pi \lesssim \theta < \pi/4$, a 120° magnetic order emerges instead of the conventional antiferromagnetic order. This result was later corroborated by series expansion techniques.

4.3 Phases and phase transitions

This discussion of the phases in the 2D case uses Fig.**??** as reference. We begin by exploring the established boundaries of the phase diagram for $\theta \in [0, \pi/4]$.

Antiferromagnetic Phase.

At $\theta = 0$, we obtain the familiar spin-1 Heisenberg model, exhibiting antiferromagnetic order. Unlike for $\theta > 0$, Quantum Monte Carlo simulations do not encounter sign problems here. The sublattice magnetisation $m = \sqrt{\langle S_x \rangle^2 + \langle S_y \rangle^2 + \langle S_z \rangle^2}$ has been accurately measured as $m = 0.805$, with tensor network results closely agreeing at $m = 0.802$. States in the antiferromagnetic phase display U(1) symmetry.

Three-sublattice antiferromagnetic phase.

At $\theta = \pi/4$, the SU(3) Heisenberg model is regained, with a three-sublattice ordered state. Slightly below $\theta = \pi/4$, this order manifests as 120° magnetic order on three sublattices, as shown in Fig. (4.1). Magnetisation per site ranges from $m \approx 0.4$ at $\theta = 0.22\pi$ to $m \approx 0.1 - 0.3$ near $\theta = \pi/4$. AFM3 states lack residual spin-rotation symmetry.

Intermediate paramagnetic phase.

Ref. [116] suggests a phase transition between the antiferromagnetic and the 120° magnetically ordered states which is direct around $\theta \approx 0.2\pi$, based on exact diagonalisation and series expansion. Further attempts using tensor networks[94], determined the critical value at $\theta_c \approx 0.21\pi$ (for bond dimension $D = 10$), matching previous antiferromagnetic predictions. However, a systematic analysis [94] indicates that the antiferromagnetic order actually vanishes before θ_c, remaining stable only up to $\theta = 0.189(2)\pi$. This suggests a paramagnetic phase between the two ordered phases [116].

Region Around $\theta = 0.2\pi$.

iPEPS simulations [94] reveal that a weakly magnetised state and a non-magnetised state with no rotational symmetry. In [94] it is proposed that the observed breaking of rotational symmetry may be due to an effect similar to coupled one-dimensional chains. In other words, given that the ground state of the bilinear biquadratic chain for $\theta \in (-\pi/4, \pi/4)$ is in the Haldane phase, one may wonder whether the intermediate two-dimensional phase could connect smoothly to the Haldane phase by taking the coupling to zero. Initial indications supporting this idea come from simulations where the iPEPS is initialised as a product of 1D chains.[94]

Anisotropic Spin-1 Model.

In studying the anisotropic spin-1 model, we set coupling strengths in the x and y directions across the (θ, J_y) plane, with $J_x = 1$. For $J_y = 0$, the system reduces to independent spin-1 chains, which exhibit the Haldane phase for $\theta \in (-\pi/4, \pi/4)$. The aim is to determine the critical coupling $J_y^c(\theta)$ that separates the Haldane phase from the antiferromagnetic or 120° magnetically ordered phases at higher θ.

To estimate $J_y^c(\theta)$ at fixed θ, Ref. [94] used iPEPS simulations initialised in the Haldane phase and the antiferromagnetic or 120° ordered phase, varying J_y

with a fixed bond dimension $D = 10$ using simple update optimisation. The resulting phase diagram provides an approximate boundary due to computational constraints, though less precise than extrapolated full update simulations used in isotropic cases.

At $\theta = 0$, $J_y^c(0)$ is determined as 0.042, aligning closely with Quantum Monte Carlo results. This value deviates significantly from the isotropic limit $J_y = 1$. Notably, $J_y^c(\theta)$ increases monotonically with θ, confirming continuity from the one-dimensional Haldane phase to the isotropic two-dimensional limit beyond $\theta_c = 0.200\pi$.

For $0.213\pi \leq \theta < \pi/4$, $J_y^c(\theta)$ marks the critical transition value between the Haldane and 120° magnetically ordered phases, decreasing with increasing θ. Comparisons with full update simulations suggest slight underestimation of the Haldane phase extent at the isotropic point, within a margin of 0.01π or less for $\theta = 0$, but still supporting a continuous phase transition between the two-dimensional and one-dimensional phases.

For the isotropic case ($J_y = 1$), precise determination of the transition from the supposed Haldane phase to the 120° magnetically ordered phase was achieved, identifying $\theta_c = 0.217(4)\pi$ where the Haldane phase state energy crosses that of the 120° state.

Claims regarding the existence of a Haldane phase remain contentious. While [94] proposed a Haldane phase in a limited region, there is no conclusive evidence of its presence within the narrow regime between the Néel magnetic order phase and the nematic spin liquid phase suggested by [58]. State-of-the-art DMRG results do not decisively support the existence of such a phase [58].

Nature of the Phase Transition from antiferromagnetic to Haldane

At $\theta = 0.189\pi$, a transition occurs between the AFM and Haldane phases. In the antiferromagnetic phase, magnetisation per site decreases as it approaches the alleged Haldane phase, this indicates a possible second-order phase transition.[94] This is atypical as both phases break different lattice translation, rotation, and spin-rotation symmetries. Although no clear hysteresis behaviour was observed, [94] indicating a second-order transition, the uncertainty in magnetisation near the transition leaves open the possibility of a weakly first-order transition. Ref. [108] first described this transition for general SU(N) of the Hamiltonian and for large N. Theoretically these phases can be described by non-linear sigma models at large distances, with the order parameter $\boldsymbol{n}$ representing the staggered magnetisation $(-1)^{x+y}\boldsymbol{S}_{(x,y)}$.

Haldane to antiferromagnetic3

At $\theta = 0.217(4)\pi$, the transition from the Haldane to the three-sublattice 120° magnetically ordered phase shows hysteresis effects,[94] allowing simulations on both sides of the transition. The sublattice magnetisation remains positive throughout the AFM3 phase, even at $\theta = 0.21\pi$, indicating it remains the lowest energy state. This contrasts sharply with the Haldane phase, where magnetisation

is zero, demonstrating a clear first-order transition with a jump to zero at the critical point.

Isotropisation Step

We propose an isotropisation step similar to that of the 1D case. Here, however, the main idea is that by using a series of SVDs we can isotropise a tensor network in 2D. This is the main result of this chapter. The main idea is shown in figure 4.3 where an SVD of the following form is performed. This step as far as we know has not been published anywhere.

$$A^{3\delta}_{7\alpha} \rightarrow B^{\chi}_{7\alpha} C^{3\delta}_{\chi} \tag{4.2}$$

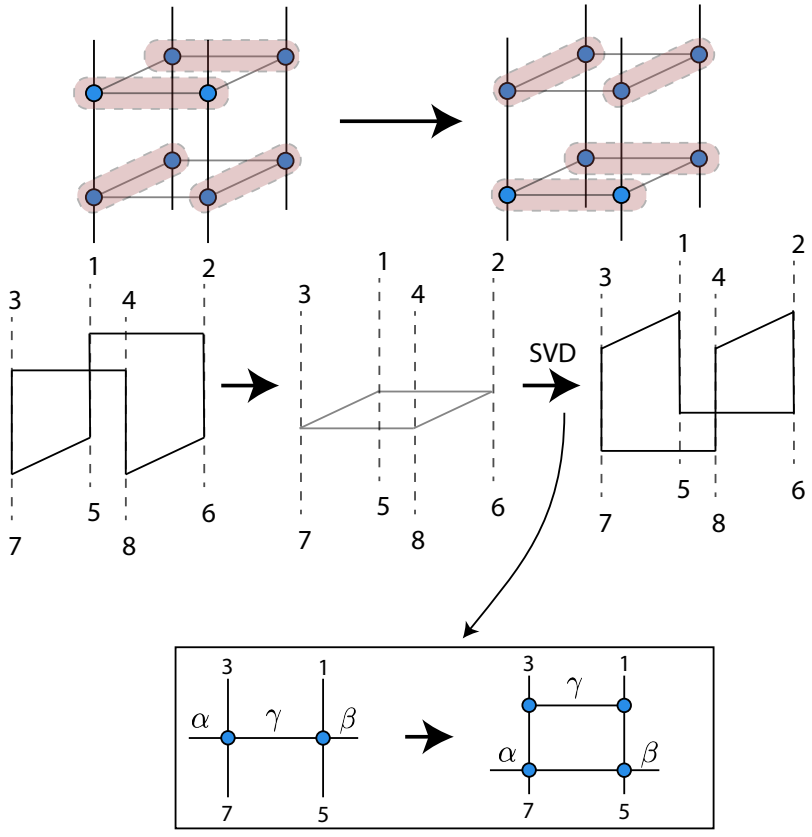

Figure 4.3: This image shows the way in which the isotropisation is done on a 3D lattice, or a 2D quantum system. The main idea is that with a series of SVDs one can isotropise the lattice and then we can work with it just as in the 1D case.

4.4 Discussion

In this section we showed an overview of the different phases that happen in the 2D spin-1 bilinear biquadratic model. The main scientific questions remain near several enhanced $SU(3)$ symmetric points, where highly entangled ground states provide no shortage of interesting possible phases. The idea that a Haldane phase may exist near one of this points is still controversial, and as in the 1D case, the best approaches have been made using tensor networks, but not using tensor renormalisation techniques.

4.5 Conclusion of first part

In this first part, we have explored the quantum phase diagram of the spin-1 bilinear-biquadratic model on 1D and on 2D on the square lattice. We have shown the basic theoretical as well as the mathematical tools to explore these systems. For the case of the 1D spin-1 system we showed a method to renormalise quantum spin chains, meaning that we developed a two-step method consisting of a so-called isotropisation step, bringing the tensor network into a more isotropic form, which is better for computations; the second step consists of a series of iterations using the tensor renormalisation network method. With this method, one can obtain proper renormalisation group flows to fixed points. As showed, the method can distinguish the different phases in the 1D case, both at criticality and ordered phases. For the 2D case we presented only the methodology and the appropriate isotropisation step.

These findings suggest exciting experimental avenues for exploring novel magnetic phases. While naturally occurring spin-1 systems with the requisite strong biquadratic interactions remain elusive, ultracold atomic systems offer a promising platform for realising the predicted phases both in 1D and 2D. Among others, the study of Mott-insulating states in optical lattices provide a strong foundation for this pursuit. Crucially, the N-independence of the exchange integral in $SU(N)$ systems suggests that achieving the relevant exchange energy scale for $SU(3)$ fermions should be feasible, given current progress with $SU(2)$ systems. Experimentally, careful selection of the Mott insulating regime is essential: it must be large enough to realise the $SU(3)$ Heisenberg model, yet sufficiently small to allow access to the exchange energy scale.

Part II

Non-Fermi liquids

Chapter 5

Introduction

This second part of the thesis studies the problem of non-Fermi liquids (NFLs). The objective is to better understand the macroscopic behaviour of interacting fermions, particularly their Fermi surfaces and associated instabilities. These phenomena are fundamental and manifest across various contexts and scales, such as in metals, neutron stars, and quark-gluon plasmas. Here, we aim to develop a formalism based on the hypothesis of a loop $U(1)$ symmetry in the infrared (IR) regime of non-Fermi liquids [32]. By quantising this group via the orbit method [69] and describing its representations, the aim is to develop a framework that aligns with observed non-Fermi liquid behaviour. This approach, while abstract, may provide some insight to these complex systems.

Non-Fermi liquids are metallic states with unconventional properties not described by the weakly coupled Fermi liquid theory. They arise from strong interactions involving soft fluctuations at the Fermi surface coupled to massless bosons. A key challenge in studying them is the absence of a clear organising principle [79]. Naively, to identify the roots of these difficulties in NFLs one can start by framing them into the broad classification of gapped and gapless systems.

Gapped systems typically exhibit topological order with no low-energy excitations, with the exception of fracton excitations [106, 110]. Gapless systems can possess either finite or infinite low-energy degrees of freedom. The former often characterise phase transitions or topological phase boundaries, while the latter, typically systems with Fermi surfaces, have a finite density of states at zero energy (e.g., conventional metals, half-filled Landau level, among others). Classifying matter within Fermi surfaces remains challenging due to their potential instabilities.

Fermi liquid theory remains the starting point in discussing non-Fermi liquids—among other reasons because Fermi-surface physics, or generalisations thereof, are crucial to understanding fundamental properties like Luttinger's theorem. The initial idea of Fermi liquid theory was to consider a free Fermi gas and introduce interactions among fermions [76, 10]. Fermi liquid theory says that these interactions do not change the excitations of a free Fermi gas, leading to the concept of quasiparticles. These low-energy quasiparticles occupy a codimension-1 surface in momentum space, which is known as the Fermi surface. Despite its success in describing dense, interacting fermions, the theory stood out among other effective theories for not using renormalisation group (RG) methods and for

being classical and phenomenological in nature. This is surprising in part because Fermi liquid theory is not a free field theory, i.e., a low-energy effective field theory governed by a kinetic equation. Nonetheless it paved the way for subsequent field theories using the renormalisation group, for example, Refs. [11, 104, 112] made possible the modern formalism. Working examples of these theories are simpler but lose spatial locality, making it not a true effective field theory as it cannot systematically list irrelevant corrections to the scale-invariant fixed point [2, 92]. An alternative local effective field theory inspired by bosonisation [50, 17, 57], also faces issues in classifying irrelevant corrections. These formalisms are thus incomplete and require further refinement [26]. The other type of interactions among fermions are long range interactions, associated with gapless modes, cannot be ignored at any energy scale and must be tracked alongside the excitations of the Fermi surface. These interactions, often strong, can unpredictably alter Fermi surface physics.

As mentioned above, non-Fermi liquids are intricate systems characterised by gapless modes that couple to the Fermi surface, inducing instabilities akin to superconductivity [30]. However, in contrast to conventional superconductivity, these instabilities arise from interactions mediated by gauge fields and their critical fluctuations. The renormalisation group flow of these systems remains poorly understood, leaving the ultimate fate of the system an open question: does it evolve into a metallic phase, a Mott insulator, or an unconventional superconducting state?

From a practical standpoint, understanding non-Fermi liquid physics is essential for comprehending materials such as the cuprates, which often exhibit a quantum critical point that drives the system towards a superconducting instability. Unlike typical renormalisation group flows between two fixed points with conformal symmetry or just scale invariance, NFLs possess a scale. In any case, given this anomalous behaviour, it is plausible to conjecture that non-Fermi liquids might harbour unconventional renormalisation group flows, different but perhaps analogous to those proposed for fractonic systems [110, 75].

Finally, a remaining theoretical question in the study of NFLs is how to construct a suitable effective field theory. Recent attempts at building effective field theories rely on sophisticated methods such as geometric quantisation [26] or holographic methods[31]. Some questions remain, however, because the scaling properties of non-Fermi liquids deviate substantially from those of their Fermi liquid counterparts. Briefly, developing a classification of irrelevant corrections both for Fermi liquids and non-Fermi liquids with well-defined scaling dimensions is crucial for advancing our understanding of them. Another question in formulating these effective theories is how to include a proper matching of UV and IR matching constraints, e.g., Luttinger's theorem, charge filling constraints, as well as more empirical constraints such as compressibility.

5.1 Review of Fermi Liquid theory

Landau introduced the initial description of Fermi liquids through a kinetic equation framework (see Ref. [76, 10] for a detailed account). The starting

point is a noninteracting Fermi gas, where Pauli's exclusion principle forbids two fermions from occupying the same state. This restricts each momentum state to accommodate only opposite-spin fermions. At zero temperature, these occupied states form a codimension-1 surface in momentum space, called the Fermi surface, below which states are occupied or empty if outside of it. At zero temperature it takes the form of a step function which depends both on momentum and spin $\epsilon(\mathbf{p}, \sigma)$—we will often disregard the spin component for simplicity:

$$n_0(\mathbf{p}, \sigma) = \Theta\left(\epsilon_F - \epsilon(\mathbf{p}, \sigma)\right),$$

this defines a Fermi sea occupied up to the Fermi momentum $\mathbf{p}_F$, an associated Fermi energy ϵ_F and $\epsilon(\mathbf{p}, \sigma)$ represents the dispersion relation and $\epsilon(\mathbf{p}) = \epsilon_F$ defines the Fermi surface at $|\mathbf{p}| = p_F$.

The semi-classical dynamics of this system is described by a distribution function

$$n(t, \mathbf{r}, \mathbf{p}) = n_0(\mathbf{p}) + \delta n(t, \mathbf{r}, \mathbf{p}), \tag{5.1}$$

obeying the kinetic equation

$$\partial_t n + \nabla_{\mathbf{p}} \epsilon(\mathbf{p}) \cdot \nabla_{\mathbf{r}} n + \mathbf{F} \cdot \nabla_{\mathbf{p}} n = 0, \tag{5.2}$$

where $\mathbf{F}$ is a force applied to the non-interacting Fermi gas. Therefore, the free Fermi gas dynamics is governed by the dispersion relation. Note that this distribution function is not enough to describe the dynamics. This is in part because when including interactions, the occupation is ill-defined. Landau's approach [76] to this problem involves starting with a free Fermi gas and adiabatically introducing interactions, the system then evolves smoothly from a non-interacting free system to an interacting one. Near the Fermi surface is where all scattering occurs, this is due to the exclusion principle. Furthermore, the spectrum should smoothly connect to that of the free Fermi gas. This suggests that particles near the Fermi surface (either a particle outside or a hole inside) will serve as the building blocks for the spectrum of the non-interacting system. As this characteristic will persist both as an effective but modified way in the low energy spectrum of the interacting theory, they are extremely relevant in writing down a Fermi liquid theory. Landau called these modified or dressed particles quasiparticles. characteristic persists as we turn adiabatically on the interactions, and they persist in an effective way within the spectrum of low energy of the Fermi liquid, These are called quasiparticles. In other words, in the interacting Fermi system, particles are replaced by quasiparticles which are emergent and which behave effectively as the original particles in terms of charge and spin, but with a different effective mass.

Quasiparticles in turn obey a different distribution

$$n(t, \mathbf{r}, \mathbf{p}) = n_0(\mathbf{p}) + \delta n(t, \mathbf{r}, \mathbf{p}), \tag{5.3}$$

where δn is the deviation of the distribution function of the quasiparticles from a system in equilibrium. This makes sense only near the Fermi surface. The disper-

sion relation of the quasiparticle is the only ingredient necessary for describing the low-energy dynamics in the interacting regime. Namely, one can write

$$\epsilon_{\mathrm{qp}}(\mathbf{r},\mathbf{p}) = \epsilon(\mathbf{p}) + \int \frac{d^d p'}{(2\pi)^d} F\left(\mathbf{p},\mathbf{p}'\right) \delta n\left(\mathbf{r},\mathbf{p}'\right), \tag{5.4}$$

where $\epsilon(\mathbf{p})$ is the dispersion relation for free fermions, and $F\left(\mathbf{p},\mathbf{p}'\right)$ is a term that represents the effective interactions exerted on a quasiparticle due to interactions with its surrounding quasiparticles. This equation is crucial for understanding the transport properties of Fermi liquids due to its inherent locality.

A kinetic equation, known as Landau's kinetic equation, captures the dynamics of the system:

$$\partial_t n + \nabla_{\mathbf{p}} \epsilon_{\mathrm{qp}}(\mathbf{p}) \cdot \nabla_{\mathbf{r}} n - \nabla_{\mathbf{r}} \epsilon_{\mathrm{qp}}(\mathbf{p}) \cdot \nabla_{\mathbf{p}} n = 0, \tag{5.5}$$

where $\nabla_{\mathbf{r}} \epsilon_{\mathrm{qp}}(\mathbf{p})$ is the force term including all the effective contributions and $\nabla_{\mathbf{p}} \epsilon_{\mathrm{qp}}(\mathbf{p})$, the quasiparticle velocity which depends on nonlinear deviations in δn.

The Landau function, which is the interaction term $F\left(\mathbf{p},\mathbf{p}'\right)$ is parametrised by angles θ, θ' near the Fermi surface. By expanding the the Landau function in terms of the angle variables

$$F\left(\theta,\theta'\right) \sim \sum_l F_l P_l^{(d)}\left(\theta,\theta'\right), \tag{5.6}$$

we obtain a family of parameters called Landau parameters, where $P_l^{(d)}\left(\theta,\theta'\right)$ are spherical harmonics or more generally they are covariant basis functions that depend on the symmetries of the system, where the index labels the representation. From (5.5) and (5.6), one can compute much of the thermodynamical properties. The theory also predicts stability conditions as lower bounds on F_l, violations of which indicate instabilities in the system, leading to Pomeranchuk instabilities. Moreover, FLs may exhibit collective excitations, distinguishable from the particle-hole continuum $\omega \leq v_F|\mathbf{q}|$.

However, despite its successes, the Landau-Fermi liquid theory has limitations. Its emergence from microscopic models remains unclear, the description based on the kinetic equation with quantum effects is limited to the Fermi-Dirac statistics and the exclusion principle. For instance, the existence of quantum critical points significantly influences the finite-temperature properties of these systems. Near these points, the conventional Fermi liquid theory breaks down, giving rise to a non-Fermi liquid state characterised by the absence of well-defined Landau quasiparticles. This anomalous behaviour stems from the intricate interplay between electronic excitations and the critical fluctuations of the order parameter. In this regime, electron-electron interactions are mediated by these critical fluctuations, leading to pronounced deviations from Fermi liquid behaviour. Ultimately, the influence of these fluctuations can be so substantial that the quasiparticle concept itself becomes invalid. To potentially overcome these limitations, a field-theoretic approach, amenable to the renormalisation group (RG) unlike Landau's theory, might provide deeper insights into the quantum aspects of Fermi liquids.

The conventional approach, which involves scaling momenta to zero, is inadequate as it integrates out the modes whose correlation functions are of interest (namely, those proximate to the Fermi level). Consequently, this method lacks predictive power as it yields a theory exclusively describing degrees of freedom deep within the Fermi sea. The Shankar-Polchinski RG scheme [112, 104] scales momenta towards the Fermi surface, preserving some physical relevance and yielding more meaningful results for the study of Fermi liquids.

This RG approach, introduced in Refs. [11, 112, 104], however incomplete, offered a first promising way to explore the quantum aspects of Fermi liquids beyond Landau's framework. Landau-Fermi liquid theory says that low-energy excitations in a Fermi liquid can be described as quasiparticles. We introduce creation and annihilation operators, $\psi^\dagger_\sigma(\mathbf{p})$ and $\psi_\sigma(\mathbf{p})$, respectively, where σ is the spin index. The operator $\psi^\dagger_\sigma(\mathbf{p})$ creates a quasiparticle with momentum $\mathbf{p}$ and spin σ, while $\psi_\sigma(\mathbf{p})$ creates a hole in the momentum state $\mathbf{p}$ with spin σ. Crucially, a hole at momentum $-\mathbf{p}$ and spin σ corresponds to a net momentum of $+\mathbf{p}$ for the system. The free action for these quasiparticles is expressed as:

$$S = \int \frac{dt\, d^d p}{(2\pi)^d} \sum_{\pm\sigma} \psi^\dagger_\sigma(\mathbf{p}) \left[i\partial_t - (\epsilon(\mathbf{p}, \sigma') - \epsilon_F) \right] \psi_\sigma(-\mathbf{p}). \tag{5.7}$$

Any momentum vector $\mathbf{p}$ can be decomposed into a component $\mathbf{p}_F$ lying on the Fermi surface and a perpendicular component $\mathbf{k}$, such that:

$$\mathbf{p} = \mathbf{p}_F + \mathbf{k}. \tag{5.8}$$

Within this renormalisation group (RG) framework, $\mathbf{p}_F$ remains unchanged under scaling, whereas $\mathbf{k}$ is rescaled by a factor $s \leq 1$ to $s\mathbf{k}$. The dispersion relation can be linearised and expanded, near the Fermi surface as follows

$$\epsilon(\mathbf{p}) - \epsilon_F = \mathbf{k} \cdot \mathbf{v}_F(\mathbf{p}_F) + \mathcal{O}(k^2),$$

The linearisation is only valid below an absolute value of momentum, which is dependent on the material. To ensure the free action remains scale-invariant, the following dimensional assignments are necessary: $[\partial_t] = [\mathbf{k}], \quad [\psi] = -\frac{1}{2}$. To understand the scaling of the system, we write all terms up to loop levels, then we select the contributions that are permissible by the system's symmetry, which leads to an interaction term that allows scattering processes

$$\int_t \int_{\mathbf{p}_1\mathbf{p}_2\mathbf{p}_3\mathbf{p}_4} V\left(\mathbf{p}_{F1}, \mathbf{p}_{F2}, \mathbf{p}_{F3}, \mathbf{p}_{F4}\right) \psi^\dagger_\sigma\left(\mathbf{p}_1\right) \psi_\sigma\left(\mathbf{p}_2\right) \psi^\dagger_\sigma\left(\mathbf{p}_3\right) \psi\left(\mathbf{p}_4\right) \delta\left(\mathbf{p}_1 + \mathbf{p}_2 - \mathbf{p}_3 - \mathbf{p}_4\right).$$

Due to the scaling dimensions of fermionic fields, all momentum-dependent terms in the interaction are deemed irrelevant under renormalisation group analysis. The remaining momentum-independent term is marginal but still exhibits angular dependence with respect to the Fermi surface for incoming and outgoing particles.

In other words, the delta function has either trivial or non-trivial scaling. Trivial scaling means that it shows some scale invariance when the sum of Fermi momenta is non-zero, while non-trivial scaling occurs when the momenta sum to zero.

That is, for configurations where the sum of Fermi momenta is non-zero, the delta function is scale-invariant, and the interaction term is irrelevant. On the other hand, for configurations where the sum of Fermi momenta is zero, then the delta function has non-trivial scale-invariance under the renormalisation group, and the quartic term is marginal. After checking that the sum is zero, then we can see if relevant configurations modify their scaling behaviour with loop corrections.

While Landau-Fermi liquid theory successfully captures forward scattering interactions, it remains blind to the pairing instabilities crucial for understanding superconductivity, a phenomenon described by the BCS coupling. The renormalisation group (RG) approach surpasses Landau theory in this regard, offering a framework to incorporate these instabilities, thereby demonstrating the efficacy of effective field theories.

However, the RG approach faces challenges. Power counting, which assigns fixed scaling dimensions to terms based on symmetry, breaks down in this context. The quartic interaction term exemplifies this issue, showing complex scaling behaviour, especially in higher dimensions and intricate Fermi surface geometries. Consequently, terms often lack well-defined scaling dimensions and need decomposition into sums with fixed scaling properties. Even then, intricate relationships arise between unrelated terms, such as the equivalence between forward scattering and BCS couplings under specific conditions. These connections result from the decomposition process, introducing redundancy into the theory.

Moreover, coupling this effective field theory to background gauge fields, a fundamental task in many systems, presents a significant challenge. Unlike Landau-Fermi liquid theory, which operates in real space, the momentum-space formulation of the effective field theory makes standard minimal coupling techniques inapplicable.

To overcome these limitations, researchers have developed alternative approaches and formalisms. Additionally, new functional RG schemes, such as those by Borges et al.[13] and Ma and Lee[84], aim to expand the RG framework beyond Shankar-Polchinski.

A key insight from the Shankar-Polchinski RG is the importance of particle-hole interactions at short momentum scales for phenomena beyond superconductivity. This leads to a strategy of discretising the Fermi surface into patches, providing a potential solution to the problem of poorly defined scaling dimensions.

The free fermion action, when expressed in spatial coordinates, adopts the form:

$$S = \sum_{\eta} \int d^{d-1}r_{\parallel} \int dt\, dr_{\perp}\, \Psi^{\dagger}_{\eta}(r_{\perp}) \left(\partial_t + v_{F\eta}\partial_{r_{\perp}}\right) \Psi_{\eta}(r_{\perp}),$$

where $r_{\perp}$ is the spatial conjugate of $\mathbf{k}$, the momentum perpendicular to the Fermi surface, and $\mathbf{r}_{\parallel}$ denotes in-plane coordinates within a specific region.

Patch-Based Approach and Its Limitations

The Shankar-Polchinski renormalisation group (RG) method partitions the Fermi surface into discrete segments labelled by η. Interactions confined to a single segment (intra-patch) are distinguished from those spanning multiple segments (inter-patch). By isolating a particular segment, η_0, inter-segment influences can be disregarded. While rescaling momenta towards the Fermi surface simplifies intra-segment couplings, it distorts the segment shape at low energies. An alternative RG approach preserves segment curvature by scaling in-plane coordinates as $(r_\perp)^{1/2}$, maintaining scale invariance of curvature terms but introducing additional segments at the fixed point.

Despite its utility in revealing non-Fermi liquid behaviour through gapless mode-mediated interactions, the fermionic patch framework suffers from inherent limitations. Notably, it lacks a local representation in physical space, is incompatible with BCS interactions, and cannot directly compute physical observables like transport coefficients without considering all segments collectively. Furthermore, while it facilitates calculations of scaling dimensions, the scaling behaviour of correlation functions remains elusive due to complex cancellations influencing infrared scaling patterns.

Bosonisation and Geometric Approaches

Drawing inspiration from bosonisation in one spatial dimension and one time dimension, a formalism that maintains locality in physical space maps each patch fermion to a chiral boson, yielding the effective action:

$$S = -p_F^{d-3} \sum_\eta \int dt\, d^d r \left(\mathbf{p}_{F_\eta} \cdot \nabla_{\mathbf{r}} \phi_\eta\right) \left(\partial_t + v_{F_\eta} \mathbf{p}_{F_\eta} \cdot \nabla_{\mathbf{r}}\right) \phi_\eta.$$

Although preserving locality, this approach encounters challenges analogous to patch theory under scaling [112], as it fails to incorporate any nonlinear contributions. These contributions may occur due to the Fermi surface's curvature or due to the dispersion relation. A geometric perspective, inspired by quantum Hall droplets, has been proposed as a step towards more advanced formalisms.

Deformation Quantisation and the Geometric Framework

This geometric perspective is rooted in the broader domain of geometric and deformation quantisation. Starting from a Poisson algebra, deformation quantisation constructs an associative algebra equipped with a product defined by:

$$F \star G = \sum_{n=0}^{\infty} \hbar^n B_n(F, G), \tag{5.9}$$

where the B_n are differential operators satisfying specific conditions. This procedure replaces Poisson brackets with commutators. By mapping functions of

coordinates and momenta to operators in Hilbert space, deformation quantisation necessitates an approximation to preserve the commutation relation:

$$[\mathcal{F}(f), \mathcal{F}(g)] = \mathcal{F}([f, g]_\star) = i\hbar\mathcal{F}(\{f, g\}) + \mathcal{O}(\hbar^2). \tag{5.10}$$

Applicable to any finite-dimensional Poisson manifold, deformation quantisation requires a quadratic field dependence in the free action for constructing a star product akin to the Moyal product in field theory.

The relevant Lie algebra comprises single-particle phase space functions endowed with a Moyal bracket, forming the Weyl algebra. The corresponding Lie group is constructed via the exponential map. While the orbit method may be applied to this algebra to describe Fermi surfaces, the Moyal bracket's power series nature limits its applicability to specific functions. To circumvent this limitation, one has to cut off the algebra which now gives the Poisson bracket

$$\begin{aligned} \{\{F, G\}\} &= \{F, G\} + \mathcal{O}\left(\nabla_{\mathbf{r}}, \nabla_{\mathbf{p}}\right)^3, \\ \{F, G\} &\equiv \nabla_{\mathbf{r}} F \cdot \nabla_{\mathbf{p}} G - \nabla_{\mathbf{p}} F \cdot \nabla_{\mathbf{r}} G, \end{aligned}$$

providing a semi-classical description of Fermi liquids through the truncated Lie algebra equipped with the Poisson bracket $\mathfrak{g} = (\{F(\mathbf{r}, \mathbf{p})\}; \{., .\})$.

An arbitrary element $F(\mathbf{r}, \mathbf{p})$ generates a canonical transformation, with transformed coordinates $\boldsymbol{r}', \mathbf{p}'$ forming canonical pairs. This transformation corresponds to Hamiltonian evolution under $F(\mathbf{r}, \mathbf{p})$, thus $\{F, G\}(\mathbf{r}, \mathbf{p})$ acts now as the commutator of two such transformations. The Lie group of Hamiltonian symplectomorphisms, denoted G, encompasses canonical transformations arising from time evolution under F.

State Space and Coadjoint Orbits

In quantum mechanics, states are represented by density matrices, which yield expectation values when acting on operators. By focusing on charge-neutral fermion bilinears, states can be distinguished based on identical expectation values for all such bilinears.

A state can be expressed using a basis $T(\mathbf{r}, \mathbf{p})$ for fermion bilinears and a dual basis $W(\mathbf{r}, \mathbf{p})$, with coefficients determined by a function $f(\mathbf{r}, \mathbf{p})$. In this language $\langle f, F \rangle$, is the expectation value of any fermionic operator. This collection of states constitutes the dual space of the Moyal algebra, denoted $\mathfrak{g}^*$, which is dual simultaneously to the Moyal and the Poisson algebras.

The coadjoint orbit method, as applied in [26], utilises the Lie algebra $\mathfrak{g}$ and its dual space $\mathfrak{g}^*$ to derive an action. This approach leads to Landau's kinetic equation for interacting Fermi liquids and higher-order corrections.

Obtaining an action through a Legendre transform necessitates restricting $\mathfrak{g}^*$ to states with values of 0 or 1, representing the Fermi surface and complying with Luttinger's theorem. This constraint is both physically justified and mathematically essential for describing well-defined Fermi surfaces at zero temperature.

Consequently, the formalism presented in [26] portrays Fermi liquid dynamics

as a fluctuating codimension-1 surface in phase space, resembling a sphere at each spatial point $\mathbf{r}$. This method is a type of bosonisation which among other things facilitates the solution of interacting fermionic problems in 1D. However for higher dimensions the bosonisation method might not be completely appropriate since the cancelations in fermion loops don't happen, except approximately. The flip side is that these near cancellations of n-point function are transparent in the bosonic picture, meaning the scaling is transparent. This is because the bosonic theory has small irrelevant interactions (rather than being a free theory in 1D) but will give the leading contributions to non-linear response.

Bosonisation in 2D establishes an isomorphism between fermionic and bosonic Fock spaces, implying a one-to-one correspondence of operators, though local operators map to non-local ones. In higher dimensions, this correspondence fails because fermionic states cannot be replicated by bosonic operators. However, in certain scenarios where fermionic fields lack gauge invariance and fermionic states are absent from the Fock space, a one-to-one correspondence might exist. Generally, though, such a correspondence is unreliable, limited by symmetry constraints. Consequently, the bosonic effective field theory can only match correlation functions of bosonic operators, and cannot, even in principle, reproduce single-particle correlation functions of fermionic operators.

Our approach diverges from [26] by centering on loop $U(1)$ groups instead of the employed space of transformations. With this in mind an effective field theory is possible in which we are not constraining by hand the possible operators that might occur.

Chapter 6

Non-Fermi liquids

Landau's Fermi liquid theory provides a successful framework for understanding most metallic phases by describing them in terms of quasiparticles and their interactions. However, certain metallic states, known as non-Fermi liquids (NFLs), exhibit unconventional properties that defy this model. These states typically emerge from strong interactions involving soft fluctuations at a Fermi surface or point, combined with massless bosonic fluctuations. Ongoing research aims to develop controlled approximations for NFL phases with a well-defined Fermi surface [92, 78, 90, 60].

Often referred to as strange metals, these states are observed in strongly correlated quantum materials such as cuprate and iron-based superconductors and heavy fermion systems [97, 5, 53, 16]. Unlike the expected quadratic temperature dependence, these materials frequently display linear resistivity across a wide temperature range, challenging conventional theories. NFL behaviour also encompasses unconventional scaling of optical conductivity and increased susceptibility to superconducting transitions [100, 29, 87].

In these systems, which maintain a well-defined Fermi surface but lack Landau quasiparticles, NFL characteristics arise from interactions between finite-density fermions and massless bosons or gauge fields at a quantum critical point [86, 25, 85]. Such states are sometimes termed critical Fermi surface states [111].

The Hertz-Millis approach models non-Fermi liquids as Fermi liquids coupled to a gapless mode, with an effective action formulated for the bosonic degrees of freedom after integrating out the fermions [54, 88]. The upper critical dimension for this coupling is $d = 3$, making the two-dimensional case particularly intriguing, as one-dimensional systems lack an extended Fermi surface and can be described using either exact or perturbative bosonisation methods, depending on dynamical exponents.

Hertz initially proposed integrating out the Fermi surface to obtain a non-local effective action for the gapless mode, but this approach lacked control. Subsequent progress was made using the Shankar-Polchinski renormalisation group (RG) scheme, employing both fermionic effective field theory [103, 2, 92, 93, 86] and bosonisation [68, 72, 78]. However, these methods are limited by the absence of a systematic expansion in fermionic theories or incompleteness in traditional bosonisation [85, 130].

A bosonised theory [26] offers advantages, capturing essential features of non-

Fermi liquids from a Gaussian theory. In two dimensions, the Gaussian truncation of the effective field theory couples to a bosonic field $\Phi(t, \mathbf{x})$ through the linearised density $S^{(2)}_{\mathrm{NFL}}$, representing a Gaussian theory tuned to criticality. The coupling includes a spin-l harmonic by multiplying with $\cos(l\theta)$.

This Gaussian action allows for an exact solution. The Φ propagator, exhibiting Landau damping, is given by:

$$\langle \Phi\Phi \rangle(\omega, \mathbf{q}) = \frac{i}{q^2 + k_0^2 - \langle \rho\rho \rangle(\omega, \mathbf{q})},$$

where $\langle \rho\rho \rangle$ is the tree-level density two-point function. For $\omega \ll v_F q$, setting $k_0^2 = -\frac{p_F \lambda^2}{2\pi v_F}$ at criticality yields:

$$\langle \Phi\Phi \rangle(\omega, \mathbf{q}) \simeq \frac{1}{q^2 - i\frac{p_F\lambda^2}{2\pi v_F^2}\frac{|\omega|}{v_F q}}, \quad \omega \ll v_F q,$$

from which the dynamical critical exponent $z = 3$ is derived.

The specific heat and its scaling in temperature can be obtained from the partition function,

$$Z(\beta) = \int D\phi D\Phi e^{-S_E},$$

where S_E is the Euclidean action, with imaginary time τ spanning $[0, \beta]$. Integrating over ϕ and then Φ shows that the partition function factorises into contributions resembling a Fermi liquid and a Landau-damped critical boson component and a Fermi liquid component:

$$Z = \det\left[q^2 + \frac{p_F\lambda^2}{2\pi v_F}\frac{|\omega_k|}{\sqrt{\omega_k^2 + v_F^2 q^2}}\right]^{-1/2} \det\left[q_n\left(-i\omega_k + v_F q_n\right)\right]^{-1/2}, \tag{6.1}$$

where $\omega_k = 2\pi T k$ are Matsubara frequencies with k taking integer values.

The free energy is

$$F = \frac{T}{V}\log Z \tag{6.2}$$

$$= -\frac{T}{2}\sum_k \int_{\mathbf{q}} \log\left[q^2 + \frac{p_F\lambda^2}{2\pi v_F}\frac{|\omega_k|}{\sqrt{\omega_k^2 + v_F^2 q^2}}\right] - \frac{T}{2}\sum_k \int_{\mathbf{q},\theta} \log\left[q_n\left(-i\omega_k + v_F q_n\right)\right]. \tag{6.3}$$

In this effective field theory, the Fermi liquid component requires appropriate ultraviolet / infrared regularisation. Its scaling behaviour can be estimated as $F_{\mathrm{FL}} \sim p_F T^2$.

The critical boson contribution at low temperature is then controled by infrared

frequencies $\omega_k \sim q^3 \ll v_F q$, simplifying the integral to:

$$\int_q \log\left(q^2 + \tilde{\lambda}^2 \frac{|\omega_k|}{q}\right) = \tilde{\lambda}^{4/3} \frac{|\omega_k|^{2/3}}{2\sqrt{3}}, \tag{6.4}$$

which is obtained after addressing a temperature-independent ultraviolet divergence. Here, $\tilde{\lambda}^2 = \frac{p_F \lambda^2}{2\pi v_F^2}$. There is one other divergent term, i.e., the Matsubara sum, which one can control by introducing an exponential term $e^{-\epsilon k}$ with $\epsilon > 0$, wiith the objective of suppressing large k contributions. Now, expanding for small ϵ and removing divergent terms gives:

$$\sum_k k^{2/3} \simeq \zeta\left(-\frac{2}{3}\right). \tag{6.5}$$

Therefore, the critical boson contribution to the pressure is:

$$P = -\frac{\zeta(-2/3)}{4\sqrt{3}} \tilde{\lambda}^{4/3} T^{5/3}. \tag{6.6}$$

As $T \to 0$, the $T^{5/3}$ term overwhelms the T^2 term, allowing us to neglect the Fermi liquid contribution. This resolves UV/IR mixing issues as the critical boson contribution remains unaffected. Consequently, the specific heat for, low temperature, should read

$$c_V = T\frac{ds}{dT} = T\frac{d^2P}{dT^2} = -\frac{5\zeta(-2/3)}{18\sqrt{3}} \tilde{\lambda}^{4/3} T^{2/3}, \tag{6.7}$$

consistent with the $T^{2/3}$ scaling observed in other studies [79].

Chapter 7

Coadjoint Orbits, Character Formulas, and Related Topics

Here's a more readable and polished version of your text:

As is well known in classical mechanics, systems with symmetries are modeled by symplectic manifolds. However, this framework is not limited to classical systems. As seen in Chapter 2.5, the time-dependent variational principle (TDVP) preserves symmetries and conservation laws by maintaining a symplectic structure.

In the following chapters, we will use these mathematical tools to propose a quantization method for loop groups. This chapter begins with an overview of Lie groups and their adjoint and coadjoint representations. For a more in-depth study of Lie groups and Lie algebras, we refer to [71, 69]. We then examine the fundamental principles of Poisson and symplectic structures, along with their realization in coadjoint orbits. Finally, we explore momentum maps and their connection to the symmetries of symplectic manifolds.

This chapter is primarily abstract, focusing on mathematical concepts.

7.1 Lie Groups

A **Lie group** G is a topological group that is also a smooth manifold, where group operations (multiplication and inversion) are smooth mappings:

$$\begin{aligned} g &\longmapsto L_f(g) = fg \\ g &\longmapsto R_f(g) = gf \end{aligned} \tag{7.1}$$

Here, L_f and R_f are diffeomorphisms, and e denotes the identity element of G.

We can define a vector field ξ as follows. A *left-invariant* vector field is such that $(L_f)_*\xi = \xi$ for every $f \in G$.

Remark 1. *The differential of a smooth map $F : \mathcal{N} \longrightarrow \mathcal{P}$ at $p \in \mathcal{N}$ is $F_{*p} : T_p\mathcal{N} \longrightarrow T_{F(p)}\mathcal{P}$, where $F_{*p}(\dot{\gamma}(0)) = \frac{d}{dt}\left[F(\gamma(t))\right]\Big|_{t=0}$, with $\gamma(t)$ a path in $\mathcal{N}$ such that $\gamma(0) = p$.*

Each left-invariant vector field on the group is given by $\xi_g = (L_g)_{*e} X$ for some tangent vector $X \in T_e G$. Hence, the tangent space at the identity element of G is isomorphic to the space of vector fields. We denote the invariant vector field associated with $X \in T_e G$ as φ_X, so that $(\varphi_X)_g = (L_g)_{*e} X$.

We can define the *Lie algebra* of G in terms of the tangent space, i.e., as a vector space $\mathfrak{g} = T_e G$, equipped with the Lie bracket

$$[X, Y] = [\varphi_X, \varphi_Y] \tag{7.2}$$

where the bracket on vector fields should be evaluated at the identity. The Lie algebra satisfies two basic properties, namely, $[X, X] = 0$, which implies $[X, Y] = -[Y, X]$ and the Jacobi identity

$$[[X, Y], Z] + [[Y, Z], X] + [[Z, X], Y] = 0. \tag{7.3}$$

For any $\mathfrak{g}$ we get a linear map $\operatorname{ad} : \mathfrak{g} \to \operatorname{End}_{\mathbb{k}} \mathfrak{g}$ given by

$$(\operatorname{ad} X)(Y) = [X, Y] \tag{7.4}$$

and thus, every $(\operatorname{ad} X)$ is a derivation. A homomorphism of Lie algebras is a linear map $\varphi : \mathfrak{g} \to \mathfrak{h}$ such that

$$\varphi_{[X,Y]} = [\varphi_X, \varphi_Y]. \tag{7.5}$$

In general any smooth homomorphism of Lie groups induces a homomorphism of Lie algebras via its derivative at the identity. In the context of symmetries, elements of $\mathfrak{g}$ represent infinitesimal symmetries near the identity. Now, as was mentioned for the case of SU(3) in the chapters above, a general Lie algebra $\mathfrak{g}$ may be expressed in terms of a basis $\{t_a \mid a = 1, \ldots, \dim \mathfrak{g}\}$ of generators obeying

$$[t_a, t_b] = f_{ab}^c t_c. \tag{7.6}$$

Here, $f_{ab}^c \in \mathbb{R}$ are the structure constants of $\mathfrak{g}$ in that particular basis.

7.1.1 Exponential Map

Above we used the tangent space to G to define the Lie algebra $\mathfrak{g}$ of G. This concept can be understood as follows: for each vector $X \in \mathfrak{g}$, there exists a unique one-parameter subgroup $\{g_t\}_{t \in \mathbb{R}}$ in G such that X is the tangent vector at the identity:

$$\left. \frac{dg_t}{dt} \right|_{t=0}. \tag{7.7}$$

The group element g_t is represented by $\exp(tX)$, and the map $X \mapsto \exp(X)$ from $\mathfrak{g}$ to G is known as the exponential map. This map establishes a one-to-one correspondence between a neighbourhood of the identity in $\mathfrak{g}$ and a neighbourhood of the identity in G, making it one of the preferred coordinate charts. The key feature of the exponential map is that it reflects many properties of G in

a neighbourhood around the identity, even though $\mathfrak{g}$ is concerned only with infinitesimal information near the identity. For closed linear groups, the Lie algebra is composed of matrices $X = c'(0)$ derived from smooth curves $c(t)$ in G that pass through the identity at $t = 0$. Among these, the curve $\exp(tX)$ is particularly noteworthy as it is smooth and exhibits the desired behaviour at $t = 0$.

For our purposes, we define the exponential map as follows. Let γ_X be the integral curve of the left-invariant vector field φ_X with $\gamma_X(0) = e$ for $X \in \mathfrak{g}$. The *exponential* map is defined by

$$\exp : \mathfrak{g} \longrightarrow G : X \mapsto \exp[X] \equiv \gamma_X(1). \tag{7.8}$$

For matrix groups, this reduces to the Taylor series $\sum_{n\in\mathbb{N}} \frac{X^n}{n!}$, often written as $\exp[X] = e^X$.

The exponential map satisfies

$$\exp[(s+t)X] = \exp[sX]\exp[tX]$$

for all $s, t \in \mathbb{R}$.

Furthermore, as hinted before, for any smooth homomorphism $\pi : G \longrightarrow H$, it holds that

$$\pi \circ \exp_G = \exp_H \circ \pi_e. \tag{7.9}$$

In other words, this shows the remarkable fact that the infinitesimal behaviour of a homomorphism near the identity determines the homomorphism in a neighbourhood of the identity. Thus, for any $X \in \mathfrak{g}$, there exists a subgroup of G consisting of elements $\exp[tX]$ for $t \in \mathbb{R}$. Notably, vector fields are complete, ensuring $\exp[tX]$ exists for all $t \in \mathbb{R}$.

7.2 Adjoint and Coadjoint Representations

A representation over a group G over a complex vector space V is a homomorphism $\rho : G \to \mathrm{GL}(V)$, where $\mathrm{GL}(V)$ denotes the general linear group of V, i.e., the group of automorphisms of V. For a Lie group G with Lie algebra $\mathfrak{g}$ as a vector space, the *adjoint representation* of G is defined as

$$\mathrm{Ad} : G \longrightarrow \mathrm{GL}(\mathfrak{g}) : g \mapsto \mathrm{Ad}_g\,. \tag{7.10}$$

i.e., as a homomorphism where Ad_g is the linear operator on $\mathfrak{g}$ given by

$$\mathrm{Ad}_g(X) = \frac{d}{dt}\left(ge^{tX}g^{-1}\right)\Big|_{t=0}. \tag{7.11}$$

In this case, e^{tX} can be replaced by any path in G with $\gamma(0) = e$ and $\dot{\gamma}(0) = X$. For matrix groups, this simplifies to $\mathrm{Ad}_g(X) = gXg^{-1}$, and it follows that

$$\exp[\mathrm{Ad}_f(X)] = f\exp[X]f^{-1}. \tag{7.12}$$

It follows almost immediately that the adjoint representation of an abelian Lie group is trivial.

As said before, the adjoint representation of the Lie algebra $\mathfrak{g}$ is defined as the differential of (7.10) at the identity:

$$\mathrm{ad}_X(Y) \equiv \frac{d}{dt}\left(\mathrm{Ad}_{e^{tX}}(Y)\right)\Big|_{t=0} = [X, Y]. \tag{7.13}$$

We now consider dual representations and their application to the adjoint representation (7.10). The dual of $\mathfrak{g}$, denoted by $\mathfrak{g}^*$, consists of linear functionals $p : \mathfrak{g} \longrightarrow \mathbb{R}$ defined by $p(X) = \langle p, X\rangle$. Thus, one can say that the elements of $\mathfrak{g}^*$ represent conserved vectors associated with the symmetries of a symmetry group G. In physical terms, given a generator X, $\langle p, X\rangle$ represents the charge when the system has conserved vectors p.

For a Lie group G with Lie algebra $\mathfrak{g}$, the *coadjoint representation* of G is the homomorphism

$$\mathrm{Ad}^* : G \longrightarrow \mathrm{GL}(\mathfrak{g}^*) : f \mapsto \mathrm{Ad}^*_f\,. \tag{7.14}$$

This is the dual homomorphism, meaning that

$$\mathrm{Ad}^*_f(p) \equiv p \circ (\mathrm{Ad}_f)^{-1}, \tag{7.15}$$

or more explicitly,

$$\left\langle \mathrm{Ad}^*_f(p), X\right\rangle = \langle p, \mathrm{Ad}_{f^{-1}}(X)\rangle\,. \tag{7.16}$$

As a specific example, take the special orthogonal group $SO(3)$ with Lie algebra $\mathfrak{so}(3)$. Then the coadjoint representation corresponds to the rotation of vectors in $\mathbb{R}^3$. If p represents a momentum vector in $\mathbb{R}^3$, then for any rotation f in $SO(3)$, the action of Ad^*_f on p yields the rotated vector $\mathrm{Ad}^*_f(p) = fp$.

7.3 Character Formulas

Character formulas provide a vital link between representation theory and Lie algebra studies. For a Lie algebra $\mathfrak{g}$ with a finite-dimensional representation V, the character of V is defined by

$$\chi_V(g) = \mathrm{Tr}(\rho(g)), \tag{7.17}$$

where ρ is the representation of G on V. The character encodes essential information about the representation, including the dimensions of its weight spaces and the multiplicities of irreducible components.

The *character* of a representation ρ is the function

$$\chi_\rho : G \to \mathbb{C} : g \mapsto \mathrm{Tr}(\rho(g)). \tag{7.18}$$

Character formulas are used to compute characters of irreducible representations, crucial for understanding the structure of the Lie algebra and its representations.

To make contact with physics we can see that partition functions or path

integrals are the objects that give us information about the spectrum of operators such as the Hamiltonian. This is clear, for example, when we have a system that is time-invariant, the Hamiltonian is the symmetry generator and the partition function or path integral may be written as

$$Z(\beta) = \mathrm{Tr}\left(e^{-\beta H}\right). \tag{7.19}$$

This formula can be generalised to the grand canonical ensembles, by simply including the appropriate symmetry generators. By working in imaginary time the trace argument is unitary, and more generally the partition function or path integral should be a symmetry transformation that depends on the specific representation that we use. By (7.17) we are guaranteed that the partition function only depends on the conjugacy classes and not on the basis elements of the Hilbert space, i.e., it is a class function.

7.4 Symplectic structures

A symplectic manifold is a smooth manifold endowed with a symplectic form, a non-degenerate, closed two-form. This geometric structure is extremely relevant for Hamiltonian mechanics, providing a framework for defining canonical coordinates and the Hamiltonian flow. It is also central to differential geometry and topology, since symplectic manifolds offer profound insights into both classical and quantum mechanics. The field of symplectic geometry encompasses the study of their properties, examples, and applications, including symplectic reduction, moment maps, and geometric quantisation.

We can define a *symplectic manifold* as a pair (M, ω) where M is a smooth manifold and ω is a symplectic form. The latter is a two-form satisfying $d\omega = 0$ (closedness) and the non-degeneracy condition that the map $v \mapsto \iota_v \omega$ is an isomorphism at every point of M. The Darboux theorem ensures that locally, any symplectic manifold can be brought into the canonical form of Euclidean space equipped with the standard symplectic structure.

Within the context of Hamiltonian mechanics, symplectic manifolds provide a natural arena. A Hamiltonian function on a symplectic manifold induces a Hamiltonian vector field whose flow preserves the symplectic form, capturing the dynamics of the system. Moreover, symplectic geometry intersects with topology through invariants such as the symplectic volume and Gromov-Witten invariants.

More precisely put, the non-degeneracy condition implies that symplectic manifolds are even-dimensional and admit what is known as a Liouville form

$$\mu = \omega \wedge \cdots \wedge \omega. \tag{7.20}$$

while the Darboux theorem says that we can describe locally any point using a canonical form with local coordinates $\{q, p\}$ written as

$$\omega = dq^i \wedge dp_i. \tag{7.21}$$

In physical terms, the phase space of a manifold representing the configuration

space of a classical system is well-known to be a cotangent bundle with a closed non-degenerate form. Thus any symplectic manifold may be identified, locally, to a cotangent bundle.

Now we want to describe more precisely some techniques which will be useful later on. Given a Lie group G, we define the Kirillov-Kostant bracket on $\mathfrak{g}^*$ as follows: given $\mathcal{A}, \mathcal{B} \in C^\infty$ from the dual Lie algebra to the real numbers we define the bracket

$$\{\mathcal{A}, \mathcal{B}\}(p) = \left\langle p, [A'_p, \mathcal{B}'_p] \right\rangle \tag{7.22}$$

where the prime denotes a differential at a point in the dual Lie algebra, and notice that the differential lives in the Lie algebra, i.e., in the dual of the dual algebra.

We define the Euler equation on $\mathfrak{g}^*$ as follows, let $\mathcal{A} \in \mathfrak{g}^*$ as before. Let δ_H be a Hamiltonian field, i.e., $\delta_H \equiv -\{H, \cdot\}$ defined over a Poisson manifold [1], where H is a C^∞ function on that manifold, and let $i_{\delta_\mathcal{A}}\omega = \omega(\delta_\mathcal{A}, \cdot) = d\mathcal{A}$ define the Hamiltonian field δ_H (which means that if there exists $\mathcal{A} \in C^\infty(\mathcal{M})$ then $\varphi = \delta_\mathcal{A}$). Then the Euler equation is

$$\dot{\gamma}(t) = (\delta_\mathcal{A})_{\gamma(t)} = \mathrm{ad}^*_{\mathcal{A}'_{\gamma(t)}}(\gamma(t)). \tag{7.23}$$

.

An interesting consequence of this is that the symplectic leaves of the above bracket are precisely the coadjoint orbits of the group. [69] In other words, it can be stated that the symplectic leaves of the Poisson manifold $(\mathfrak{g}^*, f)$ where f defines a Poisson structure, are precisely the coadjoint orbits.

By now, it should be obvious that there are many ways to obtain the symplectic structure of coadjoint orbits. The main three ways are through Poisson structures, using cotangent bundles and a third one, by using Maurer-Cartan forms [2].

The symplectic form of the coadjoint orbits of the group are defined simply as follows

$$\omega\left(\mathrm{ad}^*_X q, \mathrm{ad}^*_Y q\right)_q = \langle q, [X, Y] \rangle \tag{7.24}$$

where $q \in \mathcal{W}_p$ and $p \in \mathfrak{g}^*$ is a vector in the dual space with orbit $\mathcal{W}_p$. Note that in particular this is a closed, non-degenerate form satisfying $\left(\mathrm{Ad}^*_f\right)^*(\omega) = \omega$, thus each coadjoint orbit is a homogenous symplectic manifold. Also worth remarking is that the converse is true only up to some algebraic corrections.

---

[1] Recall that a Poisson structure on a manifold is an antisymmetric bilinear map

$$\{\cdot, \cdot\} : \mathcal{A}, \mathcal{B} \mapsto \{\mathcal{A}, \mathcal{B}\}$$

which satisfies both

$$\begin{aligned} \{\mathcal{F}, \{\mathcal{G}, \mathcal{H}\}\} + \quad & \{\mathcal{G}, \{\mathcal{H}, \mathcal{F}\}\} + \{\mathcal{H}, \{\mathcal{F}, \mathcal{G}\}\} = 0 \\ & \{\mathcal{F}, \mathcal{G}\mathcal{H}\} = \{\mathcal{F}, \mathcal{G}\}\mathcal{H} + \mathcal{G}\{\mathcal{F}, \mathcal{H}\} \end{aligned}$$

[2] A Maurer-Cartan form is a $\mathfrak{g}$ valued left-invariant 1 form on the group defined by the condition $\theta(e)X = X$ and thus $\theta(g)X = g^{-1}X$ for X defined on a point of the tangent space of the group G

7.5 Momentum maps

Let (N, η) be a symplectic manifold with symplectic form η, and let H be a Lie group acting on N via symplectomorphisms. A *momentum map* for this action is a map

$$J : N \longrightarrow \mathfrak{h}^* \tag{7.25}$$

such that for any left-invariant vector field ξ on H, the condition

$$d\langle J, \xi \rangle = -\iota_{\xi_N} \eta \tag{7.26}$$

is satisfied, where ξ_N denotes the vector field on N generated by the infinitesimal action of ξ, and $\langle \cdot, \cdot \rangle$ represents the pairing between $\mathfrak{h}^*$ and $\mathfrak{h}$. As a remark, note that the momentum map is unique up to an additive constant. Thus, if J is a momentum map, then $J + C$, where C is a constant, is also a valid momentum map.

The momentum map connects the symmetries of the manifold to conserved quantities, translating these symmetries into conserved momenta via the symplectic structure. Furthermore, the momentum map is related to universal properties of the Poisson manifolds. This is in the sense that given any homogenous Poisson manifold, a moment map defines a covering of a coadjoint orbit. Coadjoint orbits thus have peculiar properties that we are interested in. For example one can show that there is a momentum map associated with the inclusion of the coadjoint orbit in $\mathfrak{g}^*$, given a symplectic form (7.25) then coadjoint orbits have the property of always being homogenous spaces.

Chapter 8

Quantising loop groups for NFLs

In this chapter, we demonstrate the process of quantising loop groups, drawing on formal quantisation ideas [69, 59]. Typically, studying quantum systems involves extensive use of representation theory to derive geometric objects on which functional analysis and other advanced mathematical techniques can be applied. In contrast, geometric quantisation seeks to derive a representation from geometric objects by selecting a quantisation method. In the context of this thesis, the objects of interest are orbits, more specifically coadjoint orbits of a given group, which applies to various types of groups, including loop groups.

8.1 Loop groups

A loop group LG [105]consists of maps from the circle into a group G, typically a compact Lie group or its complexification. Composition in LG is defined pointwise in G. The study of loop groups extends the theory of finite Lie groups to the infinite-dimensional setting.

The groups $Map(X, \mathfrak{g})$ are particularly important. Firstly, the exponential map from the Lie algebra $\mathfrak{g}$ of G induces a locally bijective exponential map between $Map(X, \mathfrak{g})$ and $Map(X, G)$, a property uncommon in infinite-dimensional Lie groups. Secondly, these groups appear in physics in several cases. In quantum field theory, these groups serve as gauge and current groups, where X often represents physical space in three dimensions. In our case loop groups seem to parametrise correctly the symmetry of non-Fermi liquids as suggested in [32]

While not compact or Lie groups, loop groups exhibit properties reminiscent of compact groups. They are studied through their Lie algebras, known as Kac-Moody algebras. These infinite-dimensional algebras, characterised by generators and relations, generalise finite-dimensional semisimple algebras. The theory of Cartan and Killing associates an algebra to a finite integer matrix satisfying certain conditions. Relaxing the positivity condition yields affine Kac-Moody algebras, the Lie algebras of loop groups and their twisted counterparts.

Macdonald identities, generalisations of the Weyl character formula to Kac-Moody algebras, produce modular functions. Loop groups possess a rich combinatorial structure. These notes concentrate on the geometric and analytic aspects of affine Kac-Moody algebras, eschewing a more algebraic or combinatorial approach.

8.2 Why Loop Groups?

As mentioned before, to-day there is no proper effective field theory of a metal. Fermi liquid theory was a first attempt at it and several more have followed. On the other hand solving the many-body Hamiltonian for the Fermi liquid theory is still intractable. The idea of effective field theories relies on the renormalisation group flow to inform us on the relevant information to build an effective field theory. If we start from the ultraviolet, where we have a detailed microscopic physics. e.g., electrons hopping between atoms and a Coulomb repulsion, then the renormalisation group can flow to the infrared regime, where the low-energy, long-wavelength physics inhabits, e.g., we have an effective field theory of the itinerant electrons. The renormalisation group flow essentially restricts what we can eventually have at the infrared. We could have in general insulators (described by a theory with no fields), topological insulators (described by topological field theories), metals (no effective field theory), or strange metals (no effective field theory), for example. As mentioned in the sections above, Fermi liquid theory and Fermi surfaces are extremely important in describing the physics of non-Fermi liquids. The notion of strange metals has for example the class of doped cuprates where the known theories break down.

In the case of strange metals, for example, we can see in Fig. 8.1 that by suppressing the superconducting order we obtain a strange metal phase that extends all the way to $T = 0$, i.e., we have a zero temperature ground state of a many-body system. In particular we want to understand this state through an effective field theory. The main consensus about strange metals is that it should be a strongly coupled field theory which is a difficult task in general.

8.2.1 Constraining the effective field theory

In general, tere exist several types of constraints that we must have. Among the most important we have filling constraints, the UV symmetry the Lieb-Schultz-Mattis theorem and Luttinger's theorem. General statements about symmetry can be made at the UV level. For example we would expect at the ultraviolet a symmetry in clean metals consisting of some lattice translation symmetry and charge conservation, i.e., $G = \mathbb{Z}^d \times U(1)$. Then the effective field theory has to represent that symmetry subject to some constraints (even if there are spontaneously broken symmetries). The filling constraint is simply the average charge per unit cell. Furthermore we have the Lieb-Schultz-Mattis theorem where, broadly speaking, tells us that if the filling ν is not an integer, then the ground state must be metallic. Luttinger's theorem is expressed as follows

$$\frac{V_F}{(2\pi)^2} = \nu \bmod 1 \tag{8.1}$$

where V_F is the enclosed volume by the Fermi surface and ν is the microscopic filling of charge per unit cell. The main idea behind all of this is that the symmetry and the filling should provide sufficient constraints to generalise the LSM theorem by the use of anomalies. [32]

Very broadly a 't Hooft anomaly is the non-conservation of charge, or more generally the breaking of the symmetry at the infrared, in upon coupling to a background gauge field. is that the conservation law corresponding to the GIR symmetry is broken upon coupling to a background gauge field. Thus the anomaly of the emergent symmetry in the infrared is a kinematic property of the effective field theory.

To identify the emergent symmetry group at the infrared we want to derive the LSM theorem using anomalies. A defining property of Fermi liquids is that nonforward scattering are irrelevant at low energies, so the quasiparticle number at each point on the Fermi surface is separately conserved at low energies [32] . This means that the emergent symmetry group at the infrared is quite large. In general terms, what is proven in [32] is the following theorem: *if $d \geq 2$ and G_{IR} is a compact finite-dimensional Lie group, then the filling ν is a rational number. For irrational ν the emergent group G_{IR} must be an infinite dimensional group, with infinitely conserved quantities.* This is a very strong statement for clean metals where we expect infinite dimensional groups. The question of groups being finite but non-compact is an open question, but seems unlikely.

To make this precise we want to parametrise the Fermi surface using a periodic angle variable, i.e. $\theta \in S^1$. Since the infrared cutoff is a short distance cutoff in momentum space, we expect θ to take discrete values. To each one of these we attach an emergent U(1) symmetry generated by an operator N_θ, thus we have [32]

$$\exp\left(-i\sum_{\theta} f_\theta N_\theta\right) \tag{8.2}$$

where f_θ is periodic in the circle. The main assumption for obtaining a loop group is that we want the parameters f to become smooth when the cutoff of θ is sent to 0. What this means is that emergent symmetries should be in bijection with smooth functions from S^1 into U(1), i.e., the symmetry group at the infrared is a loop-U(1) group.

8.3 General idea of geometric quantisation

Geometric quantisation in its classical form [69] is a formalisation of the transition from classical to quantum mechanics that focuses on constructing quantum state spaces. This approach has its roots in [69] and its relation to path integral quantisation and coherent states is a deep one. The quantisation process begins with a symplectic manifold representing a classical mechanical system. The symplectic form ω is realised as the curvature of a principal bundle with connection, known as the prequantum bundle. In the case of a U(1)- principle bundle, this bundle is equipped with a line bundle obtained by associating the complex numbers to the $U(1)$-principal bundle.

A polarisation is then chosen to decompose the phase space into generalised coordinates and momenta. The Hilbert space of quantum states is constructed as the space of sections of the line bundle that depend only on the coordinates. Finally, classical observables, represented by functions on the symplectic manifold,

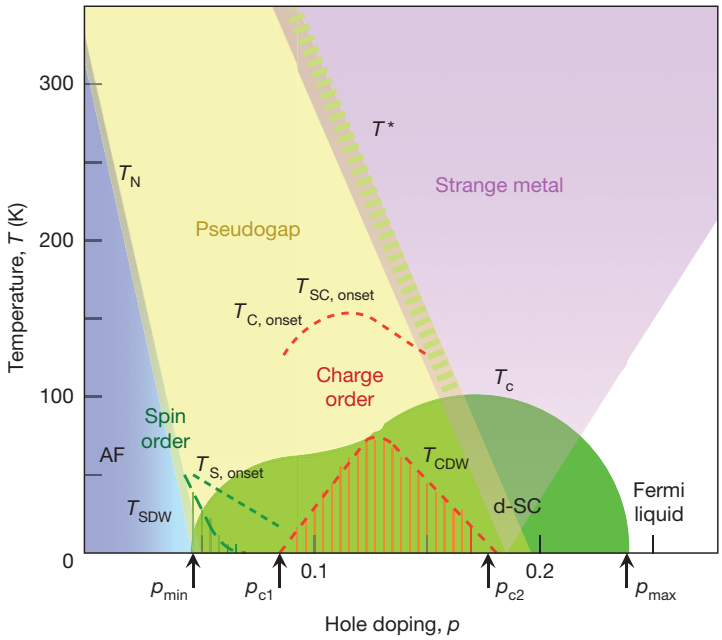

Figure 8.1: Phase diagram of the doped high temperature superconductors. AF stands for antiferromagnetic, d-SC stands for d-wave superconductivity, T_N for Normal temperature, T_{onset} stands for the onset temperatures of spin (S), charge (C) and superconductivity (SC) fluctuations; T^* stands for the crossover temperature. As can be seen in the diagram there is a strange metal phase, relevant for our discussion, which overlaps with the superconductivity dome defined by the critical temperature T_C. By suppressing the superconducting region (by applying a magnetic field for example), the strange metal region extends all the way to $T = 0$. Thus the strange metal seems to have a zero temperature ground state. [64]

are mapped to quantum observables, which are operators on the Hilbert space.

We will first focus on the prequantisation problem in geometric quantisation. The main problem of quantising a set of classical variables, i.e., a phase space with symplectic structure ω, is to find a quantum Hilbert space associated to it, that also includes an algebra of observables with some minimum structure as shown in Appendix A that remains related to the Poisson structure. As was mentioned in 5.10 we want a formalism where the linear operators A preserve some of the old structure, naively

$$[\mathcal{A}, \mathcal{B}] = i\hbar\{\mathcal{A}, \mathcal{B}\} \tag{8.3}$$

would be a first attempt, but just as in 5.10 we need to weaken the assumption and add different terms in order to make (8.3) consistent. In brief, prequantisation means that we establish some consistency conditions such as mapping identity to identity, and that the Hamiltonian fields actually satisfy (8.3). The solution relies in including the momentum map as follows

$$\mathcal{A} \mapsto -i\hbar\delta_{\mathcal{A}} - \langle \vartheta, \delta_{\mathcal{A}} \rangle + \mathcal{A} = -i\hbar\nabla_{\delta_{\mathcal{A}}} + \mathcal{A} \tag{8.4}$$

where $\omega = -d\vartheta$ is the symplectic structure of Hamiltonian fields and thus appropriately satisfies all the conditions. In particular ϑ represents the Liouville invariant form (7.20) when the subjacent manifold is a cotangent bundle. The second equality tells us that this can be also written in a covariant formulation, where now ϑ is a 1-form representing the connection, which has some straightforward physical interpretations.

Formally, the polarisation step is reminiscent of a truncation of the prequantum Hilbert space, i.e., we want to cut down the number of degrees of freedom in which the wavefunctions are allowed to live. Quite informally by taking any point in the manifold, we want to pick up specific submanifolds of the tangent space at that point. This can be viewed for example in the case of cotangent bundles, where we only choose the coordinates (and not the momenta) in each fibre of the cotangent bundle. This is very reminiscent to the Schrodinger quantisation. A generalisation of this might be the all-intresting Bergmann-Segal representation (related to coherent states) where we have a complexified phase space with a Kahler polarisation. Now polarisation of course affects the algebra of observables in the quantum case, and they must also preserve whatever polarisation procedure we choose, e.g., (8.3). In the general case, observables that may be quantised should give rise to an algebra of self-adjoint operators, which among others should contain the sums and products of these operators.

8.4 Path integrals

Let G be a connected Lie group. Let G be such a group, with $\mathfrak{g}$ denoting its Lie algebra and $\mathfrak{g}^*$ its dual. The group G acts on $\mathfrak{g}$ and $\mathfrak{g}^*$ via the adjoint and the coadjoint action, respectively.

We can assume that G, $\mathfrak{g}$, and $\mathfrak{g}^*$ are realised as matrix spaces (which, while not a general statement, is valid in this context). Consequently, we have $\mathrm{Ad}_f\, x =$

$f^{-1}xf$ and $\mathrm{Ad}^*_f \xi = f^{-1}\xi f$. For $\lambda \in \mathfrak{g}^*$, the coadjoint orbit is defined by

$$\mathcal{W}_\lambda = \left\{ \xi = f^{-1}\lambda f \mid f \in G \right\}.$$

The projection $\pi_\lambda : G \to \mathcal{W}_\lambda$ is defined by $\pi_\lambda(f) = f^{-1}\lambda f$. Given that coadjoint orbits are equipped with the Kirillov-Kostant symplectic form (7.25), we can describe the pullbacks of this form to G under the projection π_λ, denoted by $\pi_\lambda^* \omega_\lambda$.

Additionally, recall that the Liouville form ω in (7.20)—or a normalised version— serves as an invariant form on $\mathcal{W}_\lambda$.

The orbit method [69] may be seen as a correspondence between unitary irreps of G and coadjoint orbits. This correspondence is realised in several possible ways, here we'll show it using a general path integral or, mathematically, a character formula.

We will restrict the discussion to compact groups, or sometimes even to closed linear groups G. These will then be extended to loop groups below. Let $\exp(X)$ be the exponential map from the lie algebra to the group G. Let λ denote the highest weight of the irreducible representation σ_λ from the group to the space of endomorphisms $\mathrm{End}(V_\lambda)$, and let $\chi_\lambda(f) = \mathrm{Tr}_{V_\lambda} \sigma_\lambda(f)$ be the associated character formula

$$\chi_\lambda(\exp(X)) = J^{-1/2}(X) \int_{\mathcal{W}_{\lambda+\rho}} \frac{\omega^N_{\lambda+\rho}}{N!} e^{i\langle \xi, X \rangle}.$$

This is also called the Kirillov character formula where ρ is a sum of positive roots of G and $J(X)$ represents the Jacobian of $X \mapsto \exp(X)$. Notice that the measures has to be distinguished here. On one side the integration measure on $\mathfrak{g}$ will be a Lebesgue measure while for the group this has to be some volume preserving one, such as the Haar measure.

As an example, let us take SU(2). For SU(2), the highest weights are the positive half-integers, and $\rho = 1/2$. The coadjoint orbits are the two-dimensional spheres of radius $\lambda + 1/2$, centred at the origin in 3-dimensional space. It can be shown that

$$\int_{\mathcal{W}_{\lambda+1/2}} e^{i\beta(X)} d\mu_{\lambda+1/2}(\beta) = \frac{\sin((2\lambda+1)X)}{X/2}, \quad \forall X \in \mathfrak{g},$$

and

$$j(X) = \frac{\sin(X/2)}{X/2},$$

thus yielding the characters of SU(2):

$$\chi_\lambda(\exp(X)) = \frac{\sin((2\lambda+1)X)}{\sin(X/2)}.$$

In the general case, the symplectic form (7.25) will let us act on a coadjoint orbit with a Hamiltonian system. With $\lambda \in \mathfrak{g}^*$ fixed and $f : I \to G$ a map from a

segment of a circle to the group itself, the orbit action is given by the expression:

$$S(\lambda, f) = \int_I \left\langle \lambda, \mathrm{d}f\, f^{-1} \right\rangle = \int_I \left\langle f^{-1}\lambda f, f^{-1}\mathrm{d}f\, f^{-1} f \right\rangle = \int_I \left\langle \xi, f^{-1}\mathrm{d}f \right\rangle,$$

where $\xi = f^{-1}\lambda f$.

To write a path integral, let A be a connection on I. Then, for $I = S^1$, we have:

$$\chi_\lambda \left(P \exp \int_I A \right) = \int \mathcal{D}f\, e^{i\left(S(\lambda,f) + \int_I \langle \xi, A\rangle\right)}. \tag{8.5}$$

Here, we are using the coadjoint orbit $\mathcal{W}_\lambda$, but to formulate it correctly, it might be better to use it as in the Kirillov character formula (including the Jacobian).

For finite intervals, (8.5) should define the elements of the representation σ_λ as

$$\left\langle X \left| \sigma_\lambda \left(P \exp \int_I A \right) \right| Y \right\rangle = \int_{g(0), f(T)} \mathcal{D}f e^{i\left(S(\lambda,f) + \int_I \langle \xi, A\rangle\right)}. \tag{8.6}$$

Here, $\langle X|$ and $|Y\rangle$ label two vectors in V_λ, with appropriate boundary conditions corresponding to these vectors.

The action of the orbit is then

$$S(\lambda, f) + \int_I \left\langle f^{-1}\lambda f, A^h \right\rangle = S(\lambda, fh) + \int_I \left\langle (fh)^{-1}\lambda(fh), A \right\rangle. \tag{8.7}$$

under the action of a gauge transformation $A \mapsto A^h$. Here we note that $S(\lambda, f)$ is a one-cocycle for the group of paths in general (loops in particular). The fact that this is a one-cocycle implies that $\delta S = 0$ where δS is defined as follows

$$\delta S(\lambda, f, h) = S\left(\xi = f^{-1}\lambda f, h\right) - S(\lambda, fh) + S(\lambda, f).$$

This cocycle property leads to the following transformation of the path integral

$$\int \mathcal{D}f\, e^{i\left(S(\lambda,f) + \int_I \left\langle \xi(f), A^h \right\rangle\right)} = \int \mathcal{D}v\, e^{i\left(S(\lambda,v) + \int_I \langle \xi(v), A\rangle\right)},$$

where $v = fh$. We can further refine the interval and choose it to be a closed loop, i.e., we set $I = S^1$. Also, in particular, for $A = 0$, the path integral formula becomes:

$$\int_{f(0), f(T)} \mathcal{D}f\, e^{i\left(S(\lambda,f) + \int_I \left\langle \xi, dhh^{-1} \right\rangle\right)} = \left\langle a \left| \sigma_\lambda(h(T))\sigma_\lambda(h(0))^{-1} \right| b \right\rangle.$$

Now, we want to understand the idea of the orbit actions for central extensions.

Central extensions

Given a Hilbert space, a symmetry[1] is a bijective map that preserves probabilities. This map in general happens between projective spaces, i.e., $\mathbb{P}\mathcal{H} \to \mathbb{P}\mathcal{H} : [\Psi] \mapsto$

[1]We are excluding here any type of non-invertible symmetry, categorical symmetry or any such generalisation where this might not apply.

$\mathcal{S}([\Psi])$ where by $\mathbb{P}\mathcal{H}$ we mean the projective Hilbert space and by $\mathcal{S}$ the symmetry transformation. We can also represent this in terms of lines in $\mathcal{H}$ by normalised vectors. A symmetry transformation $\mathcal{S}$ must satisfy

$$|\langle \Phi \mid \Psi \rangle| = |\langle \Phi' \mid \Psi' \rangle| \tag{8.8}$$

for all normalised vectors Φ, Ψ and their images $\Phi' \in \mathcal{S}([\Phi])$, $\Psi' \in \mathcal{S}([\Psi])$.

In quantum mechanics, symmetry is understood as a transformation satisfying the equation above, and acts on states either linearly (antilinearly) and unitarily (antiunitarily) according to the symmetry representation theorem. In quantum mechanics there is a crucial subtlety. Let $g \in G$ be some symmetry transformation and let $\mathcal{U}[g]$ denote the unitary operator representing it. Since a quantum state is a line or ray of vectors in reality it determines an equivalence class of vectors in the Hilbert space, $\mathcal{U}$ does not need to be a homomorphism. Instead, what is required is that the line of $\mathcal{U}[g] \cdot \mathcal{U}[h] \cdot \Phi$ coincides with that of $\mathcal{U}[g \cdot h] \cdot \Phi$ for all $g, h \in G$ and any $\Phi \in \mathcal{H}$. Thus, $\mathcal{U}$ must be a unitary representation up to a phase factor:

$$\mathcal{U}[g] \cdot \mathcal{U}[h] = e^{i\mathtt{C}(g,h)} \mathcal{U}[f \cdot g] \quad \text{for } g, h \in G, \tag{8.9}$$

where $\mathtt{C}$ is some real function on $G \times G$. This means simply that $\mathcal{U}$ defines an action on the projective Hilbert space, thus the mapping

$$[\mathcal{U}] : G \to \mathbb{P}\mathcal{H} : g \mapsto [\mathcal{U}[g]] \tag{8.10}$$

is a homomorphism. Here, $\mathbb{P}\mathcal{H} = \mathrm{GL}(\mathcal{H})/\mathbb{C}^*$ is the projective group of $\mathcal{H}$, the quotient of the linear group of $\mathcal{H}$ by its subgroup of scalar multiples of the identity. For any operator $\mathcal{A}$ in $\mathrm{GL}(\mathcal{H})$, $[\mathcal{A}]$ denotes its equivalence class in the projective group. Any mapping $\mathcal{U}$ satisfying this condition will be referred to as a projective representation.

The function $\mathtt{C}$ in equation (8.9) is not arbitrary. It must satisfy associativity conditions, specifically:

$$\mathtt{C}(f, gh) + \mathtt{C}(g, h) = \mathtt{C}(fg, h) + \mathtt{C}(f, g) \quad \text{for all } f, g, h \in G. \tag{8.11}$$

A function $\mathtt{C} : G \times G \to \mathbb{R}$ is called a two-cocycle, with a cocycle condition. With any such function, one can define a new group

$$\widehat{G} \equiv G \times \mathbb{R} \tag{8.12}$$

where elements are pairs (f, λ), equipped with the group operation

$$(f, \lambda) \cdot (g, \mu) = (fg, \lambda + \mu + \mathtt{C}(f, g)). \tag{8.13}$$

The group (8.12) is termed a central extension of the group G.

Central extensions, loop groups and the path integral

We'll work with $\widehat{G}$ the central extension of the group G by the circle, i.e.,

$$1 \to S^1 \to \widehat{G} \to G \to 1. \tag{8.14}$$

Then, the Lie algebra $\mathfrak{g}$ also has a central extension which is given by the exact sequence

$$0 \to \mathbb{R} \to \widehat{\mathfrak{g}} \to \mathfrak{g} \to 0. \tag{8.15}$$

Assuming the S^1-bundle $\widehat{G} \to G$ is trivial with a section $s : G \to \widehat{G}$, we define objects derived from this section. The group law in $\widehat{G}$ yields a two-cocycle $\alpha : G \times G \to S^1$, where for $f, h \in G$:

$$s(f)s(h) = s(fh)e^{i\alpha(f,h)}. \tag{8.16}$$

The section s will give a two-cocycle $\omega(x, y)$:

$$[s(x), s(y)] = s([x, y]) + \omega(x, y). \tag{8.17}$$

and a splitting $\mathfrak{g} \to \widehat{\mathfrak{g}}$.

Define the 1-form $\beta(f)$ as:

$$\beta(f) = ds(f)s(f)^{-1} - df f^{-1} \in \Omega^1(G), \tag{8.18}$$

representing the central part of the Maurer-Cartan form.

It should be clear now that s gives an isomorphism $\widehat{\mathfrak{g}}^* \cong \mathfrak{g}^* \oplus \mathbb{R}$. We also have the following

$$\mathrm{Ad}^*_f(\lambda, c) = (f^{-1}\lambda f + c\gamma(f), c), \tag{8.19}$$

which means that the coadjoint action of $\widehat{G}$ descends to G and where $\lambda \in \mathfrak{g}^*$, $c \in \mathbb{R}$, and $\gamma(f) \in \mathfrak{g}^*$ accounts for the central extension.

For $(\lambda, c) \in \widehat{\mathfrak{g}}^*$, the orbit action for $\widehat{f} = s(f)e^{i\theta}$ is:

$$S_{\widehat{G}}((\lambda, c), \widehat{f}) = \int_I \left\langle (\lambda, c), d\widehat{f}\widehat{f}^{-1} \right\rangle = \int_I \left(\left\langle \lambda, df f^{-1} \right\rangle + c(d\theta + \beta(f)) \right). \tag{8.20}$$

Here, the first term represents the action of the orbit for the group corresponding to the orbit of λ. Also $S_c(\theta) = c\int_I d\theta$ denotes the orbit action for the circle.

Conclusion

The main aim of this part was to propose a path integral that can, in essence, quantise the coadjoint orbits of loop groups. While this may not yet directly address specific results related to the phenomenology of NFLs, we believe it offers a valuable mechanism for achieving such quantisation. Equation (8.8) illustrates a general method for this process, with the goal of quantising coadjoint orbits.

Appendix A

Background on quantum spin systems

Our goal here is to present the basic mathematical framework which might be useful in the thesis.

Spins

The term "spin" refers to a physical system with a Hilbert space, $\mathbb{C}^d$, where $d < \infty$. This includes physical spin states of particles like electrons, spin-$\frac{1}{2}$, represented in $\mathbb{C}^2$. This simplification aids in practical calculations and simulations. For $\mathcal{H} = \mathbb{C}^d$, the standard inner product is

$$\langle u, v \rangle = \sum_{i=1}^{d} \overline{u_i} v_i. \tag{A.1}$$

For physical spins, $d = 2S + 1$ where S is the spin quantum number.

Observables

Observables form an algebra $\mathcal{A}$ for any quantum system. Given a Hilbert space $\mathcal{H}$ this is denoted by $\mathcal{B}(\mathcal{H})$, the set of all bounded linear operators on $\mathcal{H}$. As is well-known, physically relevant observables are self-adjoint elements of $\mathcal{B}(\mathcal{H})$.

For an arbitrary spin, $\mathcal{H} = \mathbb{C}^d$ and $\mathcal{A} = M_d(\mathbb{C})$, the space of $d \times d$ complex matrices. Self-adjoint observables have real spectra.

Observables can use the Hilbert-Schmidt inner product

$$\langle A, B \rangle_{\mathrm{HS}} = \mathrm{Tr}(A^* B) \text{ for } A, B \in \mathcal{A} \tag{A.2}$$

with trace Tr. The Hilbert-Schmidt norm relates to this product, while the operator norm is

$$\|A\| = \sup_{\psi \neq 0} \frac{\|A\psi\|}{\|\psi\|}. \tag{A.3}$$

For $d = 2$, we have the Pauli matrices as a basis:

$$\mathbb{1} = \begin{pmatrix} 1 & 0 \\ 0 & 1 \end{pmatrix}, \quad \sigma^1 = \begin{pmatrix} 0 & 1 \\ 1 & 0 \end{pmatrix}, \quad \sigma^2 = \begin{pmatrix} 0 & -i \\ i & 0 \end{pmatrix}, \quad \sigma^3 = \begin{pmatrix} 1 & 0 \\ 0 & -1 \end{pmatrix}. \tag{A.4}$$

For $d = 3$, the Gell-Mann matrices form a basis for $\mathcal{A} = M_3$

$$\lambda_1 = \begin{pmatrix} 0 & 1 & 0 \\ 1 & 0 & 0 \\ 0 & 0 & 0 \end{pmatrix} \quad \lambda_2 = \begin{pmatrix} 0 & -i & 0 \\ i & 0 & 0 \\ 0 & 0 & 0 \end{pmatrix} \quad \lambda_3 = \begin{pmatrix} 1 & 0 & 0 \\ 0 & -1 & 0 \\ 0 & 0 & 0 \end{pmatrix} \tag{A.5}$$

$$\lambda_4 = \begin{pmatrix} 0 & 0 & 1 \\ 0 & 0 & 0 \\ 1 & 0 & 0 \end{pmatrix} \quad \lambda_5 = \begin{pmatrix} 0 & 0 & -i \\ 0 & 0 & 0 \\ i & 0 & 0 \end{pmatrix} \tag{A.6}$$

$$\lambda_6 = \begin{pmatrix} 0 & 0 & 0 \\ 0 & 0 & 1 \\ 0 & 1 & 0 \end{pmatrix} \quad \lambda_7 = \begin{pmatrix} 0 & 0 & 0 \\ 0 & 0 & -i \\ 0 & i & 0 \end{pmatrix} \quad \lambda_8 = \frac{1}{\sqrt{3}} \begin{pmatrix} 1 & 0 & 0 \\ 0 & 1 & 0 \\ 0 & 0 & -2 \end{pmatrix}. \tag{A.7}$$

$$\tag{A.8}$$

For general spins, a Gell-Mann basis may be found in general for SU(N), which is shown below.

Defining representation of SU(N)

The special group of unitary matrices $SU(N)$ is the group of $N \times N$ unitary matrices with determinant one. The generators of its Lie algebra $\mathfrak{su}(N)$ are the $N \times N$ traceless hermitian unitary matrices. It is well known, and particularly useful in physics, that for $N = 3$ one can use a set of Gell-Mann matrices (1.12), where the generators are usually called flavours. This is called the defining representation. We can generalise this construction to arbitrary N and choosing $\{\lambda_i\}$ to be a basis for $\mathfrak{su}(N)$ of size $N^2 - 1$. These are $N \times N$ matrices which can be embedded into an $\mathfrak{su}(N+1)$ Lie algebra by simply adding zero columns and rows to in the following manner

$$\lambda_i' = \begin{pmatrix} \lambda_i & \mathbf{0} \\ \mathbf{0} & 0 \end{pmatrix}. \tag{A.9}$$

The dimension of the group $SU(N+1)$ is $(N+1)^2 - 1$ and for $SU(N)$ is $N^2 - 1$ meaning that we need an extra set of $2N + 1$ matrices to actually be able to generate $\mathfrak{su}(N+1)$. These are simply

$$\begin{aligned} \{\lambda_{N^2+2a-2}\}_{\alpha\beta} &= \delta_{\alpha,a}\delta_{\beta,N+1} + \delta_{\alpha,N+1}\delta_{\beta,a}, \\ \{\lambda_{N^2+2a-1}\}_{\alpha\beta} &= i\left(-\delta_{\alpha,a}\delta_{\beta,N+1} + \delta_{\alpha,N+1}\delta_{\beta,a}\right), \end{aligned} \tag{A.10}$$

additionally, we need $N(N-1)$ non-diagonal matrices

$$\lambda^{\{1\}}(i,j)_{\mu\nu} = \delta_{j\mu}\delta_{i\nu} + \delta_{j\nu}\delta_{i\mu}; \quad i,j = 1,2,3,\ldots,N; \quad i<j \tag{A.11}$$

$$\lambda^{\{2\}}(i,j)_{\mu\nu} = -\mathrm{i}\left(\delta_{i\mu}\delta_{j\nu} - \delta_{i\nu}\delta_{j\mu}\right); \quad i,j = 1,2,3,\ldots,N; \quad i<j, \tag{A.12}$$

and $N-1$ diagonal matrices

$$\lambda_{k^2-1} = \sqrt{\frac{2}{k^2-k}} \begin{pmatrix} (1 & 0 & 0 & 0 & \ldots & 0 \\ 0 & 1 & 0 & 0 & \ldots & 0 \\ 0 & 0 & 1)_{k-1} & 0 & \ldots & 0 \\ 0 & 0 & 0 & -(k-1) & \ldots & 0 \\ \vdots & \vdots & \vdots & \vdots & \ddots & \ldots \\ 0 & 0 & 0 & 0 & \ldots & 0 \end{pmatrix}_{N\times N} . \tag{A.13}$$

where $k = 2,3,\ldots,N$. This is useful when working with qudits, or when we need to parametrise the unitaries in a quantum circuit.

States

The algebra of bounded linear operators $\mathcal{A} = \mathcal{B}(\mathcal{H})$ may be used to define states of quantum systems. We define a state as a normalised, positive linear functional $\omega : \mathcal{A} \to \mathbb{C}$, satisfying

$$\omega(A^*A) \geq 0 \text{ for all } A \in \mathcal{A} \text{ and } \omega(\mathbb{1}) = 1.$$

The expectation value of an observable A in state ω is $\omega(A)$. For self-adjoint observables, $\omega(A^*) = \overline{\omega(A)}$, and the variance of A is

$$\mathrm{Var}(A) = \omega\left((A-\omega(A)\mathbb{1})^*(A-\omega(A)\mathbb{1})\right) = \omega\left(A^*A\right) - |\omega(A)|^2.$$

Thus, for a unitary vector ψ, the vector state ω_ψ is

$$\omega_\psi(A) = \langle\psi, A\psi\rangle$$

for all A in the algebra.

Alternatively,

$$\omega_\psi = \mathrm{Tr}(P_\psi A)$$

where P_ψ is the projection operator:

$$P_\psi(\phi) = \langle\psi,\phi\rangle\psi \text{ for } \phi \in \mathcal{H}.$$

Bibliography

[1] Ian Affleck, Tom Kennedy, Elliott H. Lieb, and Hal Tasaki. "Rigorous results on valence-bond ground states in antiferromagnets". In: *Phys. Rev. Lett.* 59 (7 Aug. 1987), pp. 799–802. DOI: 10.1103/PhysRevLett.59.799. URL: https://link.aps.org/doi/10.1103/PhysRevLett.59.799.

[2] BL Altshuler, LB Ioffe, and AJ Millis. "Low-energy properties of fermions with singular interactions". In: *Physical Review B* 50.19 (1994), p. 14048.

[3] P. W. Anderson. "Resonating valence bonds: A new kind of insulator?" In: *Mater. Res. Bull.* 8.2 (Feb. 1973), pp. 153–160. ISSN: 00255408. DOI: 10.1016/0025-5408(73)90167-0.

[4] A. Auerbach. *Interacting Electrons and Quantum Magnetism*. Graduate Texts in Contemporary Physics. Springer New York, 1994. ISBN: 9781461208693.

[5] J. Ayres et al. "Incoherent transport across the strange-metal regime of overdoped cuprates". In: *Nature* 595.7869 (July 2021), pp. 661–666. ISSN: 1476-4687. DOI: 10.1038/s41586-021-03622-z. URL: https://doi.org/10.1038/s41586-021-03622-z.

[6] M. Bal, M. Mariën, J. Haegeman, and F. Verstraete. "Renormalization Group Flows of Hamiltonians Using Tensor Networks". In: *Phys. Rev. Lett.* 118.25, 250602 (June 2017), p. 250602. DOI: 10.1103/PhysRevLett.118.250602. arXiv: 1703.00365 [cond-mat.stat-mech].

[7] M. Bal, M. M. Rams, V. Zauner, J. Haegeman, and F. Verstraete. "Matrix product state renormalization". In: *Phys. Rev. B* 94.20, 205122 (Nov. 2016), p. 205122. DOI: 10.1103/PhysRevB.94.205122. arXiv: 1509.01522 [quant-ph].

[8] A Balatsky and A Chubukov. "On the excitations in a S= 1 linear chain Heisenberg antiferromagnet with S= 1/2 impurities". In: *Journal of Physics: Condensed Matter* 3.10 (1991), p. 1359.

[9] Bela Bauer and Chetan Nayak. "Area laws in a many-body localized state and its implications for topological order". In: *J. Stat. Mech. Theory Exp.* 2013.09 (Sept. 2013), P09005. ISSN: 1742-5468. DOI: 10.1088/1742-5468/2013/09/P09005. arXiv: 1306.5753. URL: https://iopscience.iop.org/article/10.1088/1742-5468/2013/09/P09005.

[10] Gordon Baym and Christopher Pethick. *Landau Fermi-liquid theory: concepts and applications*. John Wiley & Sons, Inc., 2008.

[11] G Benfatto and Giovanni Gallavotti. "Renormalization-group approach to the theory of the Fermi surface". In: *Physical Review B* 42.16 (1990), p. 9967.

[12] Adam D. Bookatz. "QMA-complete problems". In: *Quantum Inf. Comput.* 14.5-6 (Dec. 2012), pp. 361–383. ISSN: 15337146. arXiv: 1212.6312. URL: http://arxiv.org/abs/1212.6312.

[13] Francisco Borges, Anton Borissov, Ashutosh Singh, Andrés Schlief, and Sung-Sik Lee. "Field-theoretic functional renormalization group formalism for non-Fermi liquids and its application to the antiferromagnetic quantum critical metal in two dimensions". In: *Annals of Physics* 450 (2023), p. 169221.

[14] K Buchta, Gábor Fáth, Örs Legeza, and Jenő Sólyom. "Probable absence of a quadrupolar spin-nematic phase in the bilinear-biquadratic spin-1 chain". In: *Physical Review B—Condensed Matter and Materials Physics* 72.5 (2005), p. 054433.

[15] Boye Buyens, Jutho Haegeman, Karel Van Acoleyen, Henri Verschelde, and Frank Verstraete. "Matrix Product States for Gauge Field Theories". In: *Phys. Rev. Lett.* 113 (Aug. 2014), p. 91601. ISSN: 0031-9007. DOI: 10.1103/PhysRevLett.113.091601. URL: https://ui.adsabs.harvard.edu/abs/2014PhRvL.113i1601B.

[16] Yuan Cao, Debanjan Chowdhury, Daniel Rodan-Legrain, Oriol Rubies-Bigorda, Kenji Watanabe, Takashi Taniguchi, T. Senthil, and Pablo Jarillo-Herrero. "Strange Metal in Magic-Angle Graphene with near Planckian Dissipation". In: *Physical Review Letters* 124.7 (Feb. 2020). ISSN: 1079-7114. URL: http://dx.doi.org/10.1103/PhysRevLett.124.076801.

[17] A. H. Castro Neto and Eduardo Fradkin. "Bosonization of Fermi liquids". In: *Phys. Rev. B* 49 (16 Apr. 1994), pp. 10877–10892. DOI: 10.1103/PhysRevB.49.10877. URL: https://link.aps.org/doi/10.1103/PhysRevB.49.10877.

[18] Olalla A Castro-Alvaredo and Benjamin Doyon. "Entanglement entropy of highly degenerate states and fractal dimensions". In: *Physical Review Letters* 108.12 (2012), p. 120401.

[19] M. A. Cazalilla, A. F. Ho, and M. Ueda. "Ultracold gases of ytterbium: Ferromagnetism and Mott states in an SU(6) Fermi system". In: *New J. Phys.* 11.6 (2009). ISSN: 13672630. DOI: 10.1088/1367-2630/11/10/103033.

[20] J. G. Cheng, G. Li, L. Balicas, J. S. Zhou, J. B. Goodenough, Cenke Xu, and H. D. Zhou. "High-Pressure Sequence of $Ba_3NiSb_2O_9$ Structural Phases: New $S = 1$ Quantum Spin Liquids Based on Ni^{2+}". In: *Phys. Rev. Lett.* 107 (19 Nov. 2011), p. 197204. DOI: 10.1103/PhysRevLett.107.197204. URL: https://link.aps.org/doi/10.1103/PhysRevLett.107.197204.

[21] Andrew M. Childs, David Gosset, and Zak Webb. "The Bose-Hubbard model is QMA-complete". In: *Lect. Notes Comput. Sci. (including Subser. Lect. Notes Artif. Intell. Lect. Notes Bioinformatics)*. PART 1. Springer Verlag, 2014, pp. 308–319. ISBN: 9783662439470. DOI: 10.1007/978-3-662-43948-7_26. arXiv: 1311.3297.

[22] Goffredo Chirco, Daniele Oriti, and Mingyi Zhang. "Ryu-Takayanagi formula for symmetric random tensor networks". In: *Phys. Rev. D* 97.12 (2018), p. 126002. ISSN: 24700029. DOI: 10.1103/PhysRevD.97.126002. arXiv: 1711.09941. URL: https://doi.org/10.1103/PhysRevD.97.126002.

[23] William J. Cunningham, Bianca Dittrich, and Sebastian Steinhaus. "Tensor network renormalization with fusion charges: applications to 3d lattice gauge theory". In: (2020), pp. 1–43. arXiv: 2002.10472. URL: http://arxiv.org/abs/2002.10472.

[24] Yan-Wei Dai, Qian-Qian Shi, Huan-Qiang Zhou, and Ian P McCulloch. "Absence of a critical nematic phase in the vicinity of the $SU(3)$ ferromagnetic point for the one-dimensional spin-1 bilinear-biquadratic model". In: *arXiv preprint arXiv:2201.01434* (2022).

[25] Denis Dalidovich and Sung-Sik Lee. "Perturbative non-Fermi liquids from dimensional regularization". In: *Phys. Rev. B* 88 (24 Dec. 2013), p. 245106. DOI: 10.1103/PhysRevB.88.245106. URL: http://link.aps.org/doi/10.1103/PhysRevB.88.245106.

[26] Luca V Delacrétaz, Yi-Hsien Du, Umang Mehta, and Dam Thanh Son. "Nonlinear bosonization of Fermi surfaces: The method of coadjoint orbits". In: *Physical Review Research* 4.3 (2022), p. 033131.

[27] P. A.M. Dirac. "Note on Exchange Phenomena in the Thomas Atom". In: *Math. Proc. Cambridge Philos. Soc.* 26.3 (1930), pp. 376–385. ISSN: 14698064. DOI: 10.1017/S0305004100016108. URL: /core/journals/mathematical-proceedings-of-the-cambridge-philosophical-society/article/note-on-exchange-phenomena-in-the-thomas-atom/6C5FF7297CD96F49A8B8E9E3EA50E412.

[28] J Dubail and N Read. "Tensor network trial states for chiral topological phases in two dimensions and a no-go theorem in any dimension". In: *Phys. Rev. B* 92 (Nov. 2015), p. 205307. ISSN: 0163-18291098-0121. DOI: 10.1103/PhysRevB.92.205307. URL: https://ui.adsabs.harvard.edu/abs/2015PhRvB..92t5307D.

[29] Andreas Eberlein, Aavishkar A. Patel, and Subir Sachdev. "Shear viscosity at the Ising-nematic quantum critical point in two-dimensional metals". In: *Phys. Rev. B* 95 (7 Mar. 2017), p. 075127. DOI: 10.1103/PhysRevB.95.075127. URL: https://link.aps.org/doi/10.1103/PhysRevB.95.075127.

[30] GM Eliashberg. "Interactions between electrons and lattice vibrations in a superconductor". In: *Sov. Phys. JETP* 11.3 (1960), pp. 696–702.

[31] Dominic V Else. "Holographic models of non-Fermi liquid metals revisited: An effective field theory approach". In: *Physical Review B* 109.3 (2024), p. 035163.

[32] Dominic V Else, Ryan Thorngren, and T Senthil. "Non-Fermi liquids as ersatz Fermi liquids: general constraints on compressible metals". In: *Physical Review X* 11.2 (2021), p. 021005.

[33] G. Evenbly and G. Vidal. "Tensor Network Renormalization". In: *Phys. Rev. Lett.* 115.18, 180405 (Oct. 2015), p. 180405. DOI: 10.1103/PhysRevLett.115.180405. arXiv: 1412.0732 [cond-mat.str-el].

[34] G. Evenbly and G. Vidal. "Tensor Network Renormalization Yields the Multiscale Entanglement Renormalization Ansatz". In: *Phys. Rev. Lett.* 115.20, 200401 (Nov. 2015), p. 200401. DOI: 10.1103/PhysRevLett.115.200401. arXiv: 1502.05385 [cond-mat.str-el].

[35] G. Evenbly and G. Vidal. "Tensor Network States and Geometry". In: *Journal of Statistical Physics* 145.4 (Nov. 2011), pp. 891–918. DOI: 10.1007/s10955-011-0237-4. arXiv: 1106.1082 [quant-ph].

[36] Glen Evenbly. "Algorithms for tensor network renormalization". In: *arXiv e-prints*, arXiv:1509.07484 (Sept. 2015), arXiv:1509.07484. DOI: 10.48550/arXiv.1509.07484. arXiv: 1509.07484 [cond-mat.str-el].

[37] M. Fannes, B. Nachtergaele, and R. F. Werner. "Finitely correlated states on quantum spin chains". In: *Commun. Math. Phys.* 144.3 (Mar. 1992), pp. 443–490. ISSN: 00103616. DOI: 10.1007/BF02099178. URL: http://link.springer.com/10.1007/BF02099178.

[38] Gábor Fáth and Jenő Sólyom. "Search for the nondimerized quantum nematic phase in the spin-1 chain". In: *Physical Review B* 51.6 (1995), p. 3620.

[39] P. Fazekas and P. W. Anderson. "On the ground state properties of the anisotropic triangular antiferromagnet". In: *Philos. Mag.* 30.2 (1974), pp. 423–440. ISSN: 00318086. DOI: 10.1080/14786439808206568.

[40] A. V. Gorshkov et al. "Two-orbital S U(N) magnetism with ultracold alkaline-earth atoms". In: *Nat. Phys.* 6.4 (Apr. 2010), pp. 289–295. ISSN: 1745-2473. DOI: 10.1038/nphys1535. arXiv: 0905.2610. URL: http://www.nature.com/articles/nphys1535.

[41] A. G. Green, C. A. Hooley, J. Keeling, and S. H. Simon. "Feynman Path Integrals Over Entangled States". In: (July 2016). arXiv: 1607.01778. URL: http://arxiv.org/abs/1607.01778.

[42] Martin Greiter, Darrell F. Schroeter, and Ronny Thomale. "Parent Hamiltonian for the non-Abelian chiral spin liquid". In: *Phys. Rev. B* 89 (16 Apr. 2014), p. 165125. DOI: 10.1103/PhysRevB.89.165125. URL: https://link.aps.org/doi/10.1103/PhysRevB.89.165125.

[43] Zheng-Cheng Gu and Xiao-Gang Wen. "Tensor-entanglement-filtering renormalization approach and symmetry-protected topological order". In: *Phys. Rev. B* 80 (Oct. 2009), p. 155131. ISSN: 0163-18291098-0121. DOI: 10.1103/PhysRevB.80.155131. URL: https://ui.adsabs.harvard.edu/abs/2009PhRvB..80o5131G.

[44] Zheng-Cheng Gu and Xiao-Gang Wen. "Tensor-entanglement-filtering renormalization approach and symmetry-protected topological order". In: *Phys. Rev. B* 80.15, 155131 (Oct. 2009), p. 155131. DOI: 10.1103/PhysRevB.80.155131. arXiv: 0903.1069 [cond-mat.str-el].

[45] Jutho Haegeman, J. Ignacio Cirac, Tobias J. Osborne, Iztok PiÅorn, Henri Verschelde, and Frank Verstraete. "Time-dependent variational principle for quantum lattices". In: *Phys. Rev. Lett.* 107.7 (2011), pp. 1–5. ISSN: 00319007. DOI: 10.1103/PhysRevLett.107.070601. arXiv: 1103.0936.

[46] Jutho Haegeman, J. Ignacio Cirac, Tobias J. Osborne, Iztok Pižorn, Henri Verschelde, and Frank Verstraete. "Time-Dependent Variational Principle for Quantum Lattices". In: *Phys. Rev. Lett.* 107.7, 070601 (Aug. 2011), p. 070601. DOI: 10.1103/PhysRevLett.107.070601. arXiv: 1103.0936 [cond-mat.str-el].

[47] Jutho Haegeman, Tobias J Osborne, and Frank Verstraete. "Post-matrix product state methods: To tangent space and beyond". In: *Phys. Rev. B* 88 (Aug. 2013), p. 75133. ISSN: 0163-18291098-0121. DOI: 10.1103/PhysRevB.88.075133. URL: https://ui.adsabs.harvard.edu/abs/2013PhRvB..88g5133H.

[48] F. D. M. Haldane. "Nonlinear Field Theory of Large-Spin Heisenberg Antiferromagnets: Semiclassically Quantized Solitons of the One-Dimensional Easy-Axis Néel State". In: *Phys. Rev. Lett.* 50 (15 Apr. 1983), pp. 1153–1156. DOI: 10.1103/PhysRevLett.50.1153. URL: https://link.aps.org/doi/10.1103/PhysRevLett.50.1153.

[49] F.D.M. Haldane. "Continuum dynamics of the 1-D Heisenberg antiferromagnet: Identification with the O(3) nonlinear sigma model". In: *Physics Letters A* 93.9 (1983), pp. 464–468. ISSN: 0375-9601. DOI: https://doi.org/10.1016/0375-9601(83)90631-X. URL: https://www.sciencedirect.com/science/article/pii/037596018390631X.

[50] FDM Haldane. "Luttinger's theorem and bosonization of the fermi surface". In: *arXiv preprint cond-mat/0505529* (2005).

[51] Kenji Harada and Naoki Kawashima. "Quadrupolar order in isotropic Heisenberg models with biquadratic interaction". In: *Phys. Rev. B - Condens. Matter Mater. Phys.* 65.5 (Jan. 2002), pp. 1–4. ISSN: 1550235X. DOI: 10.1103/PhysRevB.65.052403. arXiv: 0109431 [cond-mat]. URL: https://link.aps.org/doi/10.1103/PhysRevB.65.052403.

[52] Markus Hauru, Clement Delcamp, and Sebastian Mizera. "Renormalization of tensor networks using graph-independent local truncations". In: *Phys. Rev. B* 97.4, 045111 (Jan. 2018), p. 045111. DOI: 10.1103/PhysRevB.97.045111. arXiv: 1709.07460 [cond-mat.str-el].

[53] Ian M. Hayes, Ross D. McDonald, Nicholas P. Breznay, Toni Helm, Philip J. W. Moll, Mark Wartenbe, Arkady Shekhter, and James G. Analytis. "Scaling between magnetic field and temperature in the high-temperature superconductor BaFe2(As1?xPx)2". In: *Nature Physics* 12.10 (May 2016), 916?919. ISSN: 1745-2481. DOI: 10.1038/nphys3773. URL: http://dx.doi.org/10.1038/nphys3773.

[54] John A. Hertz. "Quantum critical phenomena". In: *Phys. Rev. B* 14 (3 Aug. 1976), pp. 1165–1184. DOI: 10.1103/PhysRevB.14.1165. URL: https://link.aps.org/doi/10.1103/PhysRevB.14.1165.

[55] Sebastian Holtz, Thorsten Rohwedder, and Reinhold Schneider. "On manifolds of tensors of fixed TT-rank". In: *Numer. Math.* 120.4 (2012), pp. 701–731. ISSN: 0029599X. DOI: 10.1007/s00211-011-0419-7.

[56] Roger A. Horn and Charles R. Johnson. *Matrix Analysis*. Cambridge University Press, 2012. ISBN: 9780521839402. DOI: https://doi.org/10.1017/9781139020411. URL: /core/books/matrix-analysis/FDA3627DC2B9F5C3DF2FD8C3CC136B48.

[57] A Houghton, H-J Kwon, and JB Marston. "Multidimensional bosonization". In: *Advances in Physics* 49.2 (2000), pp. 141–228.

[58] Wen Jun Hu, Shou Shu Gong, Hsin Hua Lai, Haoyu Hu, Qimiao Si, and Andriy H. Nevidomskyy. "Nematic spin liquid phase in a frustrated spin-1 system on the square lattice". In: *Phys. Rev. B* 100.16 (Oct. 2019), p. 165142. ISSN: 24699969. DOI: 10.1103/PhysRevB.100.165142.

[59] Alan Huckleberry and Tilmann Wurzbacher. *Infinite dimensional Kähler manifolds*. Vol. 31. Birkhäuser, 2012.

[60] Hong-Chen Jiang, Matthew S. Block, Ryan V. Mishmash, James R. Garrison, D. N. Sheng, Olexei I. Motrunich, and Matthew P. A. Fisher. "Non-Fermi-liquid d-wave metal phase of strongly interacting electrons". In: *Nature* 493.7430 (2013), pp. 39–44. DOI: 10.1038/nature11732. URL: https://doi.org/10.1038/nature11732.

[61] Juan José García-Ripoll. "Time evolution of Matrix Product States". In: *New Journal of Physics* 8.12 (Dec. 2006), p. 305. DOI: 10.1088/1367-2630/8/12/305. arXiv: cond-mat/0610210 [cond-mat.str-el].

[62] L.P. Kadanoff. "Scaling laws for Ising models near Tc". In: *Physics (Long Island City, N.Y.)* 263.2 (1966).

[63] Anton Kapustin, Alex Turzillo, and Minyoung You. "Topological field theory and matrix product states". In: *Phys. Rev. B* 96.7 (2017), pp. 1–13. ISSN: 24699969. DOI: 10.1103/PhysRevB.96.075125. arXiv: 1607.06766.

[64] B. Keimer, S. A. Kivelson, M. R. Norman, S. Uchida, and J. Zaanen. "From quantum matter to high-temperature superconductivity in copper oxides". In: *Nature* 518.7538 (2015), pp. 179–186. DOI: 10.1038/nature14165. URL: https://doi.org/10.1038/nature14165.

[65] Julia Kempe, Alexei Kitaev, and Oded Regev. "The complexity of the local hamiltonian problem". In: *SIAM J. Comput.* 35.5 (2006), pp. 1070–1097. ISSN: 00975397. DOI: 10.1137/S0097539704445226.

[66] Tom Kennedy and Slava Rychkov. "Tensor Renormalization Group at Low Temperatures: Discontinuity Fixed Point". In: *Annales Henri Poincaré* 25.1 (2024), pp. 773–841. DOI: 10.1007/s00023-023-01289-y. URL: https://doi.org/10.1007/s00023-023-01289-y.

[67] Tom Kennedy and Slava Rychkov. "Tensor RG Approach to High-Temperature Fixed Point". In: *Journal of Statistical Physics* 187.3 (2022), p. 33. DOI: 10.1007/s10955-022-02924-4. URL: https://doi.org/10.1007/s10955-022-02924-4.

[68] D. V. Khveshchenko. "Geometrical approach to bosonization of $D > 1$ dimensional (non)-Fermi liquids". In: *Phys. Rev. B* 52 (7 Aug. 1995), pp. 4833–4841. DOI: 10.1103/PhysRevB.52.4833. URL: https://link.aps.org/doi/10.1103/PhysRevB.52.4833.

[69] Aleksandr Aleksandrovich Kirillov. *Lectures on the orbit method*. Vol. 64. American Mathematical Soc., 2004.

[70] Alexei Kitaev. "Anyons in an exactly solved model and beyond". In: *Annals of Physics* 321.1 (2006). January Special Issue, pp. 2–111. ISSN: 0003-4916. DOI: https://doi.org/10.1016/j.aop.2005.10.005. URL: https://www.sciencedirect.com/science/article/pii/S0003491605002381.

[71] Anthony W Knapp and Anthony William Knapp. *Lie groups beyond an introduction*. Vol. 140. Springer, 1996.

[72] H.-J. Kwon, A. Houghton, and J. B. Marston. "Gauge interactions and bosonized fermion liquids". In: *Phys. Rev. Lett.* 73 (2 July 1994), pp. 284–287. DOI: 10.1103/PhysRevLett.73.284. URL: https://link.aps.org/doi/10.1103/PhysRevLett.73.284.

[73] Claudine Lacroix, Philippe Mendels, and Frédéric Mila. *Introduction to Frustrated Magnetism*. Ed. by Claudine Lacroix, Philippe Mendels, and Frédéric Mila. Vol. 164. Springer Series in Solid-State Sciences. Berlin, Heidelberg: Springer Berlin Heidelberg, 2011, p. 500. ISBN: 978-3-642-10588-3. DOI: 10.1007/978-3-642-10589-0. arXiv: 0306542 [cond-mat]. URL: http://link.springer.com/10.1007/978-3-642-10589-0%20http://books.google.com/books?id=utSV09ZuhOkC%7B%5C&%7Dpgis=1.

[74] Hsin Hua Lai, Wen Jun Hu, Emilian M. Nica, Rong Yu, and Qimiao Si. "Antiferroquadrupolar Order and Rotational Symmetry Breaking in a Generalized Bilinear-Biquadratic Model on a Square Lattice". In: *Phys. Rev. Lett.* 118.17 (Apr. 2017), p. 176401. ISSN: 10797114. DOI: 10.1103/PhysRevLett.118.176401. arXiv: 1603.03027.

[75] Ethan Lake. "Renormalization group and stability in the exciton Bose liquid". In: *Phys. Rev. B* 105 (7 Feb. 2022), p. 075115. DOI: 10.1103/PhysRevB.105.075115. URL: https://link.aps.org/doi/10.1103/PhysRevB.105.075115.

[76] LD Landau. "On the theory of the Fermi liquid". In: *Sov. Phys. JETP* 8.1 (1959), p. 70.

[77] Andreas Läuchli, Guido Schmid, and Simon Trebst. "Spin nematics correlations in bilinear-biquadratic S=1 spin chains". In: *Phys. Rev. B - Condens. Matter Mater. Phys.* 74.14 (Oct. 2006), p. 144426. ISSN: 10980121. DOI: 10.1103/PhysRevB.74.144426. arXiv: 0607173 [cond-mat].

[78] Michael J. Lawler, Daniel G. Barci, Victoria Fernández, Eduardo Fradkin, and Luis Oxman. "Nonperturbative behavior of the quantum phase transition to a nematic Fermi fluid". In: *Phys. Rev. B* 73 (8 Feb. 2006), p. 085101. DOI: 10.1103/PhysRevB.73.085101. URL: https://link.aps.org/doi/10.1103/PhysRevB.73.085101.

[79] Sung-Sik Lee. "Recent developments in non-fermi liquid theory". In: *Annual Review of Condensed Matter Physics* 9.1 (2018), pp. 227–244.

[80] Michael Levin and Cody P. Nave. "Tensor Renormalization Group Approach to Two-Dimensional Classical Lattice Models". In: *Phys. Rev. Lett.* 99.12, 120601 (Sept. 2007), p. 120601. DOI: 10.1103/PhysRevLett.99.120601. arXiv: cond-mat/0611687 [cond-mat.stat-mech].

[81] Elliott Lieb and Daniel Mattis. "Ordering energy levels of interacting spin systems". In: *Journal of Mathematical Physics* 3.4 (1962), pp. 749–751.

[82] Zheng Xin Liu, Hong Hao Tu, Ying Hai Wu, Rong Qiang He, Xiong Jun Liu, Yi Zhou, and Tai Kai Ng. "Non-Abelian S=1 chiral spin liquid on the kagome lattice". In: *Phys. Rev. B* 97.19 (May 2018), p. 195158. ISSN: 24699969. DOI: 10.1103/PhysRevB.97.195158.

[83] E. Y. Loh, J. E. Gubernatis, R. T. Scalettar, S. R. White, D. J. Scalapino, and R. L. Sugar. "Sign problem in the numerical simulation of many-electron systems". In: *Phys. Rev. B* 41.13 (May 1990), pp. 9301–9307. ISSN: 01631829. DOI: 10.1103/PhysRevB.41.9301.

[84] Han Ma and Sung-Sik Lee. "Fermi liquids beyond the forward-scattering limit: The role of nonforward scattering for scale invariance and instabilities". In: *Physical Review B* 109.4 (2024), p. 045143.

[85] Ipsita Mandal and Sung-Sik Lee. "Ultraviolet/infrared mixing in non-Fermi liquids". In: *Phys. Rev. B* 92 (3 July 2015), p. 035141. DOI: 10.1103/PhysRevB.92.035141. URL: https://link.aps.org/doi/10.1103/PhysRevB.92.035141.

[86] Max A Metlitski and Subir Sachdev. "Quantum phase transitions of metals in two spatial dimensions. I. Ising-nematic order". In: *Physical Review B—Condensed Matter and Materials Physics* 82.7 (2010), p. 075127.

[87] Max A. Metlitski, David F. Mross, Subir Sachdev, and T. Senthil. "Cooper pairing in non-Fermi liquids". In: *Phys. Rev. B* 91 (11 Mar. 2015), p. 115111. DOI: 10.1103/PhysRevB.91.115111. URL: http://link.aps.org/doi/10.1103/PhysRevB.91.115111.

[88] A. J. Millis. "Effect of a nonzero temperature on quantum critical points in itinerant fermion systems". In: *Phys. Rev. B* 48 (10 Sept. 1993), pp. 7183–7196. DOI: 10.1103/PhysRevB.48.7183. URL: https://link.aps.org/doi/10.1103/PhysRevB.48.7183.

[89] Ashley Milsted and Guifre Vidal. *Tensor networks as conformal transformations*. May 2018. URL: https://ui.adsabs.harvard.edu/abs/2018arXiv180512524M.

[90] David F. Mross, John McGreevy, Hong Liu, and T. Senthil. "Controlled expansion for certain non-Fermi-liquid metals". In: *Phys. Rev. B* 82 (4 July 2010), p. 045121. DOI: 10.1103/PhysRevB.82.045121. URL: https://link.aps.org/doi/10.1103/PhysRevB.82.045121.

[91] Satoru Nakatsuji, Yusuke Nambu, Keisuke Onuma, Seth Jonas, Collin Broholm, and Yoshiteru Maeno. "Coherent behaviour without magnetic order of the triangular lattice antiferromagnet {NiGa}2S4". In: *J. Phys. Condens. Matter* 19.14 (Mar. 2007), p. 145232. DOI: 10.1088/0953-8984/19/14/145232. URL: https://doi.org/10.1088%7B%5C%%7D2F0953-8984%7B%5C%%7D2F19%7B%5C%%7D2F14%7B%5C%%7D2F145232.

[92] Chetan Nayak and Frank Wilczek. "Non-Fermi liquid fixed point in 2 + 1 dimensions". In: *Nuclear Physics B* 417.3 (1994), pp. 359–373. ISSN: 0550-3213. DOI: https://doi.org/10.1016/0550-3213(94)90477-4. URL: https://www.sciencedirect.com/science/article/pii/0550321394904774.

[93] Chetan Nayak and Frank Wilczek. "Renormalization group approach to low temperature properties of a non-Fermi liquid metal". In: *Nuclear Physics B* 430.3 (1994), pp. 534–562.

[94] Ido Niesen and Philippe Corboz. "A tensor network study of the complete ground state phase diagram of the spin-1 bilinear-biquadratic Heisenberg model on the square lattice". In: *SciPost Phys.* 3.4 (Oct. 2017), p. 030. ISSN: 2542-4653. DOI: 10.21468/SciPostPhys.3.4.030. arXiv: 1707.01953. URL: https://scipost.org/10.21468/SciPostPhys.3.4.030.

[95] Ido Niesen and Philippe Corboz. "Emergent Haldane phase in the S=1 bilinear-biquadratic Heisenberg model on the square lattice". In: *Phys. Rev. B* 95.18 (May 2017), p. 180404. ISSN: 24699969. DOI: 10.1103/PhysRevB.95.180404. arXiv: 1701.05142.

[96] J. Oitmaa and C. J. Hamer. "S=1 bilinear biquadratic spin model on the square lattice: A series expansion study". In: *Phys. Rev. B - Condens. Matter Mater. Phys.* 87.22 (June 2013), p. 224431. ISSN: 10980121. DOI: 10.1103/PhysRevB.87.224431.

[97] S. Ono, Seiki Komiya, and Yoichi Ando. "Strong charge fluctuations manifested in the high-temperature Hall coefficient of high-T_c cuprates". In: *Phys. Rev. B* 75 (2 Jan. 2007), p. 024515. DOI: 10.1103/PhysRevB.75.024515. URL: https://link.aps.org/doi/10.1103/PhysRevB.75.024515.

[98] Román Orús. "Tensor networks for complex quantum systems". In: 1.9 (2019), pp. 538–550. ISSN: 25225820. DOI: 10.1038/s42254-019-0086-7. arXiv: 1812.04011. URL: http://dx.doi.org/10.1038/s42254-019-0086-7.

[99] N. Papanicolaou. "Unusual phases in quantum spin-1 systems". In: *Nucl. Physics, Sect. B* 305.3 (Nov. 1988), pp. 367–395. ISSN: 05503213. DOI: 10.1016/0550-3213(88)90073-9.

[100] Aavishkar A. Patel, Philipp Strack, and Subir Sachdev. "Hyperscaling at the spin density wave quantum critical point in two-dimensional metals". In: *Phys. Rev. B* 92 (16 Oct. 2015), p. 165105. DOI: 10.1103/PhysRevB.92.165105. URL: https://link.aps.org/doi/10.1103/PhysRevB.92.165105.

[101] D. Perez-Garcia, F. Verstraete, M. M. Wolf, and J. I. Cirac. "Matrix Product State Representations". In: *Quantum Inf. Comput.* 7.5-6 (Aug. 2006), pp. 401–430. ISSN: 15337146. arXiv: 0608197 [quant-ph]. URL: http://arxiv.org/abs/quant-ph/0608197.

[102] Lorenzo Piroli and J. Ignacio Cirac. "Quantum Cellular Automata, Tensor Networks, and Area Laws". In: 1 (2020), pp. 1–7. arXiv: 2007.15371. URL: http://arxiv.org/abs/2007.15371.

[103] J. Polchinski. "Low-energy dynamics of the spinon-gauge system". In: *Nuclear Physics B* 422 (July 1994), pp. 617–633. DOI: 10.1016/0550-3213(94)90449-9.

[104] Joseph Polchinski. "Effective Field Theory and the Fermi Surface". In: *arXiv e-prints*, hep-th/9210046 (Oct. 1992), hep–th/9210046. DOI: 10.48550/arXiv.hep-th/9210046. arXiv: hep-th/9210046 [hep-th].

[105] Andrew Pressley and G Segal. "Loop groups". In: *Encyclopedia of Physical Science and Technology* 1 (1987), p. 151.

[106] Michael Pretko, Xie Chen, and Yizhi You. "Fracton phases of matter". In: *International Journal of Modern Physics A* 35.06 (2020), p. 2030003.

[107] Mykhailo V Rakov and Michael Weyrauch. "Bilinear-biquadratic spin-1 rings: an SU (2)-symmetric MPS algorithm for periodic boundary conditions". In: *Journal of Physics Communications* 1.1 (2017), p. 015007.

[108] N Read and Subir Sachdev. "Valence-bond and spin-Peierls ground states of low-dimensional quantum antiferromagnets". In: *Physical review letters* 62.14 (1989), p. 1694.

[109] Ulrich Schollwöck. "The density-matrix renormalization group in the age of matrix product states". In: *Ann. Phys. (N. Y).* 326.1 (2011), pp. 96–192. ISSN: 00034916. DOI: 10.1016/j.aop.2010.09.012. arXiv: 1008.3477.

[110] Nathan Seiberg and Shu-Heng Shao. "Exotic symmetries, duality, and fractons in 2+ 1-dimensional quantum field theory". In: *SciPost Physics* 10.2 (2021), p. 027.

[111] T. Senthil. "Theory of a continuous Mott transition in two dimensions". In: *Phys. Rev. B* 78 (4 July 2008), p. 045109. DOI: 10.1103/PhysRevB.78.045109. URL: https://link.aps.org/doi/10.1103/PhysRevB.78.045109.

[112] Rev Shankar. "Renormalization-group approach to interacting fermions". In: *Reviews of Modern Physics* 66.1 (1994), p. 129.

[113] Daniel Stanek, Oleg P. Sushkov, and Götz S. Uhrig. "Self-consistent spin-wave theory for a frustrated Heisenberg model with biquadratic exchange in the columnar phase and its application to iron pnictides". In: *Phys. Rev. B - Condens. Matter Mater. Phys.* 84.6 (Aug. 2011), p. 064505. ISSN: 10980121. DOI: 10.1103/PhysRevB.84.064505. arXiv: 1104.1954.

[114] Leonard Susskind. "Entanglement is not enough". In: *Fortschritte der Physik* 64.1 (2016), pp. 49–71.

[115] L Tagliacozzo and G Vidal. "Entanglement renormalization and gauge symmetry". In: *Phys. Rev. B* 83 (Mar. 2011), p. 115127. ISSN: 0163-18291098-0121. DOI: 10.1103/PhysRevB.83.115127. URL: https://ui.adsabs.harvard.edu/abs/2011PhRvB..83k5127T.

[116] Tamás A. Tóth, Andreas M. Läuchli, Frédéric Mila, and Karlo Penc. "Competition between two- and three-sublattice ordering for S=1 spins on the square lattice". In: *Phys. Rev. B - Condens. Matter Mater. Phys.* 85.14 (Apr. 2012), p. 140403. ISSN: 10980121. DOI: 10.1103/PhysRevB.85.140403.

[117] Hirokazu Tsunetsugu and Mitsuhiro Arikawa. "Spin nematic phase in S = 1 triangular antiferromagnets". In: *J. Phys. Soc. Japan* 75.8 (Aug. 2006). ISSN: 00319015. DOI: 10.1143/JPSJ.75.083701.

[118] Kouji Ueda, Chenglong Jin, Naokazu Shibata, Yasuhiro Hieida, and Tomotoshi Nishino. "Least Action Principle for the Real-Time Density Matrix Renormalization Group". In: (2006), pp. 1–5. arXiv: 0612480 [cond-mat]. URL: http://arxiv.org/abs/cond-mat/0612480.

[119] Laurens Vanderstraeten, Jutho Haegeman, and Frank Verstraete. "Simulating excitation spectra with projected entangled-pair states". In: *Phys. Rev. B* 99.16 (Apr. 2019), p. 165121. ISSN: 24699969. DOI: 10.1103/PhysRevB.99.165121. arXiv: 1809.06747. URL: https://ui.adsabs.harvard.edu/abs/2019PhRvB..99p5121V.

[120] Laurens Vanderstraeten, Jutho Haegeman, and Frank Verstraete. "Simulating excitation spectra with projected entangled-pair states". In: *Phys. Rev. B* 99.16 (2019), pp. 1–5. ISSN: 24699969. DOI: 10.1103/PhysRevB.99.165121. arXiv: 1809.06747.

[121] Laurens Vanderstraeten, Jutho Haegeman, and Frank Verstraete. "Tangent-space methods for uniform matrix product states". In: *SciPost Phys. Lect. Notes* 7 (2019), pp. 1–77. ISSN: 2590-1990. DOI: 10.21468/scipostphyslectnotes.7. arXiv: 1810.07006.

[122] F Verstraete and J I Cirac. "Matrix product states represent ground states faithfully". In: *Phys. Rev. B* 73 (Mar. 2006), p. 94423. ISSN: 0163-18291098-0121. DOI: 10.1103/PhysRevB.73.094423. URL: https://ui.adsabs.harvard.edu/abs/2006PhRvB..73i4423V.

[123] Guifré Vidal. "Efficient Simulation of One-Dimensional Quantum Many-Body Systems". In: *Phys. Rev. Lett.* 93.4, 040502 (July 2004), p. 040502. DOI: 10.1103/PhysRevLett.93.040502. arXiv: quant-ph/0310089 [quant-ph].

[124] Haruki Watanabe. "Counting rules of Nambu–Goldstone modes". In: *Annual Review of Condensed Matter Physics* 11.1 (2020), pp. 169–187.

[125] Alexander Weiße, Gerhard Wellein, Andreas Alvermann, and Holger Fehske. "The kernel polynomial method". In: *Reviews of Modern Physics* 78.1 (Jan. 2006), pp. 275–306. DOI: 10.1103/RevModPhys.78.275. arXiv: cond-mat/0504627 [cond-mat.other].

[126] Christopher David White, ChunJun Cao, and Brian Swingle. "Conformal field theories are magical". In: *Physical Review B* 103.7 (2021), p. 075145.

[127] Steven R. White and Adrian E. Feiguin. "Real-time evolution using the density matrix renormalization group". In: *Phys. Rev. Lett.* 93.7 (Aug. 2004), p. 076401. ISSN: 00319007. DOI: 10.1103/PhysRevLett.93.076401. arXiv: 0403310 [cond-mat].

[128] Sebastian Wouters, Naoki Nakatani, Dimitri Van Neck, and Garnet Kin-Lic Chan. "Thouless theorem for matrix product states and subsequent post density matrix renormalization group methods". In: *Phys. Rev. B, vol. 88, Issue 7, id. 075122* 88 (Aug. 2013), p. 75122. DOI: 10.1103/PhysRevB.88.075122. URL: https://ui.adsabs.harvard.edu/abs/2013PhRvB..88g5122W.

[129] Shuo Yang, Zheng-Cheng Gu, and Xiao-Gang Wen. "Loop Optimization for Tensor Network Renormalization". In: *Phys. Rev. Lett.* 118.11, 110504 (Mar. 2017), p. 110504. DOI: 10.1103/PhysRevLett.118.110504.

[130] Weicheng Ye, Sung-Sik Lee, and Liujun Zou. "Ultraviolet-Infrared Mixing in Marginal Fermi Liquids". In: *Phys. Rev. Lett.* 128 (10 Mar. 2022), p. 106402. DOI: 10.1103/PhysRevLett.128.106402. URL: https://link.aps.org/doi/10.1103/PhysRevLett.128.106402.

[131] Rong Yu and Qimiao Si. "Antiferroquadrupolar and Ising-Nematic Orders of a Frustrated Bilinear-Biquadratic Heisenberg Model and Implications for the Magnetism of FeSe". In: *Phys. Rev. Lett.* 115.11 (Sept. 2015), p. 116401. ISSN: 10797114. DOI: 10.1103/PhysRevLett.115.116401. arXiv: 1501.05926.

[132] V. Zauner-Stauber, L. Vanderstraeten, M. T. Fishman, F. Verstraete, and J. Haegeman. "Variational optimization algorithms for uniform matrix product states". In: *Phys. Rev. B* 97.4, 045145 (Jan. 2018), p. 045145. DOI: 10.1103/PhysRevB.97.045145. arXiv: 1701.07035 [quant-ph].